AN INVESTIGATION INTO THE VISCOSITY OF C-MASSECUITE USING A PIPELINE VISCOMETER

Shaista Shah

Student number 204 503 886

Submitted in fulfilment of the academic requirements for the degree of Master of Science in Engineering in the School of Chemical Engineering at the College of Agriculture, Engineering and Science, University of KwaZulu-Natal.

Supervisor: Dr David Lokhat Co-Supervisor : Mr Stephen David Peacock

June 2017

EXAMINER'S COPY

DECLARATION 1 - PLAGIARISM

I, Shaista Shah, declare that

1. The research reported in this thesis, except where otherwise indicated, is my original research.
2. This thesis has not been submitted for any degree or examination at any other university.
3. This thesis does not contain other persons' data, pictures, graphs or other information, unless specifically acknowledged as being sourced from other persons.
4. This thesis does not contain other persons' writing, unless specifically acknowledged as being sourced from other researchers. Where other written sources have been quoted, then:
    a. Their words have been re-written but the general information attributed to them has been referenced
    b. Where their exact words have been used, then their writing has been placed in italics and inside quotation marks, and referenced.
5. This thesis does not contain text, graphics or tables copied and pasted from the Internet, unless specifically acknowledged, and the source being detailed in the thesis and in the References sections.

Candidate : Shaista Shah

Signature : …… Date : ……

This dissertation is submitted for examination with approval from the candidate's supervisors.

Supervisor : Dr David Lokhat

Signature : …… Date : ……

Co-Supervisor : Mr Stephen David Peacock

Signature : …… Date : ……

DECLARATION 2 - PUBLICATIONS

DETAILS OF CONTRIBUTION TO PUBLICATIONS that form part and/or include research presented in this thesis (include publications in preparation, submitted, *in press* and published and give details of the contributions of each author to the experimental work and writing of each publication)

Publication 1

Shah, S., Lokhat, D., Peacock, S.D., 2017. An investigation into the viscosity of C-massecuite using a pipeline viscometer. *Proc. S. Afr. Sugar Technol. Ass.* (in press)

Author : Shaista Shah

Co-authors : David Lokhat, Stephen David Peacock

Signature : …… Date : ……

ACKNOWLEDGEMENTS

I would like to thank my Supervisor Dr David Lokhat and co-Supervisor Mr Stephen Peacock for sharing their wealth of knowledge and providing insightful guidance in the development of this dissertation. I would also like to thank Mr Chandresh Narotam, Mr Patrick Moodley, Mr Sibonelo Goodman Mchunu, Mr Sphakamiso Zondi and the team at Tongaat Hulett's Maidstone mill and Technology Group for their unreserved support and assistance with the construction of the pipeline viscometer and experimental work. And lastly to my parents Mr Ajay and Dr Pretha Shah, you are both an inspiration and I love you; thank you for your continued encouragement and support.

ABSTRACT

Sugar is recovered by three stages of evaporative crystallisation, with each stage producing a two-phase mixture of sugar crystal and mother liquor commonly referred to as massecuite. The composition of each massecuite changes as increased amounts of sucrose crystallises out of solution, increasing the concentration of residual non-sugars and organic salts with each evaporative stage and resulting in C-massecuite possessing the lowest purity and highest viscosity. Tongaat Hulett maintains an interest in the viscosity of C-massecuite from a process and equipment design perspective as viscosity is a critical physical property in the selection of pumps and design of piping networks, evaporative and cooling crystallisers, crystalliser drives and reheaters in the C-station of a sugar factory. In the absence of a well-established correlation, viscosity data published by Andre Rouillard in 1984 is widely-used at Tongaat Hulett, however, this chart and other widely published data resulted from experimentation with a rotating viscometer that is believed to be unsuitable for this application. The rotating viscometer results in displacement of sugar crystals, interfering with the accuracy of the measurements. Whilst the rotational viscometer was accepted by the International Commission for Uniform Methods of Sugar Analysis as the standard technique for measurement of molasses viscosity, no standard technique is available for massecuite viscosity measurement. An investigation into alternative methods of viscosity measurement rendered the pipeline viscometer as best suited to this product as the method of measurement is not affected by the heterogeneous nature of the massecuite. The aim of this study is thus to design, construct and validate a pipeline viscometer which is to be used, together with non-Newtonian theory, to investigate the viscosity of C-massecuite. The pipeline viscometer was successfully constructed, validated and used, together with the power law model, to describe the viscosity of C-massecuite in terms of two rheological parameters; the flow behaviour index and consistency. The results of this study indicate that the average flow behaviour index of C-massecuite is 0.85. An empirical correlation for C-massecuite consistency as a function of temperature, dissolved solids concentration and crystal content was proposed with a regression coefficient of 0.7672 as well as additional equations to guide the estimation of C-massecuite viscosity. The massecuite consistency, assumed to be equivalent to apparent viscosity at a shear rate of $1s^{-1}$, was compared with the C-massecuite viscosity data currently used. A more rapid increase in massecuite viscosity with a reduction in temperature was found, however, the experimental data was found to fall within the recommended range for C-massecuite viscosity currently used. It is with confidence that the power law model can thus be used with a flow behaviour index of 0.85 and a consistency as predicted by the empirical correlation and guiding equations to yield an apparent viscosity for C-massecuite.

TABLE OF CONTENTS

LIST OF FIGURES

LIST OF TABLES

NOMENCLATURE

Greek Symbols

Δh = Hydrostatic head, m

ΔP_e = Pressure drop due to entrance effects, kPa

ΔP_c = Corrected pressure drop due to entrance effects, kPa

ΔP = Pressure drop, kPa

ϕ = Volume fraction of crystal

ϕ_m = Maximum volume fraction of crystals

γ = Shear rate, s^{-1}

μ = Dynamic viscosity, Pa.s

ρ = Density, kg/m^3

σ_j = Deviation associated with variable j

τ = Shear stress, Pa

τ_w = Shear stress at the pipe wall, Pa

Variables

B = Massecuite brix, %

CC = Crystal content, %

CV = Coefficient of variation

D = Pipe diameter, m

DS = Dry substance, %

g = Acceleration due to gravity, 9.81m/s^2

K = Consistency, Pa.s^n

l = Mean crystal size by mass (as determined by sieve analysis), mm

l_{sgs} = Specific grain size or mean crystal size by area, mm

L = Pipe length, m

L_{eff} = Effective length, m

l_{sgs} = Specific grain size or mean crystal size by area, mm

n = Flow behaviour index

N = Speed, rps

NS = Non-sucrose, %

P = Pressure, kPa

P = Purity, %

Q = Volumetric flow, m^3/s

Q_{ns} = Non-slip volumetric flow, m^3/s

Q_s = Volumetric flow due to wall slip, m^3/s

R = Pipe radius, m

R_s = Radius of spindle, m

Re = Reynold's number

RS/Ash = Reducing sugar to ash ratio

S/NS = Sucrose to Non-sucrose ratio

SS_E = Error sum of squares

SS_R = Residual sum of squares

SS_T = Total sum of squares

T = Temperature, °C (unless otherwise stated)

t = Torque, N.m

TS = Total solids, %

u = Fluid velocity, m/s

u_c = Corrected fluid velocity, m/s

u_{ns} = Non-slip fluid velocity, m/s

u_s = Wall slip fluid velocity, m/s

x_j = Measured statistical value for variable j

X = Volume fraction of liquid phase

z = Height, m

CHAPTER 1: INTRODUCTION

Sucrose is produced in the sugar cane stalk during photosynthesis and is extracted, purified and crystallised in a sugar mill. Sugar is recovered by three stages of evaporative crystallisation producing a two-phase mixture of sugar crystal and mother liquor referred to as massecuite.

The composition of massecuite is highly dependent on cane quality and changes as increased amounts of sucrose crystallises out of solution. Massecuite consists of sugars, non-sugars and inorganic salts (Walford, 1996). The sugars contained in massecuite include sucrose (sugar), fructose and glucose (reducing sugars), oligosaccharides and polysaccharides. Organic non-sugars include organic acids, amino acids, starch, gums, waxes and dextran.

Concentrated syrup is used as the feed to the first stage of evaporative crystallisation producing a high-grade A-massecuite. A-sugar is separated from A-molasses, which is then used as feed to the second stage of evaporative crystallisation to produce B-massecuite. B-sugar is separated from B-molasses which is then used as feed to the third stage of evaporative crystallisation to produce C-massecuite. The concentration of residual non-sugars and organic salts increases with each boiling, resulting in C-massecuite possessing the lowest purity and highest viscosity. B- and C- sugars are re-melted and returned to syrup for re-processing whilst A-sugar is sold to the local market as raw sugar or used as feed to a sugar refinery.

Tongaat Hulett maintains an interest in the viscosity of C-massecuite from a process and equipment design perspective as viscosity is a critical physical property that is used in the selection of pumps and design of piping networks, evaporative and cooling crystallisers, crystalliser drives and reheaters in the C-station of a sugar factory. In the absence of a well-established correlation, viscosity data published by Rouillard (1984) as a function of temperature is widely used to estimate C-massecuite viscosity (Figure 2-9), however, the recommended range for C-massecuite viscosity is broad and the effect of shear rate was not considered, allowing room for optimisation in prediction of this parameter. Accurate prediction of C-massecuite viscosity provides the greatest benefit as this type of massecuite possesses the highest viscosity and is the most difficult to process and thus allows for the greatest capital saving in the back end of a sugar mill.

Extensive research was carried out on the viscosity of massecuite from the 1950s onwards using a rotating viscometer. Whilst the International Commission for Uniform Methods of Sugar Analysis (ICUMSA) accepted the rotational viscometer as the standard technique for measurement of molasses viscosity (Ananta et al., 1989), this instrument was believed to be unsuitable for massecuite due to the heterogeneous nature of the product (Ananta et al., 1989). No standard technique was available then (Ananta et al., 1989; Maudarbocus, 1980) or is available now for massecuite viscosity measurement. However, pipeline

viscometry has been favoured for massecuite measurements (Behne, 1964) as no mechanical rotation is involved, limiting the impact of crystal interference or crystal migration on viscosity measurements. Pipeline viscometry uses compressed air as a driving force, which acts evenly upon the massecuite surface, propagating massecuite through the pipeline and is thus a suitable measuring technique for heterogeneous fluids.

A research project was thus undertaken to investigate the viscosity of C-massecuite using a pipeline viscometer with the aim to achieve the following:

a) Design, construct and validate a pipeline viscometer
b) Use the pipeline viscometer, together with non-Newtonian theory, to determine the flow behaviour index and consistency for C-massecuite as a function of temperature, dissolved solids concentration and crystal content
c) Establish a correlation and guidelines that can be used to assist in the estimation of C-massecuite viscosity

A review of literature pertaining to fluid behaviour and non-Newtonian fluid rheology will be presented in order to outline the theoretical considerations involved in the design of the experimental apparatus and method. A review of literature pertaining to the physical properties of massecuite will be presented including a review of factors affecting massecuite viscosity and observations of non-Newtonian behaviour of massecuite. Published literature and proposed correlations for massecuite viscosity will then be presented based on various methods of viscometry previously employed in order to provide the basis for this study. The design and validation of the pipeline viscometer together with the experimental method is to be presented followed by the results obtained during experimentation with C-massecuite. Following an analysis of the results, a correlation and guidelines to assist in the estimation of C-massecuite viscosity is to be proposed.

CHAPTER 2: LITERATURE REVIEW

Rheology is the study of fluid flow and involves the expression of fluid behaviour in terms of fundamental governing equations and physical properties. A rheology bulletin outlines the historical developments in the field of rheology (Doraiswamy, 2002) beginning with the study of ideal, inviscid fluid flow pioneered by Blaise Pascal. Pascal first observed that pressure exerted on an incompressible fluid in a confined space acted equally in all directions (Pascal, 1663).

When a pressure driving force is applied to a fluid, the applied shear stress acts upon the surface area of the fluid element and results in a shear rate i.e. a velocity gradient between adjacent layers within the fluid. The concept of viscosity describes the internal friction that results from one fluid layer moving across another and can be broadly defined as the relationship between shear stress and shear rate. Viscosity is inversely related to fluidity and is measured in units of Pa.s or Poise ($g.cm^{-1}.s^{-1}$), where 10P equals 1Pa.s.

The concept of viscosity was first introduced by Isaac Newton who stated that the internal shear stress of a fluid is linearly related to the resulting shear rate by a constant of proportionality defined as viscosity (Holland & Bragg, 1995). All fluids obeying Newton's law of viscosity are classified as Newtonian fluids.

Gotthilf Hagen conducted the first explicit study of viscosity of Newtonian fluids and proposed that the pressure drop across a pipe was the sum of a viscosity term and a kinetic energy correction term (Hagen, 1839). Jean Leonard Poiseuille expanded on the work of Hagen and showed that the flow rate of Newtonian fluids in a pipe was proportional to pressure drop and R^4 (Poiseuille, 1841).

It was only much later that experiments were carried out by Schwedoff (1890) with non-Newtonian fluids using the Couette device and viscosity proposed to be a function of shear rate. Shear stress and shear rate data were first obtained by Eisenschitz et al. (1929) and Mooney (1931), with the latter going on to address concerns relating to wall slip relevant to this study.

In this chapter, theoretical considerations involved in the design of the experiment and subsequent calculations are outlined based on the flow of incompressible, non-Newtonian fluids with reference to equations developed by Pascal, Bernoulli and Rabinowitsch-Mooney. The physical properties of massecuite are summarised and factors affecting massecuite viscosity are discussed, together with observations of non-Newtonian behaviour of massecuite. A review of published literature and proposed correlations for massecuite viscosity are outlined providing a foundation for the purpose of this study.

2.1 Continuum hypothesis

Gases and liquids are collectively classified as fluids and are composed of a number of molecules. These molecules travel an average distance, called the mean free path, before colliding with each other, resulting in a change of path or transfer of energy. The continuum hypothesis can be employed where the length scale of the apparatus is significantly greater than that of the mean free path (Holland & Bragg, 1995). The mean free path is inversely proportional to the density of the medium and is thus significant for low pressure gases.

Research into the molecular theory of the viscosity of low density gases was pioneered separately by Sydney Chapman and David Enskog. The Chapman-Enskog kinetic theory allows for the determination of the mean free path and viscosity of gases at low density (Bird et al., 2002), however, this work is not directly applicable to the suspension of solid particles in a liquid medium.

All fluids, except for low pressure gases and high velocity gases, can be assumed to act as a continuous medium where the microstructure of the fluid is ignored and the fluid properties represent that of the average prevailing conditions. (Holland & Bragg, 1995). The continuum hypothesis applies to homogenous and heterogeneous fluids and was applied to massecuite during experimentation with the pipeline viscometer. C-massecuite consists of a suspension of particles 0.12mm in diameter with a mean free path between collisions estimated to be in the region of a fraction of a millimetre. Laminar flow within the pipeline viscometer implies fluid flow in neat layers with little axial mixing. As a result of the length scale of the apparatus (1.4m) being largely greater than that of the mean free path of the suspending particles (a fraction of a millimetre), the continuum hypothesis can be employed assuming a uniform distribution of particles up to the pipe wall. The effect of the interaction of crystals at the pipe wall was thereafter accounted for by the associated wall slip (Holland & Bragg, 1995) and will be discussed in further detail in chapter 2.4.4.

2.2 Compressibility of fluids

The response of a fluid to an applied pressure allows the fluid to be classified as compressible or incompressible. Gases possess a large specific volume and are capable of being compressed. Liquids, however, are effectively incompressible therefore implying a constant density under applied pressure. Massecuite was assumed to act as an incompressible fluid under the prevailing experimental conditions.

2.3 Classification of fluid behaviour

2.3.1 Real vs. Ideal fluid

Fluids can be classified as real or ideal. When an external source of pressure is applied to an ideal, inviscid, incompressible fluid flowing within a smooth pipe, the fluid moves across the pipe surface at a specific

flow rate. Due to the absence of the fluid viscosity, the ideal fluid may continue moving at this rate indefinitely as there is no frictional loss within the system to reduce the pressure driving force.

With a real fluid, however, the interaction of the moving fluid element, represented by δr, with the stationary pipe surface results in a shearing stress τ which acts upon the circumferential area of the pipe, as shown in Figure 2-1, therefore reducing the pressure of the fluid.

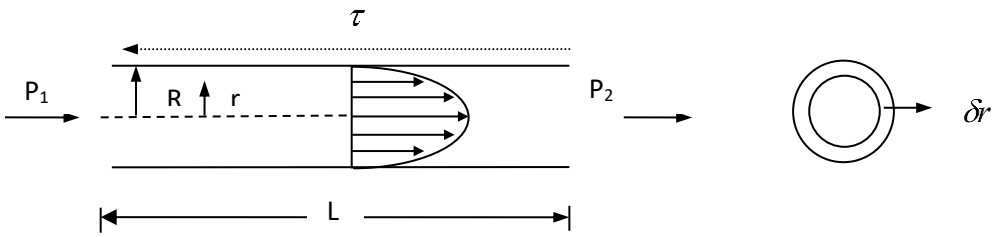

Figure 2-1: Fluid flow in a pipe, adapted from Chhabra & Richardson (2008)

The velocity profile within a pipe is initially flat, thereafter assuming a parabolic profile for Newtonian fluids under laminar flow conditions, as seen in Figure 2-2 (see Appendix 7.1 for a more detailed proof).

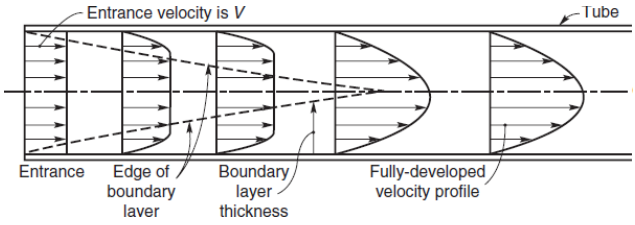

Figure 2-2: Velocity profile in a pipe (Chhabra & Richardson, 2008)

The pressure drop associated with the developing velocity profile was calculated as a correction for end effects ΔP_e. A pipe length L_e was required before the fluid flow was assumed to become fully developed. Once the velocity profile is developed, the subsequent pressure drop for a homogeneous fluid was assumed to be a result of the inherent resistance of the fluid itself.

The viscosity of a real fluid μ can be defined as the resistance to flow and is expressed as the ratio of the resulting shear stress τ to shear rate γ shown in equation 2-1.

$$\mu = \frac{\tau}{\gamma} \qquad 2\text{-}1$$

The shear rate γ can be defined as the velocity gradient that develops perpendicular to the applied shear. The change in fluid viscosity with shear rate allows the fluid behaviour to be classified as either Newtonian or non-Newtonian.

2.3.2 Newtonian behaviour

Newtonian fluids are characterised by a constant viscosity independent of shear rate and shear time and as obeying the full set of Navier-Stokes equations. The behaviour of such fluids is well understood and can be predicted with great accuracy. Additional information on Newtonian fluid behaviour can be found in Holland & Bragg (1995) and further explanation of the Navier-Stokes equations can be found in Chhabra & Richardson (2008).

2.3.3 Non-Newtonian behaviour

The complex behaviour of non-Newtonian fluids results in viscosity measurements becoming more complex. Non-Newtonian fluids exhibit a dependence of viscosity on the applied rate of shear and, in some cases, a dependence on time.

Time-independent fluids experiencing a decrease in viscosity with an increase in shear rate are classified as pseudoplastic. The shear stress-shear rate relationship for time independent fluids is shown in Figure 2-3, where the apparent viscosity is defined as the slope of the plot of shear stress vs. shear rate. The constant viscosity associated with Newtonian fluids is thus expressed as a straight-line plot with a constant slope starting at the origin. Non-Newtonian fluid viscosity, however, is expressed as a plot with a non-uniform slope. A shear stress-shear rate plot starting above the origin is indicative of an internal resistance required to be overcome before fluid flow can be achieved.

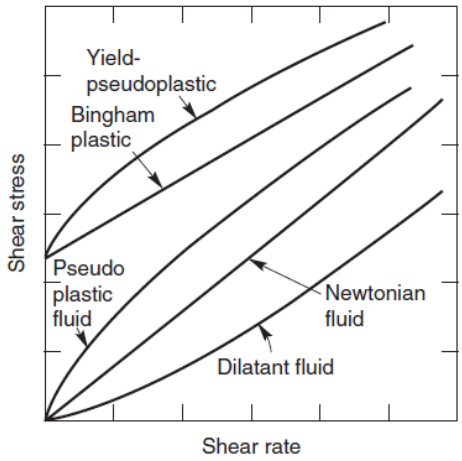

Figure 2-3: Shear stress-shear rate behaviour for time independent fluids (Chhabra & Richardson, 2008)

Pseudoplastic fluid behaviour is of interest to this study and is most commonly expressed by the power law or Ostwald de Waele model (Rouillard, 1985; Chhabra & Richardson, 2008). The plot of shear stress vs. shear rate is referred to as the flow curve and the relationship between shear stress and shear rate can be described by equation 2-2 for a power law fluid, where K represents the fluid consistency and n represents the flow behaviour index.

$$\tau = K.\gamma^{n} \qquad 2\text{-}2$$

Pseudoplastic fluids are characterised by a flow behaviour index less than 1 whilst fluids experiencing an increase in viscosity are classified as dilatant with a flow behaviour index greater than 1. Newtonian fluids can be expressed with a flow behaviour index of 1, allowing equation 2-2 to revert to equation 2-1, where consistency *K* equals viscosity μ .

Where significant deviations from the power law model exist at very high and low shear rates, the Carreau model or Cross model can be used to approximate the fluid viscosity. Where deviations from the Power law model occur only at low shear rates, the Ellis fluid model can be used to express the fluid viscosity. Additional information on fluid viscosity models for time independent fluids can be found in Chhabra & Richardson (2008).

Under conditions of constant shear over a period of time, time-dependent fluids experiencing a reduction in viscosity are classified as exhibiting thixotropic behaviour whilst an increase in viscosity characterises rheopectic behaviour. The shear stress-shear rate relationship for time dependent fluids is shown in Figure 2-4 and additional information can be found in Chhabra & Richardson (2008).

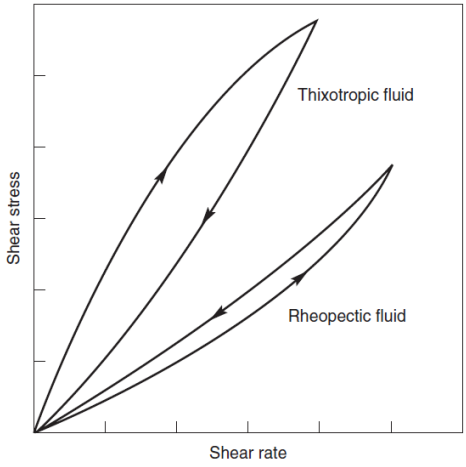

Figure 2-4: Shear stress-shear rate behaviour for time dependent fluids (Chhabra & Richardson, 2008)

2.4 Non-Newtonian fluid rheology

The calculations for shear stress and shear rate as well as the method for correcting for wall slip and entrance effects are outlined using theory of fluid dynamics and non-Newtonian rheology as outlined by Jastrzebski (1967), Rouillard (1981), Ness (1983), Mathlouthi & Kasprzyk (1984), Holland & Bragg (1995), Chhabra & Richardson (2008) and Barker (2008).

2.4.1 Calculation of shear stress

Pascal's law states that a pressure applied to an incompressible fluid acts equally in all directions. Hydrostatic pressure can be expressed mathematically according to equation 2-3.

$$\Delta P = \rho g z \qquad 2\text{-}3$$

Building on the work of Pascal (1663), Bernoulli (1738) went on to propose a principle of conservation of energy for inviscid fluids most simply expressed according to equation 2-4.

$$\frac{1}{2}u^2 + gz + \frac{P}{\rho} = \text{constant} \qquad 2\text{-}4$$

For a fluid flowing within a horizontal pipe as seen in Figure 2-1, the resulting shearing stress τ reduces the pressure of the fluid along the length of the pipe and corresponds to a shear stress at radius *r*. In order to maintain flow, a force is to be applied with an order of magnitude large enough to overcome the internal resistance inherent in the fluid, characterised by the fluid viscosity and prevailing flow conditions.

For incompressible fluid flow within a horizontal pipe, Bernoulli's equation can be re-written according to equation 2-5.

$$\frac{1}{2}u_1^{\,2} + gz_1 + \frac{P_1}{\rho} = \frac{1}{2}u_2^{\,2} + gz_2 + \frac{P_2}{\rho} - \tau \qquad 2\text{-}5$$

The velocity of the fluid element within the pipe is assumed to be constant allowing the kinetic energy terms to be cancelled out. The orientation of the pipe is assumed to be horizontal with elevation $z_1 = z_2$, allowing the potential energy term to be cancelled out. Assuming the fluid density remains constant within the pipe, Bernoulli's equation for the conservation of energy within the horizontal pipe can therefore be reduced to equation 2-6.

$$P_1 = P_2 - \tau \qquad 2\text{-}6$$

Applying a force balance allows for the development of equation 2-7.

$$P\pi r^2 = (P + \Delta P)\pi r^2 - \tau.2\pi rL \qquad 2\text{-}7$$

The shear stress at the wall surface τ_w occurs at a radius $r = R$. Substituting $\tau = \tau_w$ at $r = R$ allows equation 2-7 to be re-written, as shown in equation 2-8 (Chhabra & Richardson, 2008).

$$\tau_w = \frac{R}{2}\left(\frac{-\Delta P}{L}\right) \qquad 2\text{-}8$$

The equation above for shear stress at the pipe wall (equation 2-8) holds true for both Newtonian and non-Newtonian fluids (Chhabra & Richardson, 2008).

2.4.2 Calculation of corrected shear stress at the wall for end effects

In order for the pressure drop used in equation 2-8 to accurately represent the pressure loss due to the inherent resistance to flow, all other sources of pressure must be accounted for. The loss of pressure associated with a developing velocity profile must be correctly accounted for and is commonly referred to as the correction for entrance effects or end effects. The corrected pressure drop for each shear rate can be calculated according to equation 2-9.

$$\left(-\Delta P_c\right) = \left(-\Delta P\right) - \left(-\Delta P_e\right) \qquad 2\text{-}9$$

The shear stress at the pipe wall can then be calculated using the corrected pressure drop according to equation 2-10.

$$\tau_w = \frac{R}{2}\left(\frac{-\Delta P_c}{L}\right) \qquad 2\text{-}10$$

The correction for end effects can be evaluated by conducting experiments with at least three pipes of the same diameter, but with varying lengths. The generation of flow curves allows the shear stress to be calculated at several pre-determine shear rates for all three pipelines, as seen in chapter 4.2.1. The effect of the developing pressure profile can therefore be calculated as a pressure drop, as per a procedure proposed by Chhabra & Richardson (2008).

A plot of the length-to-diameter ratio (*L/D*) against the pressure drop for each shear rate can be developed. Extending the *L/D* ratio to zero allows the pressure drop at the entrance to be calculated for each constant

shear rate as the intercept on the y-axis. A correlation to predict pressure drop due to entrance effects as a function of shear rates can thus be established, as seen in equation 4-7.

2.4.3 Calculation of shear rate

The velocity gradient perpendicular to the direction of fluid flow is referred to as the shear rate. For an incompressible Newtonian fluid flowing through a pipe, the shear rate can be calculated according to equation 2-11 (Chhabra & Richardson, 2008).

$$\gamma = \frac{8u}{D} \qquad 2\text{-}11$$

For an incompressible, non-Newtonian fluid flowing through a pipe, assuming no wall slip, the shear rate at the pipe wall can be calculated according to the Rabinowitsch-Mooney equation (Equation 2-12) expressed as a function of shear stress at the pipe wall (τ_w) and shear rate $\left(\frac{8u}{D}\right)$ (Holland & Bragg, 1995).

$$-\gamma_w = \frac{8u}{D}\left[\frac{3}{4} + \frac{1}{4}\frac{d\ln\left(\frac{8u}{D}\right)}{d\ln\tau_w}\right] \qquad 2\text{-}12$$

For a power law fluid, the gradient of a ln-ln plot of shear stress at the pipe wall as a function of shear rate represents the flow behaviour index *n* (Chhabra & Richardson, 2008). The flow behaviour index can be expressed according to equation 2-13 (as seen in chapter 2.4.5, equation 2-30).

$$n = \frac{d\ln\tau_w}{d\ln\left(\frac{8u}{D}\right)} \qquad 2\text{-}13$$

Substitution of equation 2-13 into equation 2-12 yields a simplified equation for the non-Newtonian shear rate at the wall as a function of flow behaviour index, as seen in equation 2-14 (Chhabra & Richardson, 2008).

$$\gamma_w = \frac{8u}{D}\left[\frac{3n+1}{4n}\right] \qquad 2\text{-}14$$

The non-Newtonian shear rate is thus calculated for each data point only once the flow curve is developed using the corrected shear rate accounting for wall slip.

2.4.4 Calculation of corrected shear rate at the wall due to wall slip

Whilst the continuum hypothesis can be applied to heterogeneous fluids with uniform dispersions up to the pipe wall, the effect of the solid particles against the pipe wall cannot be ignored. An acceleration of particles at the pipe wall is a phenomenon commonly encountered with multi-phase products resulting in a higher system pressure drop. The acceleration results from a smaller fluid layer at the pipe wall with a lower viscosity resulting in "wall slip" (Chhabra & Richardson, 2008).

For homogeneous fluids, the wall slip velocity u_s is assumed to be zero, simplifying the calculation. However, for a heterogeneous fluid, the wall slip velocity must be accounted for. The total flow rate for a heterogeneous fluid can be calculated as the sum of the wall slip flow Q_s and bulk fluid flow or non-slip flow Q_{ns}, as seen in equation 2-15.

$$Q = Q_s + Q_{ns} \qquad 2\text{-}15$$

In order to evaluate the wall slip velocity, it is necessary to manipulate the above equation such that the dependence of the wall slip velocity on pipe radius can be evaluated.

The differential volumetric flow of a fluid element through a circumferential section of pipe can be written according to equation 2-16 where the velocity component is a function of the radius.

$$Q = \int_0^R 2\pi r u.dr \qquad 2\text{-}16$$

Integration by parts therefore yields equation 2-17.

$$Q = 2\pi\left[\left(\frac{r^2}{2}u\right)\Big|_0^R + \left(\int_0^R \frac{r^2}{2}\frac{-du}{dr}dr\right)\right] \qquad 2\text{-}17$$

As referenced by Chhabra & Richardson (2008), Mooney (1931) recommended applying a boundary condition for wall slip where $u = u_s$ at $r = R$, resulting in the development of equation 2-18.

$$Q = \pi R^2 u_s + \pi\int_0^R r^2\frac{-du}{dr}.dr \qquad 2\text{-}18$$

Applying the non-slip boundary condition at the wall where $u = 0$ at $r = R$ allows for the development of equation 2-19 and 2-20.

$$Q_{ns} = 2\pi\left[0 + \left(\int_0^R \frac{r^2}{2}\frac{-du}{dr}dr\right)\right] \qquad 2\text{-}19$$

$$Q_{ns} = \pi\int_0^R r^2\left(\frac{-du}{dr}\right)dr \qquad 2\text{-}20$$

Substituting the equation for non-slip flow (Equation 2-20) into the equation for total flow (Equation 2-18) results in the development of equation 2-21.

$$Q = \pi R^2 u_s + Q_{ns} \qquad 2\text{-}21$$

Dividing through by $\pi R^3 \tau_w$ results in the development of equation 2-22.

$$\frac{Q}{\pi R^3 \tau_w} = \frac{u_s}{R\tau_w} + \frac{Q_{ns}}{\pi R^3 \tau_w} \qquad 2\text{-}22$$

The procedure outlined by Chhabra & Richardson (2008) recommended manipulating the equation above such that it can be expressed in terms of shear rate. The total cross sectional flow *Q* can be expressed according to 2-23.

$$Q = \frac{u.\pi D^2}{4} \qquad 2\text{-}23$$

Substituting equation 2-23 into 2-22 allows for the development of equations 2-24 and 2-25.

$$\frac{2u}{D\tau_w} = \frac{2u_s}{D\tau_w} + \frac{2u_{ns}}{D\tau_w} \qquad 2\text{-}24$$

$$\left(\frac{8u}{D}\right)\times\frac{1}{\tau_W} = \frac{8u_s}{D\tau_w} + \frac{8u_{ns}}{D\tau_w} \qquad 2\text{-}25$$

Re-arranging equation 2-25 above allows the non-slip velocity to be expressed as a function of non-slip volumetric flow, shown in equation 2-26

$$u_{ns} = \frac{4Q_{ns}}{\pi D^2} \qquad 2\text{-}26$$

Substituting equation 2-26 into 2-25 allows the shear rate to be expressed as a function of non-slip volumetric flow.

$$\left(\frac{8u}{D}\right)\times\frac{1}{\tau_W}=\frac{8u_s}{D\tau_w}+\frac{32Q_{ns}}{\pi D^3\tau_w} \qquad 2\text{-}27$$

The correction for wall slip, carried out as per the procedure outlined in Chhabra & Richardson (2008), begins with experimentation with three pipelines with a constant length and varying diameters and generation of the flow curves, as seen in chapter 4.2.2. The linear ln-ln plot of shear stress vs. shear rate allows the shear rate to be calculated at seven pre-determined shear stresses, for all three pipelines.

For a constant shear stress, the gradient of a plot of shear rate $\frac{8u}{D}$ vs. $\frac{1}{D}$ is represented by $8u_s$, dividing the gradient by 8 allows the wall slip velocity to be calculated for constant values of shear stress, as seen in chapter 4.2.2. A plot of wall slip velocity vs. shear stress can therefore be used to estimate the wall slip velocity for varying shear stresses as seen in equation 4-14. Once the wall slip velocity u_s is calculated, the corrected velocity can be substituted into equation 2-14 to calculate the corrected shear rate for a non-Newtonian fluid, as seen in equation 2-28.

$$\gamma_{\text{corrected}}=\frac{8u_c}{D}\left[\frac{3n+1}{4n}\right]=\frac{8(u-u_s)}{D}\left[\frac{3n+1}{4n}\right] \qquad 2\text{-}28$$

2.4.5 Application of the power law model and calculation of flow behaviour index and consistency

A flow curve can be developed for each data set based on the corrected shear stress (equation 2-10) as a function of corrected shear rate (equation 2-28). It must be noted that the calculation of corrected shear stress and corrected shear rate is an iterative one as each correction is dependent on the other.

The power law model, discussed in chapter 2.3.3 and 2.8.1 and expressed according to equation 2-2, allows for graphical determination of the flow behaviour index and consistency from a ln-ln plot of shear stress and shear rate. Substituting equation 2-28 into 2-2 yields the following expression for non-Newtonian fluids.

$$\tau=K.\left(\frac{8u_c}{D}\right)^n\left[\frac{3n+1}{4n}\right]^n \qquad 2\text{-}29$$

Applying the natural logarithm to both sides of equation 2-29 allows the corrected shear stress to be plotted as a function of corrected shear rate to yield a straight-line plot.

$$\ln(\tau_w) = n\ln\left(\frac{8u_c}{D}\right) + \ln\left(K\left[\frac{3n+1}{4n}\right]^n\right) \qquad 2\text{-}30$$

The flow behaviour index and the consistency can be calculated from equation 2-30 using equations 2-31 and 2-32 respectively.

$$n = \text{slope} \qquad 2\text{-}31$$

$$K = \frac{e^{\text{intercept}}}{\left[\frac{3n+1}{4n}\right]^n} \qquad 2\text{-}32$$

Having established the flow behaviour index and consistency, an apparent viscosity for non-Newtonian fluids can be expressed according to equation 2-33.

$$\mu_{\text{apparent}} = \frac{\tau}{\gamma} = K\gamma^{n-1} \qquad 2\text{-}33$$

From equation 2-33, it can be seen that for Newtonian fluids with a flow behaviour index of 1, consistency is equivalent to viscosity.

2.4.6 Fluid flow regime and Reynold's number

Fluid flow can be characterised as either laminar, transitional or turbulent. The theoretical equations used to calculate the consistency and flow behaviour index described above assume that fluid flow is in the laminar region (Chhabra & Richardson, 2008). Laminar flow results in a fluid flowing in neat layers and can be characterised by the Reynolds number. For a Newtonian fluid, the Reynold's number can be calculated according to equation 2-34 where laminar flow is associated with a Reynold's number less than 2100.

$$\text{Re} = \frac{\rho D u}{\mu} \qquad 2\text{-}34$$

For a non-Newtonian fluid, however, the Reynold's number becomes a function of the apparent viscosity and can be calculated from a generalised correlation as shown by equation 2-35.

$$\mathrm{Re}' = \frac{\rho D u}{\mu_{\text{apparent}}} \qquad 2\text{-}35$$

Substituting equation 2-33 into 2-35 yields the correlation for the generalised Reynold's number. The generalised Reynold's number was calculated according to equation 2-36 to ensure the fluid flow remained in the laminar regime during experimentation.

$$\mathrm{Re}' = \frac{\rho u^{2-n} D^{n}}{8^{n-1} K} \qquad 2\text{-}36$$

For non-Newtonian fluids, the transition from laminar to turbulent flow occurs at a Reynold's number that is dependent on the flow behaviour index, as shown in Figure 2-5. Whilst it is difficult to produce turbulent massecuite flow with the pressures used during experimentation, the Reynold's number was calculated to determine whether the flow regime remained laminar.

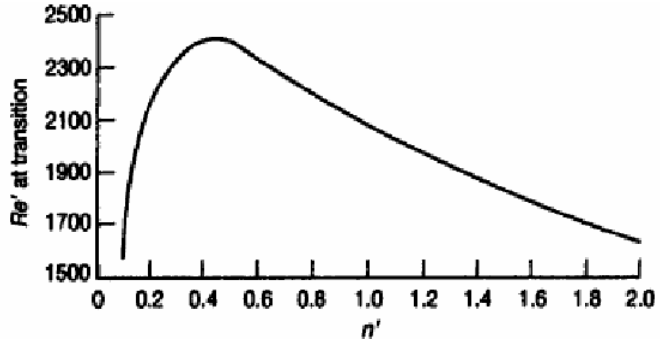

Figure 2-5: Critical Reynold's number as a function of flow behaviour index (Gan, 2012)

Having established the non-Newtonian theory relevant to this study, the physical properties of massecuite are to be outlined in order to better understand the factors affecting the non-Newtonian behaviour of massecuite.

2.5 Physical properties of C-massecuite

C-massecuite is characterised as a low grade massecuite with a dissolved solids concentration of 95-97%, an apparent sucrose purity of approximately 55% and crystal content of approximately 28%. The crystal size of C-sugar crystals within C-massecuite is typically 0.12mm compared to a raw sugar crystal size of 0.65mm.

2.5.1 Brix

Brix is a measure of the dissolved solids concentration of a sugar solution measured using a refractometer, as shown in Figure 2-6. The refractometer brix measurement is based on the refraction of light when passing through a sugar solution. The analysis for massecuite brix requires dilution of the massecuite sample and dissolution of crystals and is carried out according to the laboratory test method outlined in the South African sugar industry laboratory manual (Anon., 2005).

Figure 2-6: Refractometer used to measure massecuite brix

2.5.2 Pol

The apparent sucrose content or polarization is commonly referred to as pol and is measured using a polarimeter as shown in Figure 2-7. The pol measurement is based on the optical rotation of polarised light passing through a sugar solution (Rein, 2007). The analysis for massecuite pol requires dilution of the massecuite sample and dissolution of crystals and is carried out according to the laboratory test method outlined in the South African sugar industry laboratory manual (Anon., 2005).

Figure 2-7: Polarimeter used to measure massecuite pol

2.5.3 Purity

The apparent sucrose purity, commonly referred to as purity, represents the portion of dissolved solids (brix) that is measured as pol and is calculated according to equation 2-37.

$$Purity = \frac{Pol}{Refractometer\ Brix} \qquad 2\text{-}37$$

2.5.4 Nutsch molasses

Nutsch molasses is produced by filtering the mother liquor from a massecuite using an apparatus known as a nutsch bomb, as shown in Figure 2-8, so as to allow the properties of the nutsch molasses (mother liquor) to be determined.

Figure 2-8: Nutsch bomb used to produce nutsch molasses

A sample of massecuite is placed in a nutsch bomb, compressed air is applied to the sealed unit and molasses is purged through the perforated screen whilst crystals are retained on the screen. Analysis of nutsch molasses allows the properties of the mother liquor to be obtained without interference from sugar crystals that may dissolve during analysis.

2.5.5 Density

Massecuite density is calculated as a bulk density as shown in equation 2-38 based on the crystal content of massecuite CC measured in kg/kg, crystal density of 1553kg/m^3 and an ICUMSA approved molasses density correlation published by Kadlec et al. (1983) as referenced by Peacock (1995).

$$\frac{1}{\rho_{massecuite}} = \frac{CC}{\rho_{crystal}} + \frac{1-CC}{\rho_{molasses}} \qquad 2\text{-}38$$

The density of the sugar crystal itself is invariable and will not impact viscosity measurements from one sample to the next.

2.5.6 Crystal content

Crystal content is a measure of the mass fraction of crystals expressed as a percentage of the total mass of massecuite and is calculated according to equation 2-39 using massecuite purity, nutsch molasses (mother liquor) purity and massecuite brix.

$$Crystal\,content = \frac{100(Mscte\,purity - Nutsch\,Mol\,purity)}{Mscte\,purity(100 - Nutsch\,Mol\,purity)} \times Mscte\,brix \qquad 2\text{-}39$$

2.5.7 Crystal size and shape

C-massecuite crystals are typically 0.12mm in size and rectangular in shape, with a length-to-width ratio of 1.5 – 2 (Rein, 2007). The inclusion of impurities can inhibit growth on two opposite faces of the crystal resulting in elongated needle-shaped crystals. Partial dissolution of crystal corners may also result in the formation of D-shaped crystals.

2.5.8 Dry substance

Massecuite dry substance is a measure of dry solids by titration using the Karl-Fischer method or under vacuum oven drying (Love, 2002), however, due to the long test procedure and large number of samples to be tested, a correlation developed by Love (2002) to estimate dry substance using massecuite brix and pol was used, as shown by equation 2-40.

$$DS = Brix\left(1 - 0.00066\ \left[Brix - Pol\right]\right) \qquad 2\text{-}40$$

2.5.9 Reducing sugars to ash ratio

Reducing sugars refer to invert sugars produced by the degradation of sucrose i.e. fructose and glucose. The ash content in sugar cane juice remains constant throughput the process. The reducing sugars to ash ratio thus represents a useful measure of sucrose degradation on a fixed basis throughout the process.

2.5.10 Impurities

A large portion of impurities in sugarcane juice are removed during clarification, however, any impurities that remain in the sugar cane juice are concentrated in massecuite and molasses. These impurities include inorganic salts and organic non-sugars such as dextran, starch, gums, waxes, organic acids, amino acids or colourants (Walford, 1996) all of which are believed to contribute to an increase in massecuite viscosity. Colloids are reported to increase massecuite viscosity and refer to an agglomeration of organic non-sugars that are dispersed in the suspending fluid.

2.5.11 Viscosity

A correlation proposed by Genotelle (1978) as referenced by Peacock (1995) is used widely within the sugar industry to predict the viscosity of sucrose solutions as a function of temperature and brix, as shown in equation 2-41. However, this correlation is applicable only for pure, homogeneous sucrose solutions with concentrations up to 85% brix.

$$\log_{10}\mu_{solution} = 22.46N - 0.114 + (30 - T) \times \frac{\left(1.1 + 43.1N^{1.25}\right)}{91 + T} \qquad 2\text{-}41$$

Where $N = \frac{B}{1900 - 18B}$

No correlation for massecuite viscosity exists, neither is there an ICUMSA recommended standard technique for massecuite viscosity measurement. It was this finding that initiated the study of massecuite viscosity.

2.6 Factors affecting massecuite viscosity

The viscosity of crystal suspensions is often expressed as a function of the properties of the suspending mother liquor and/or of the crystals in suspension (Kelly, 1958). The viscosity of massecuite is no different and was historically expressed either as an absolute viscosity or as a function of molasses and sugar crystals, as seen in equation 2-42.

$$\mu_{relative} = \frac{\mu_{massecuite}}{\mu_{molasses}} \qquad 2\text{-}42$$

This method of expressing massecuite viscosity was convenient as previous studies included experimentation with massecuite samples prepared in a laboratory by mixing known quantities of molasses and sugar crystals. As a result, the crystal size distribution of dried sugar could be easily determined using a vibrating sieve before addition to molasses and the properties of molasses could be determined directly before mixing i.e. molasses temperature, dry substance and quantity of impurities.

2.6.1 Molasses viscosity

The viscosity of massecuite was found to be highly dependent on the viscosity of the molasses surrounding the crystal as shown by Silina (1953), Kelly (1958), Artyukhov & Garyazha (1970), Awang & White (1976), Metzler (1996), Broadfoot et al. (1998) and Bruhns (2004). In addition, molasses viscosity was found to be dependent on molasses temperature and dry substance, as shown by Rouillard & Koenig (1980) and Broadfoot (1984) as well as impurities present. The risk associated with expressing massecuite viscosity

as a function of molasses viscosity was highlighted by Kelly (1958) in that deviations of molasses viscosity from predicted behaviour could be transferred to massecuite viscosity predictions.

A widely used correlation for molasses viscosity was reported by Rouillard & Koenig (1980) as shown in equation 2-52, where the effect of impurities was taken into account by using the sucrose/non-sucrose ratio and reducing sugar to ash ratio. Molasses viscosity correlations by Broadfoot (1984) and Broadfoot et al. (1998) are also widely used and account for the effect of impurities using molasses purity.

2.6.2 Temperature

As massecuite temperature increases, the vibration of molecules increases and facilitates flow with less friction. A strong dependence of massecuite viscosity on temperature was reported either directly by Rouillard (1984), Durgueil (1987) and Rein (2007) or indirectly as a function of molasses viscosity by Rouillard & Koenig (1980) and Broadfoot (1984).

Rein (2007) noted a strong dependence of massecuite consistency on temperature referencing the viscosity chart developed by Rouillard (1984) as shown in Figure 2-9, noting a two-fold change in massecuite viscosity with a change in temperature of 10°C. Rein (2007) referenced the work of Keast & Sichter (1984) and Barker (1998) as supporting this observation. Broadfoot (1984) and Durgueil (1987) reported a similar change in massecuite viscosity but with a temperature difference of 7°C and 9°C, respectively. Following a review of the massecuite viscosity literature, Rein (2007) proposed the use of Figure 2-10 to determine the range of massecuite and molasses viscosities assuming a two-fold change in viscosity with a temperature difference of 9°C. Viscosity charts as shown in Figure 2-9 and 2-10 are commonly used to represent the viscosity-temperature relationship for liquids (Seeton, 2006). The viscosity-temperature relationship presented on a log-log plot is often found to be linear (Perry, 1950) until a critical viscosity is reached, breaking down thereafter to an exponential relationship.

The temperature dependence of massecuite consistency was referenced by Mathlouthi and Kasprzyk (1984) as following the form shown in equation 2-43.

$$K = Ae^{-mT} \; or \; \ln K = \ln A - mT \qquad 2\text{-}43$$

The dependence of fluid viscosity on temperature can be expressed generically according to equation 2-44 as referenced by Mesaadi et al. (2015). Constants *A, B, C, D, E, F, a, b, c, n* represent fitted parameters.

$$\ln(\mu) = A + \frac{B}{T+C} + a.\log T + b.T + cT^2 + \frac{D}{T^2} + \frac{E}{T^3} + \frac{F}{T^n} \qquad 2\text{-}44$$

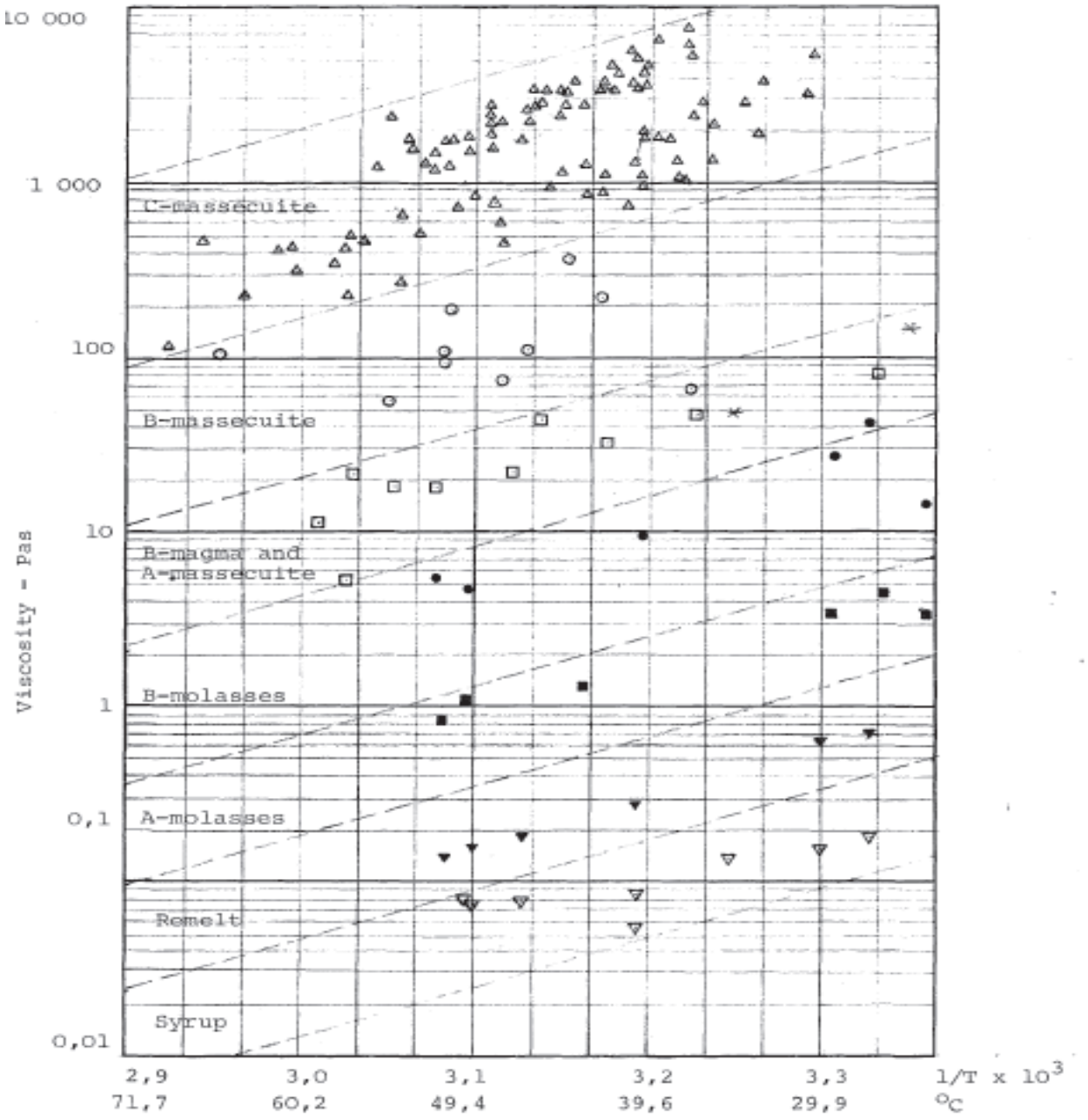

Figure 2-9: Massecuite viscosity as a function of temperature (Rouillard, 1984)

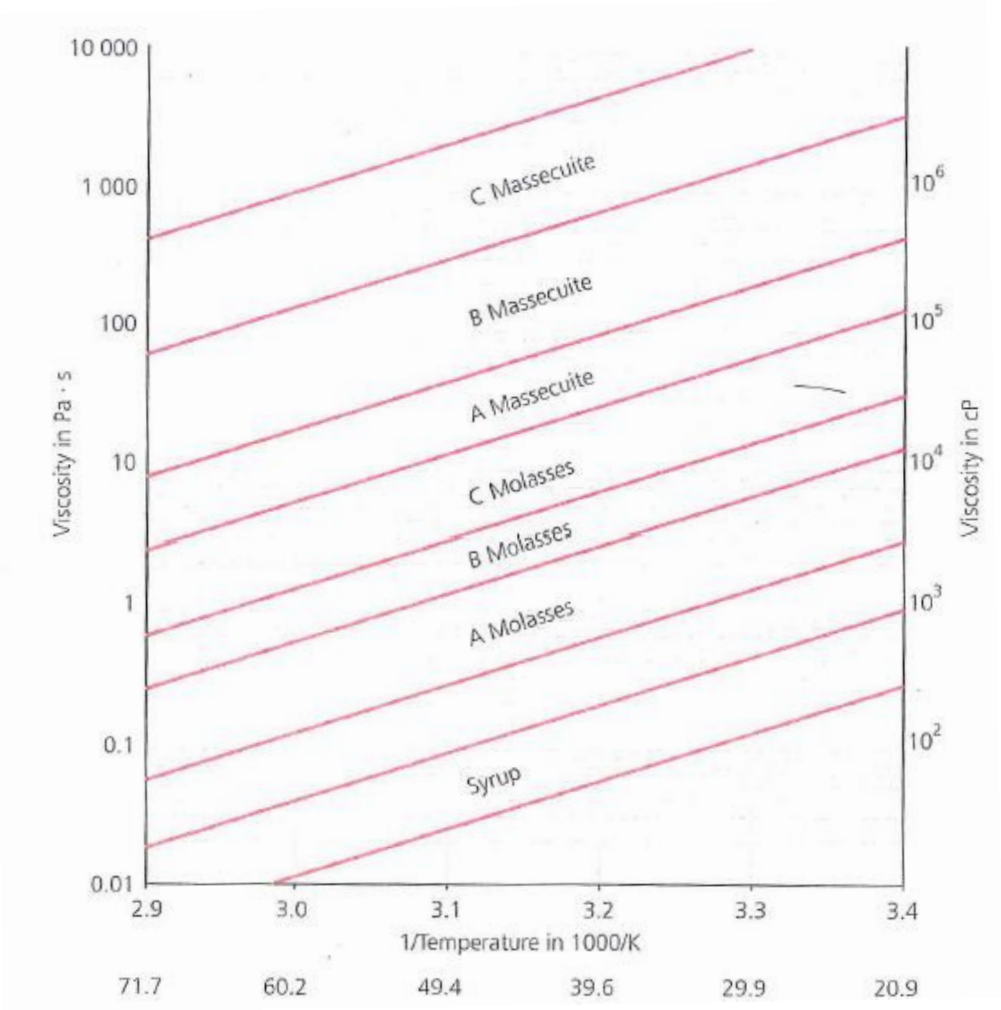

Figure 2-10: Massecuite viscosity as a function of temperature (Rein, 2007)

2.6.3 Dry substance

Molasses and massecuite viscosity correlations were reported to be strongly dependent on molasses dry substance and was reported either directly (Ness, 1980) or indirectly as a function of molasses viscosity as shown by Silina (1953), Kelly (1958), Artyukhov and Garyazha (1970), Awang and White (1976), Rouillard and Koenig (1980), Broadfoot (1984), Metzler (1996), Broadfoot et al. (1998) and Bruhns (2004).

The dry substance, or solids concentration, increases as the volume fraction of water decreases. The mobility of suspended crystals is reduced and there is a greater resistance to flow. Kelly (1958) described a generalised relationship for relative viscosity as a function of volume fraction of water as shown in equation 2-45, where X represents the volume fraction of liquid phase and *l* represents the particle size in millimetres.

$$\mu_{\text{relative}} = X^{a} \qquad \text{2-45}$$

Where $a = -6.49l^{0.276}$

The exponent *a* is reported to be dependent on particle shape as well as size, however, the relationship proposed by Kelly (1958) implies an exponential increase in viscosity with an increase in dry substance.

2.6.4 Crystal content

The viscosity of massecuite was found to be highly dependent on the crystal content as a mass fraction of crystals (Ness, 1980) or on the volume fraction of crystals, as shown by Silina (1953), Kelly (1958), Artyukhov and Garyazha (1970), Awang and White (1976), Rouillard and Koenig (1980), Broadfoot (1984); Metzler (1996), (Broadfoot et al. (1998) and Bruhns (2004).

The friction caused by particle-fluid and particle-particle interaction in heterogeneous fluids results in a higher resistance to flow. This phenomenon is more pronounced as the quantity of crystals (either mass fraction or volume fraction) increases, and is associated with an increase in viscosity. The relationship for relative consistency as a function of volume fraction of crystals proposed by Maron and Pierce (1956), as referenced by Mueller et al. (2011), was reported to be widely used and is shown in equation 2-46. The volume fraction of crystals is represented by ϕ and K_{relative} represents the suspension consistency as a function of the suspending fluid consistency.

$$K_{\text{relative}} = \left(1 - \frac{\phi}{\phi_m}\right)^{-2} \qquad \text{2-46}$$

Where ϕ_m = Maximum volume fraction of crystals (ordered packing = 0.74, random = 0.64)

The general form of this relationship was evident in correlations proposed by Metzler (1996) and later modified by Broadfoot et al. (1998) as well as that of Bruhns (2004).

The volume fraction of crystals can be calculated based on the crystal content, density of crystals and properties of nutsch molasses. Work carried out by Bruhns in 1996, as referenced by Bruhns (2004), reviewed the effect of volume fraction of crystals on the relative viscosity predicted by various correlations proposed before 1996, as seen in Figure 2-11. The correlation by Awang & White (1976) was reported to represent relative massecuite viscosity well, illustrates an exponential increase in relative viscosity with crystal content.

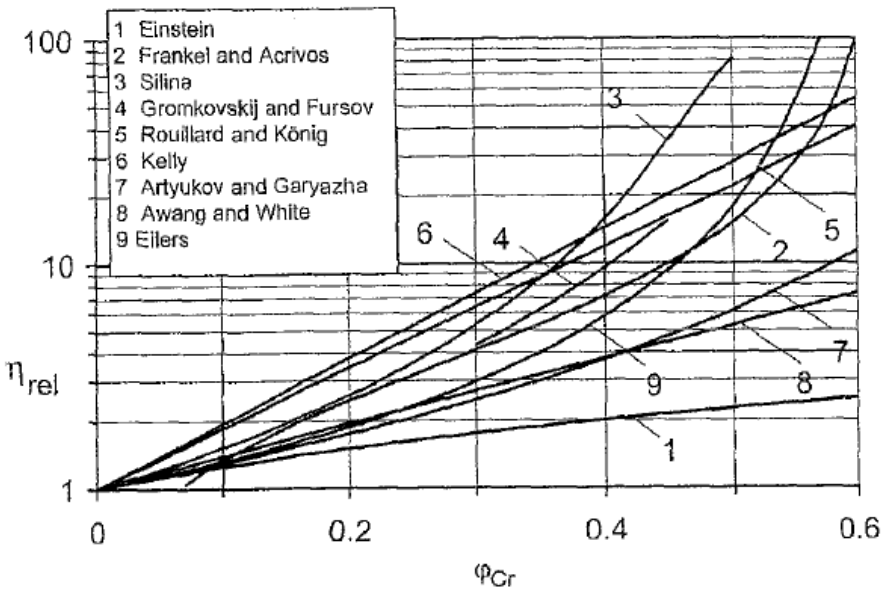

Figure 2-11: Impact of volume fraction of crystals on correlation outputs (Bruhns, 2004)

2.6.5 Crystal shape

The shape of suspended particles impacts the viscosity of the suspension as the particle orientation during flow and volume required for rotation changes as the particle shape changes (Mueller et al., 2011). It is thus understandable that the viscosity of massecuite was found to be dependent on crystal shape, as reported by Kelly (1958), Awang & White (1976), Metzler (1996) and Rouillard and Koenig (1980). Crystals can be classified as rectangular, D-shaped, elongated or irregular. Rectangular and D-shaped crystals can be seen in Figure 2-12.

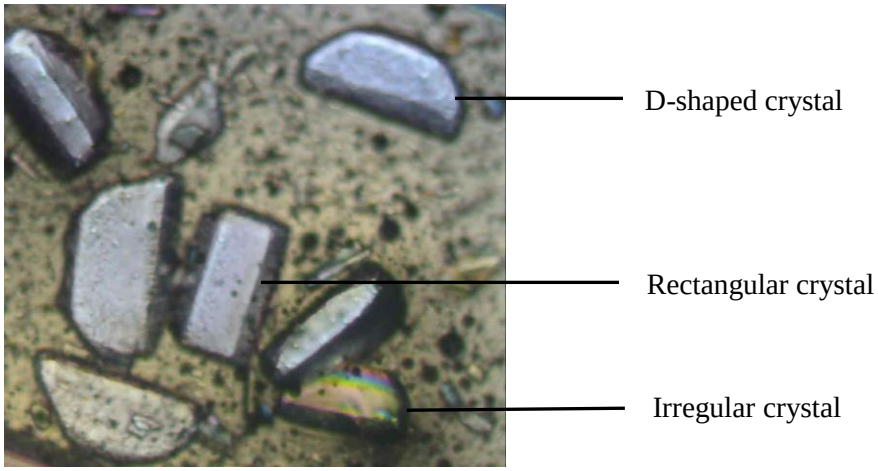

Figure 2-12: Crystal shape

A rectangular crystal shape is desired, however, the inclusion of impurities on the crystal surface can inhibit growth on a surface, resulting in elongated crystals. Partial dissolution or crystal breakage may result in irregular crystal shapes.

2.6.6 Crystal size distribution

Awang and White (1976) illustrated a dependence of massecuite viscosity on crystal size distribution reinforced by Rouillard and Koenig (1980) and later confirmed by Metzler (1996) and Broadfoot et al. (1998). A uniform crystal size distribution is desired, however, spontaneous nucleation results in mixed grain. Rouillard and Koenig (1980) reported that a mixture of crystal sizes causes a reduction in massecuite viscosity for the same crystal content.

2.6.7 Impurities

Rouillard and Koenig (1980) identified possible sources of error in massecuite viscosity prediction due to the presence of colloids, dextran or suspended matter present in molasses that is seen to increase the viscosity of massecuite. Rouillard (1983) reported that the presence of gums increases massecuite viscosity but noted that insoluble matter and colloids have no measurable effect on the viscosity of factory products. Dextran was believed to increase molasses and thus massecuite viscosity significantly (Rein, 2007). The dextran content on massecuite was measured but used for information purposes only.

2.6.8 Air

The aeration of molasses was believed to inflate molasses viscosity (Rein, 2007) and thus implies an increase in massecuite viscosity. Kelly & McAntee (1942) proposed a method for degassing of molasses samples by exposure to vacuum, prior to mixing with sugar crystals to produce massecuite samples. Seeing as massecuite samples were taken directly from the plant and the volumes were larger than could be accommodated for vacuum de-gassing, an alternative method was employed. Massecuite samples were at a temperature of approximately 60°C and cooled overnight to 45°C in a sealed massecuite tank, with the vent valve closed. The cooling effect resulted in the creation of a vacuum and upon opening the vent valve the following day, allowed for de-aeration of each sample.

2.6.9 Shear rate

The non-Newtonian nature of massecuite implies an inherent non-linear dependence on shear rate. At higher shear rates, massecuite behaviour was reported to approach Newtonian behaviour (Ness, 1983) and was reflected in the higher flow behaviour indices calculated by Kot et al. (1968) and Awang & White (1976) as shown in Table 2-1. It is important that experimentation be carried out within the industrially-relevant range of shear rates. Broadfoot & Miller (1990) reported a range of $0.1 – 10s^{-1}$ as being a practical range of

shear rates encountered in operation, however, a range of 0.01-4s^{-1} was investigated in order to include massecuite flow under gravity and pumped flow.

2.6.10 Summary of factors affecting massecuite viscosity

A review of the factors affecting massecuite viscosity highlights the dependence of massecuite viscosity on the properties of the crystal (crystal content, shape and crystal size distribution) as well as the properties of the molasses layer surrounding the crystal (molasses dry substance, temperature and purity).

Experimental work was carried out on massecuite samples taken directly from the plant and not samples prepared in a laboratory by addition of molasses and sugar. The properties of massecuite (temperature, dry substance, crystal content and purity) were thus taken into account directly rather than in relation to molasses properties.

The crystal size distribution can only be calculated accurately for dried sugar using a vibrating sieve. It is possible to estimate the crystal size distribution from a photograph of massecuite using a microscope, however, the calculated distribution may not be representative of the entire sample and is not considered accurate. For the purpose of this study, crystal size distribution will not be taken into account.

For the purpose of this study, the crystal size, shape and dextran content will be measured for informational purposes but will not be included in a correlation.

2.7 Non-Newtonian behaviour of massecuite

The classification of massecuite as a non-Newtonian fluid is well established (Rein, 2007), however, the type of time independent flow behaviour observed has varied and is summarised below.

2.7.1 Time independent behaviour

Massecuite is accepted to exhibit time-independent pseudoplastic behaviour, characterised by a reduction in viscosity with an increasing rate of shear as shown in Figure 2-3 and confirmed by Behne (1964), Ness (1980), Ness (1983), Rouillard (1985), Broadfoot & Miller (1990), Echeverri et al. (2005) and Rein (2007).

As referenced by Awang & White (1976) and Ness (1983), literature from Done, Znamenskii and Popov & Troino reported massecuite to exhibit Bingham plastic behaviour. Bingham plastic fluids are characterised as having an initial yield stress that prevents the fluid from flowing unless overcome by an external force, thereafter exhibiting Newtonian behaviour as shown in Figure 2-3. However, Awang & White (1976) referenced work by Adkins (1951), Silina (1953) and Kot et al. (1968) who conducted more detailed experimental work confirming that massecuite will flow under all conditions of shear stress.

Adkins (1951) conducted tests with a Searle viscometer designed by the Bureau of Sugar Experiment Stations in Brisbane. The Searle viscometer consisted of a freely-rotating cylinder within a second insulated cylinder, as shown in Figure 2-13. Two mass pieces were attached by a cord and guide pulleys and resulted in rotation of the cylinder as the mass pieces fall under the effects of gravity. The use of two identical mass pieces allowed for the application of a constant torque on the sample. The rate of shear was thus dependent only on the mass on the mass pieces and the viscosity of the sample.

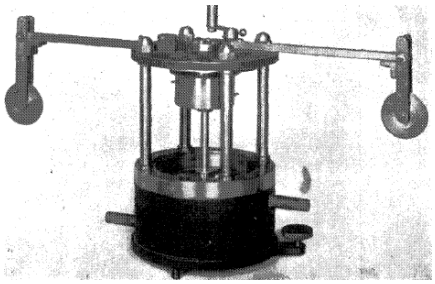

Figure 2-13: Searle viscometer used by Adkins (1951)

Massecuite samples with crystal contents between 20% and 40% were tested by Adkins (1951) and confirmed to exhibit pseudoplastic behaviour, as shown in Figure 2-14. Observed Bingham plastic behaviour was attributed to extrapolation of results from tests carried out at a higher shear stress where the shear stress-shear rate relationship was largely linear. However, upon closer examination at a lower shear stress, massecuite was found to remain fluid (Adkins, 1951), overcoming an inherent resistance before achieving a linear flow curve, characteristic of pseudoplastic behaviour.

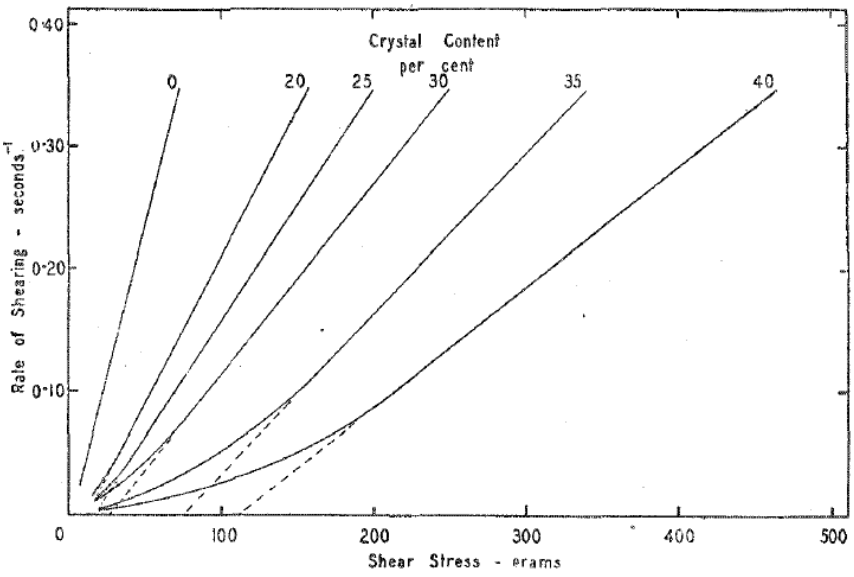

Figure 2-14: Flow curve developed by Adkins (1951) of shear rate (s^{-1}) vs. shear stress (grams)

2.7.2 Observations of time dependent behaviour

As referenced by Ness (1983), work carried out by Done illustrated thixotropic behaviour of massecuite characterised by time-dependent shear thinning. However, with experimentation using a Brookfield Synchro-Lectric rotating viscometer, Behne (1964) found that the observed time-dependent shear-thinning behaviour was attributed to the displacement of crystals during rotation of the spindle, resulting in the spindle rotating in a pool of molasses and recording a decrease in viscosity with time.

The instability of crystal suspensions can also contribute toward the observation of time-dependent behaviour, where sedimentation of crystals results in a reduction in the recorded shear stress. Massecuite containing crystals smaller than 0.1mm with a crystal content less than 30% was reported to create a stable suspension that enables the use of a rotational viscometer (Ananta et al., 1989). However, whilst C-massecuite allowed for a stable suspension of crystals, with typical crystal sizes of 0.12mm and a crystal content of 28%, the void created by the rotating spindle is still problematic.

Extensive research into the viscosity of massecuite was carried out from the 1950s onward using mainly rotating viscometers, however, efforts were abandoned in the 1990s due to the difficulty with obtaining accurate results and a belief that massecuite viscosity added little value to the sugar milling operations. However, Tongaat Hulett maintains an interest in the viscosity of C-massecuite from a process and equipment design perspective as viscosity is a critical physical property in the selection of pumps and design of piping networks and equipment in the C-station of a sugar factory. A comprehensive review of published literature is outlined based on empirical correlations and the method of viscometry employed.

2.8 Empirical correlations for massecuite viscosity

2.8.1 Earlier Correlations

Bruhns (2004) reviewed previous work on the viscosity of massecuite starting with that of Einstein (1906) who proposed a theoretical correlation for the viscosity of suspensions with a volume fraction less than 10%, not applicable to massecuite which contains higher volume fractions of crystals. Bruhns (2004) referenced the work of Frankel & Acrivos (1967) who proposed a theoretical correlation valid for high volume fractions of crystal.

2.8.2 Ackermann & Shen (1979)

Rouillard and Koenig (1980) referenced an empirical correlation developed by Ackermann & Shen (1979) for massecuite viscosity based on the interaction of solid-liquid mixtures, as shown by equation 2-47.

$$\mu_{\text{relative}} = \left[1 - \frac{\pi}{4\alpha^2}\right] + \left[\frac{\pi}{4} - \frac{\pi}{6\alpha}\right]\left[\frac{1}{\alpha^2 - 1}\right]\left[1 + \frac{2}{\sqrt{\alpha^2 - 1}} \tan^{-1}\left(\sqrt{\frac{\alpha + 1}{\alpha - 1}}\right)\right] \qquad 2\text{-}47$$

Where $\alpha = \left(\frac{\phi_\infty}{\phi}\right)^{\frac{1}{3}}$ and

ϕ_∞ = Maximum volume fraction of crystals = 0.625

The correlation by Rouillard & Koenig (1980) for molasses viscosity used in conjunction with the correlation developed by Ackermann & Shen (1979) for relative massecuite viscosity was reported to have the highest correlation co-efficient of 0.918 when compared to correlations by Silina (1953), Kelly (1958), Artyukhov and Garyazha, (1970), Awang and White (1976) and a modified Awang & White correlation developed by Rouillard & Koenig (1980).

2.9 Rotating viscometry and associated correlations for massecuite viscosity

The Brookfield rotating viscometer is the most widely used viscometer among the sugar industry and is based on the measurement of the drag force imposed on a spindle as it rotates within a viscous fluid at constant speed (Behne, 1964). The spindles used can be cylindrical, disc-type spindles or T-spindles.

There are concerns surrounding the accuracy of massecuite viscosity measurement using rotating viscometry due to the interaction and displacement of crystals around the rotating spindle. Despite widespread concerns as documented in section 2.7.2, an abundance of literature is available based on measurements with rotating viscometry and is reviewed in more detail.

2.9.1 Silina (1953)

Awang & White (1976) and Rouillard & Koenig (1980) referenced a correlation developed by Silina (1953) representing the viscosity of massecuite as a function of the molasses viscosity and concentration of sugar crystals per unit volume, as seen in equation 2-48. Ness (1983) reported that a rotating viscometer was used to determine massecuite viscosities.

$$\frac{\mu_{\text{massecuite}}}{\mu_{\text{molasses}}} = \frac{1}{1 - 3.8047\phi + 3.6586\phi^2} \qquad 2\text{-}48$$

2.9.2 Kelly (1958)

Awang and White (1976) and Rouillard and Koenig (1980) referenced a correlation developed by Kelly (1958) using a rotating viscometer with a cylindrical spindle. The correlation expressed massecuite

viscosity as a function of molasses viscosity, particle size as well as the volume concentration of crystals, as seen in equation 2-49.

$$\log_{10}\left(\frac{\mu_{\text{massecuite}}}{\mu_{\text{molasses}}}\right) = 1.93.(l+1).\phi \qquad \textit{2-49}$$

2.9.3 Artyukhov & Garyazha (1970)

Awang & White (1976) and Rouillard & Koenig (1980) referenced the work of Artyukhov & Garyazha (1970) who developed a correlation for massecuite viscosity expressed as a function of molasses viscosity and volume fraction of crystals to molasses ϕ as seen in equation 2-50.

$$\frac{\mu_{\text{massecuite}}}{\mu_{\text{molasses}}} = 1 + \frac{2\phi}{\left(1 - 0.85.\phi^{\frac{2}{3}}\right)^2} \qquad \textit{2-50}$$

2.9.4 Awang & White (1976)

Awang & White (1976) proposed a correlation to determine massecuite viscosity using unpublished data from Nicklin and from measurements carried out with C-massecuite using a Contraves Rheomat rotational viscometer with a range of shear rates between 2-100s^{-1}. The viscosity of massecuite was proposed to be a function of the molasses viscosity surrounding the crystal as well as the number of crystals and crystal size distribution. Massecuite samples were first subjected to a high vacuum to remove air bubbles, a procedure originally proposed by Kelly & M^{c}Antee (1942). The molasses brix, purity and temperature were identified as impacting the massecuite viscosity. Awang & White (1976) found that the apparent viscosity of massecuite related well to that of the surrounding molasses, and was greatly influenced by the crystal content, proposing the relationship illustrated by equation 2-51.

$$\log_{10}\left(\frac{\mu_{\text{massecuite}}}{\mu_{\text{molasses}}}\right) = 1.65.\phi.l^{0.15}.\left(1 - \frac{CV}{12}\right) \qquad \textit{2-51}$$

The co-efficient of variation *CV* is associated with the uniformity of crystal sizes and can be calculated as the standard deviation of the distribution divided by the mean crystal size.

The flow behaviour index is indicative of the degree of non-Newtonian behaviour where a value of 1 is indicative of Newtonian behaviour. Studies by Awang & White (1976) showed the flow behaviour index for massecuite to lie between 0.8 - 0.9 and was confirmed by Barker (2008). However, Broadfoot & Miller

(1990) reported flow behaviour indices closer to 1. A comparison of published data for the flow behaviour indices for massecuite, as summarised by Awang & White (1976), are shown in Table 2-1.

Table 2-1: Flow behaviour indices for massecuite by Awang and White (1976)

Source	Number of experiments	Temperature	Crystal content	Crystal size range	Shear rate	Range of n	
		^{0}C	%	mm	s-1		
Done, 1950	12	40-50	15-45	0.3-0.8	0.1-1.5	0.85	+/- 0.04
Adkins, 1951	5	room	20-40	N/A	0.1-4	0.6 - 0.9	
Nicklin, 1958	36	room	5-30	0.3-2.1	0.1-4	0.9	+/- 0.05
Kot et al, 1968	-	20-30	15-50	0.2-0.4	1-30	0.8 - 1	
Awang and White, 1976	22	30-60	15-30	0.3	2-100	0.92	+/- 0.07

Awang & White (1976) proposed that the flow behaviour index was found to be independent of crystal content and crystal size but may be dependent on the range of shear rate.

2.9.5 Rouillard & Koenig (1980)

Rouillard and Koenig (1980) reviewed the work carried out on massecuite viscosity and proposed a correlation for molasses viscosity that can be used in the expression of massecuite viscosity.

A correlation for the viscosity of molasses was developed as a function of dry substance, temperature, reducing sugar to ash ratio and sucrose to non-sucrose ratio, as seen in equation 2-52, with temperature measured in Kelvin, *S/NS* representing the sucrose/non-sucrose ratio and *RS/Ash* representing the reducing sugar to ash ratio.

$$\mu_{\text{molasses}} = \frac{1.03\times10^{-17}\left(\frac{DS}{100-DS}\right)^{5.82}}{\left(\frac{T-273.15}{T^2}\right)^{4.45}.e^{\left[0.187\left(\frac{S}{NS}\right)^3+0.689\left(\frac{RS}{\text{Ash}}\right)\right]}} \qquad 2\text{-}52$$

Rouillard & Koenig (1980) identified the crystal content as having the greatest impact on massecuite viscosity. Massecuite was produced by mixing crystals of recorded crystal size with degassed molasses. The viscosity of de-gassed molasses was measured prior to mixing with the intention to express massecuite viscosity as a function of molasses viscosity. Massecuite viscosity measurements were carried out using a Brookfield HBT rotating viscometer. The correlation for massecuite viscosity, expressed as a function of molasses viscosity, was obtained by modifying the equation proposed by Awang & White (1976) to give a correlation co-efficient similar to the best fit correlation of Ackermann & Shen (1979). Rouillard & Koenig

(1980) thus recommended the following modified Awang & White correlation for massecuite viscosity, illustrated by equation 2-53, where l_{sgs} represents the crystal specific grain size.

$$\ln\left(\frac{\mu_{\text{massecuite}}}{\mu_{\text{molasses}}}\right) = 2.84.l_{sgs}^{\ 0.0377}.\phi.\left(1-\frac{CV}{12}\right) \qquad 2\text{-}53$$

It must be noted that the specific grain size represents the mean crystal size by surface area and is mathematically different from the particle size, which is often determined as a mean crystal size by mass, as determined by sieve analysis.

Rouillard and Koenig (1980) identified possible sources of error in massecuite viscosity prediction due to the presence of colloids, dextran or suspended matter present in molasses that is seen to increase the viscosity of massecuite.

2.9.6 Rouillard (1981), (1983), (1984) and (1985)

Rouillard (1981) carried out extensive research on the rheological properties of molasses and massecuite using a Brookfield rotating viscometer with cylindrical spindles, culminating in the completion of a PhD thesis in 1985 relating to massecuite boiling.

Rouillard (1983) noted that insoluble matter and colloids have no measurable effect on the viscosity of factory products. In addition, he noted that the factors greatly affecting massecuite viscosity included temperature, dry substance, sucrose, gums, reducing sugars and ash.

Rouillard (1984) reported on the lack of published data for the range of massecuite viscosities and carried out measurements of various sugar factory products using a Brookfield rotational viscometer, leading to the development of the viscosity chart used by Tongaat Hulett, as shown in Figure 2-9. Rouillard (1984) also concluded that repeated evaporative crystallisation stages do not significantly increase the viscosity of sugar products.

Rouillard (1985) confirmed the applicability of the power law model to characterise massecuite behaviour, referencing findings from Awang and White (1976) regarding a flow behaviour index of 0.8 - 0.9 for C-massecuite. Whilst the viscosity chart was not published in this document, Rouillard (1985) reported a range for massecuite viscosities at 70°C that appear in line with the viscosity chart as seen in Figure 2-9. The viscosity of A massecuite was reported as falling within a range of 2 – 10 Pa.s. For B massecuite, this range increased to 10 - 90 Pa.s where the greatest range of viscosities was reported for C-massecuite, falling between 90 – 1000Pa.s.

2.9.7 Broadfoot (1984)

Similar to the approach of Rouillard & Koenig (1980), Broadfoot (1984) referenced a correlation for molasses viscosity proposed by Broadfoot & Steindl (1980) as shown in equation 2-54.

$$\mu_{\text{molasses}} = 0.111P^{-1.3}\gamma^{-0.16}\exp\left(\frac{3.7\left[DS-0.19(T-50)\right]}{113.5-\left[DS-0.19(T-50)\right]}\right) \qquad 2\text{-}54$$

Massecuite viscosity was thereafter recommended to be calculated using the original correlation proposed by Awang and White (1976) as shown in equation 2-51.

2.9.8 Durgueil (1987)

Durgueil (1987) used an HBT Brookfield viscometer to investigate the consistency of C-massecuite as a function of temperature, crystal content, total solids and pol content using an Arrhenius-type correlation.

Durgueil (1987) carried out a statistical analysis on the viscosity results of 43 samples of massecuite from Maidstone Mill during the 1985/ 1986 season and proposed the following correlation, shown by equation 2-55, where temperature is reported in Kelvin.

$$K = \frac{\exp\left[-21.33+15.90\text{Pol}-35.49CC+\dfrac{6802.37+3618.15[TS-CC]-13129.53CC+3042.79[1-TS]+19356.86[\text{Pol}-CC][1-TS]}{([4.187-2.3(\text{Pol}-CC)(1-TS)][1-TS]+1.19CC+1.7[TS-CC])T}\right]}{(1-TS)^{2.88}} \qquad 2\text{-}55$$

Durgueil (1987) reported a multiple correlation co-efficient of 0.972 and a residual error of 0.465. A comparison of the calculated and measured consistencies can be seen in Figure 2-15.

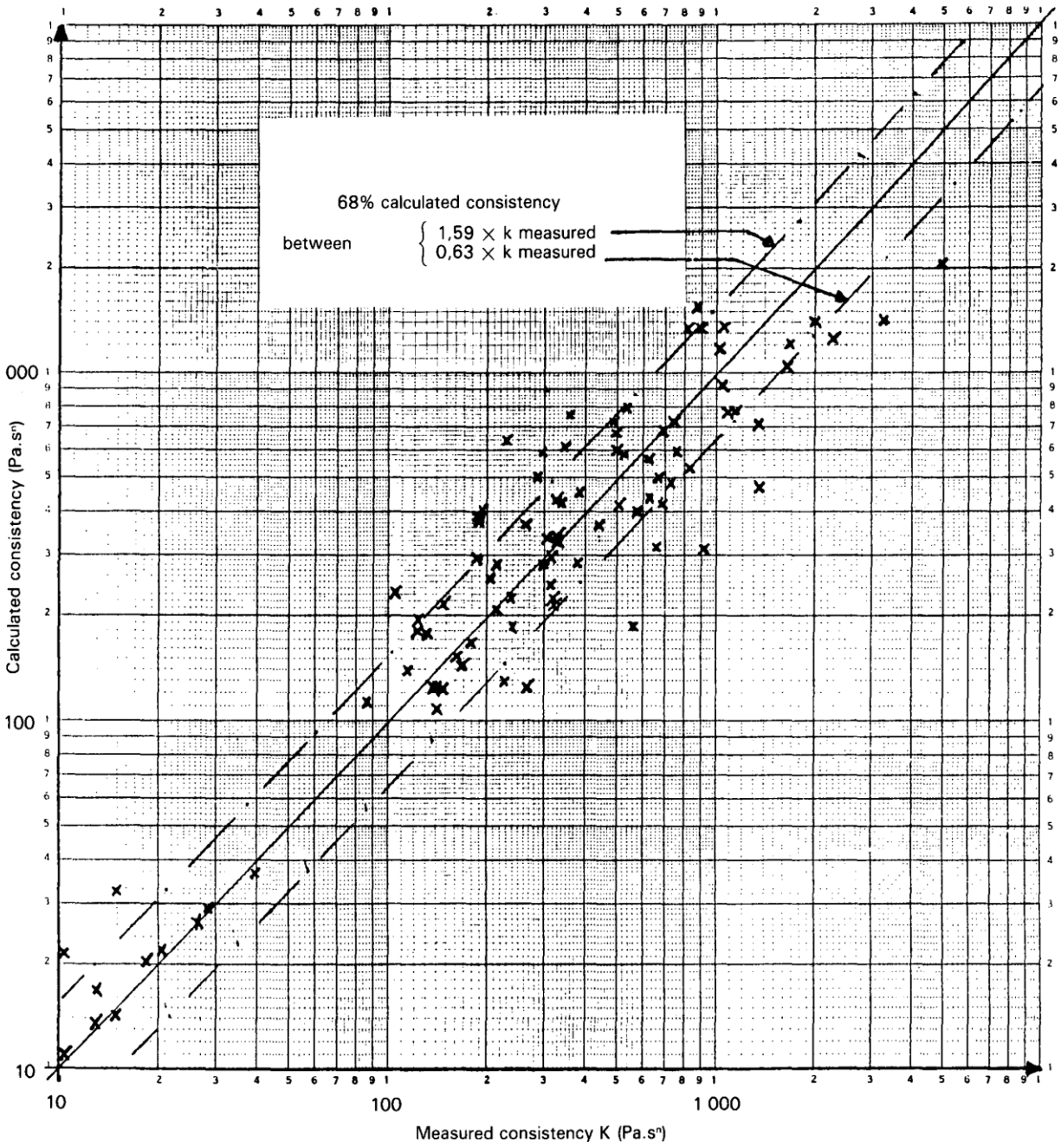

Figure 2-15: Comparison of calculated and measured consistencies for C-massecuite (Durgueil, 1987)

2.9.9 Metzler (1996)

Broadfoot et al. (1998) referenced a correlation developed by Metzler (1996) for the relative consistency of molasses to massecuite as shown below. The correlation is reported to have an accuracy of 30% and is shown by equation 2-56 and 2-57, where ψ represents the sphericity of crystals, typically 0.85 for sugar.

$$\frac{K_{\text{massecuite}}}{K_{\text{molasses}}} = \left(\frac{1+3.8\phi}{1-\frac{\phi}{\phi_m}} \right)^{1.4} \qquad 2\text{-}56$$

$$\varphi_m = 1 - \left[0.41 + 0.45(1-\psi)^4\right]\left[1 - 0.51.CV\right] \qquad 2\text{-}57$$

Later studies by Broadfoot et al. (1998) found this correlation to overstate the consistency of massecuite, when compared with experimental data.

2.9.10 Broadfoot, Miller and McLaughlin (1998)

Broadfoot et al. (1998) referenced a correlation for the consistency of molasses as developed by Broadfoot & Steindl (1980) as shown by equation 2-58.

$$K_{\text{molasses}} = 0.111P^{-1.3} \exp\left(\frac{3.7\left[DS - 0.19(T-50)\right]}{113.5 - \left[DS - 0.19(T-50)\right]} \right) \qquad 2\text{-}58$$

Using the correlation for molasses consistency in equation 2-58, the correlations of Metzler (1996) and Awang & White (1976) were adjusted by Broadfoot et al. (1998), proposing modified correlations for the consistency of massecuite. Experimental results using high and low grade massecuite was compared with the modified correlations, as seen in Figure 2-16.

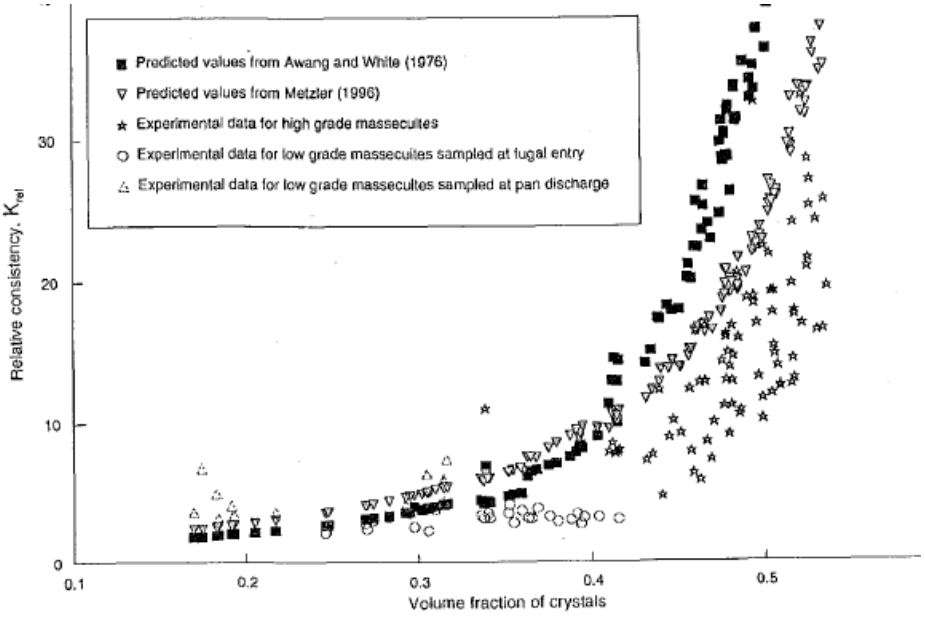

Figure 2-16: Comparison of experimental data with existing correlations

The Awang & White (1976) correlation was modified by Broadfoot et al. (1998) as shown in equation 2-59 and provides a good fit to the experimental data with slight over-estimation of the relative consistency for volume fractions of 0.3 and below, seen in Figure 2-17.

$$\log_{10}\left(\frac{K_{\text{massecuite}}}{K_{\text{molasses}}}\right) = 1.14.\phi.l^{0.13}.(1+0.14.CV) \qquad 2\text{-}59$$

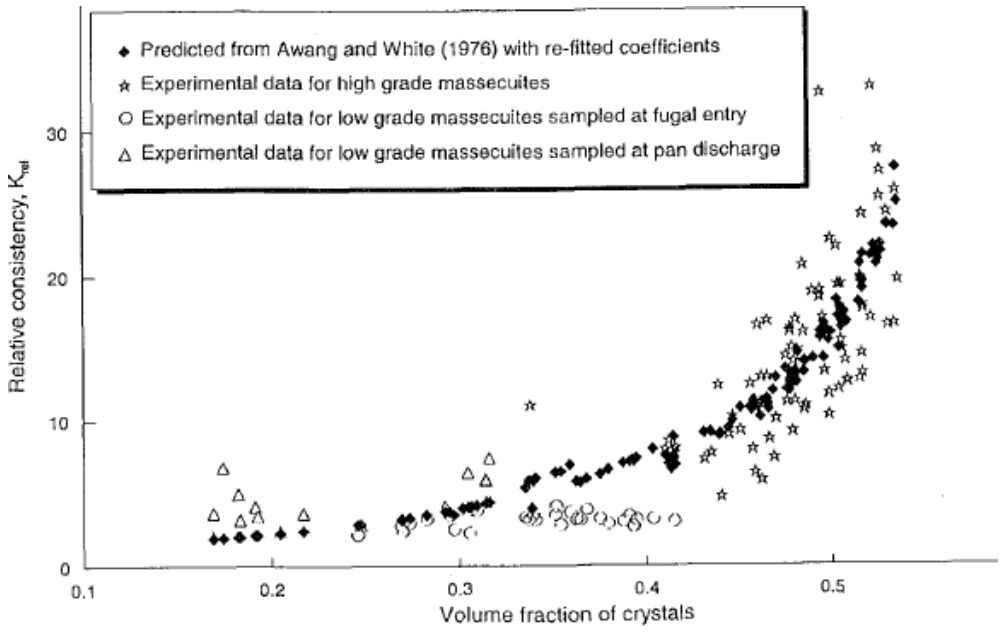

Figure 2-17: Comparison of experimental data with modified Awang and White (1976) correlation

The Metzler (1996) correlation was modified by Broadfoot et al. (1998) as shown in equation 2-60 (ϕ_m is represented by equation 2-57) and provides a good fit to the experimental data, especially for high grade massecuites with a high crystal content, seen in Figure 2-18.

$$\frac{K_{\text{massecuite}}}{K_{\text{molasses}}} = \left(\frac{1+4.76\phi}{1-\frac{\phi}{\phi_m}}\right)^{1.13} \qquad 2\text{-}60$$

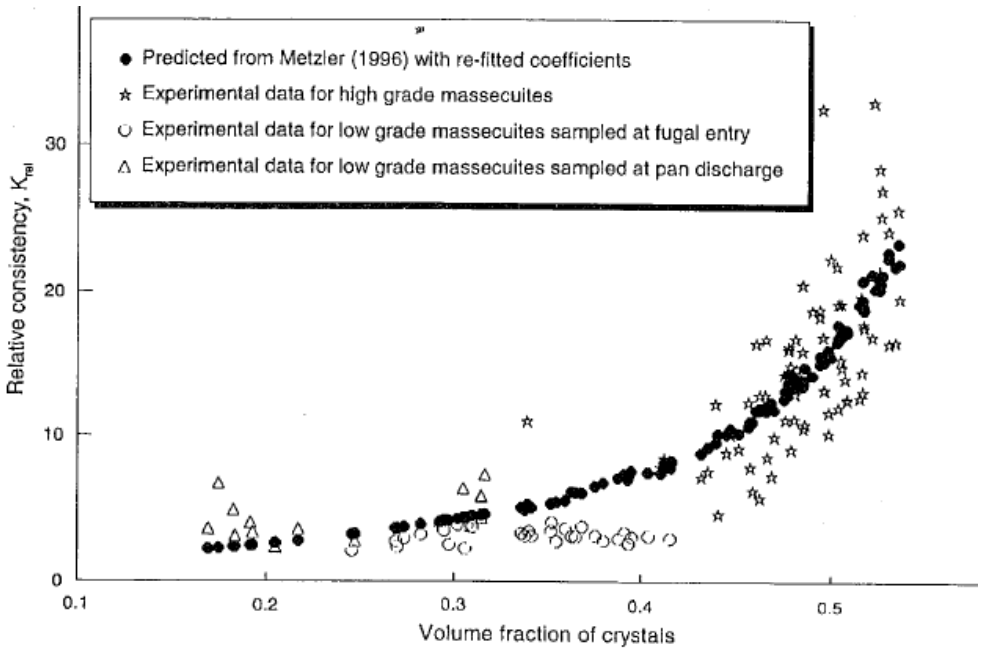

Figure 2-18: Comparison of experimental data with modified Metzler (1996) correlation

2.9.11 Rein (2007)

Peter Rein is the author of the Cane Sugar Engineering textbook that includes contributions from leading experts in the sugar industry. Rein (2007) references the modified correlations of Metzler (1996) and Awang & White (1976), as referenced by Broadfoot et al. (1998), to determine the consistency of massecuite.

As shown in section 2.6.3, Rein (2007) noted a strong dependence of massecuite consistency on temperature referencing the viscosity chart (Figure 2-9) developed by Rouillard (1984), noting a two-fold change in massecuite viscosity with a change in temperature of 10°C. Rein (2007) proposed the use of Figure 2-10 to determine the range of massecuite and molasses viscosities assuming a two-fold change in viscosity with a temperature difference of 9°C.

2.10 Glass Capillary Viscometry and associated correlations for massecuite viscosity

The use of the glass capillary viscometer is based on the principle of the time taken for a viscous medium to flow through a capillary. Once measured, the data is then ratioed to that of the test fluid used to calibrate the instrument, often found to be distilled water. Whilst yielding highly accurate data for dilute sugar products, the apparatus was found to be suitable for Newtonian fluids only (Ness, 1984).

The study of the viscosity of pure sucrose solutions was first undertaken with the use of the glass capillary viscometer which measures the time taken for a known volume of the product to drain from the capillary under gravity (Ness, 1984). Micheli & de Gyulay (1938) noted difficulty in the measurement of the viscosity of molasses with the glass capillary viscometer. The time required for the draining of molasses under gravity was found to be too long and thus a pressurised gas stream was used to propel the molasses through the viscometer. The gas pressure, however, was limited by the design pressure of the glass capillary, which was found to be too low for the pressurised gas to have any significant impact on the drainage time. The equipment was thus modified and constructed with a steel tank and capillary, the beginning of what would later become the pipeline viscometer.

2.11 Pipeline viscometry and associated correlations for massecuite viscosity

Research on the use of the pipeline viscometer for massecuite viscosity measurement was propagated by the Australian Sugar Industry with very little research done in South Africa. Behne (1964) undertook an investigation into the viscosity of C-massecuite following the inclusion of continuous centrifugals in the Australian sugar industry. Viscosity measurements were carried out using a Brookfield Synchro-Lectric Rotating viscometer and with pipelines of three different lengths, each with low length-to-diameter ratios. Behne (1964) found that the Brookfield viscometer indicated thixotropic behaviour, a time-dependent shear-thinning behaviour that was attributed to the displacement of crystals resulting in the spindle rotating in a pool of molasses. Even as early as 1964, Behne (1964) laid the foundation for the move away from the Brookfield viscometer for massecuite viscosity measurement toward a pipe flow measurement for massecuite viscosity.

The design of the pipeline viscometer is based on the principle that when a fluid flows in the pipeline, a pressure drop results as there is an inherent resistance to flow. Compressed air is used as a driving force, pushing the massecuite through the pipe and the pressure drop is measured using pressure indicators.

2.11.1 Ness (1980)

The work carried out by Ness (1980) took cognisance of the learnings from Adkins (1951), Behne (1964) and Awang & White (1976) and laid the foundations for the practical use of pipeline viscometry for the measurement of massecuite viscosity. A pipeline viscometer was built at the university of Queensland and used to develop a correlation for massecuite viscosity as a function of crystal content and molasses dry solids at a constant temperature of 50°C as shown by equation 2-61.

$$\ln \mu_{\text{massecuite}} = -9.74 + 0.078CC + 0.162DS_{\text{mol}} \qquad 2\text{-}61$$

2.11.2 Ness (1983)

Ness (1983) carried out a comparative study where the viscosity of massecuite was measured using both a pipeline viscometer and a Brookfield RVT rotational viscometer. Both studies showed massecuite to exhibit pseudoplastic behaviour with a good fit to the power law model. Results from the pipeline viscometer illustrated that the flow behaviour index was the same irrespective of the tube dimensions, with changes noted only with the consistency.

Comparing the two methods of viscometry, Ness (1983) observed that the flow behaviour index, n, based on data from the rotational viscometers were found to be lower than that of the pipeline viscometer, with the rotational viscometer illustrating a greater degree of non-Newtonian behaviour.

2.11.3 Broadfoot & Miller (1990)

An extensive study on the rheology of molasses and massecuite was carried out by Broadfoot & Miller (1990) using a pipeline viscometer. A combination crystalliser-pipeline viscometer was used with water-jacketted tubes with different length-to-diameter ratios.

Massecuite samples were prepared by mixing raw sugar and final molasses to produce a massecuite with a 30% crystal content by weight. Results from the pipeline viscometer were corrected for end effects and the flow behaviour indices were found to range from 0.86 – 1. Comparison of results with the rotating viscometer was difficult due to the difference in the range of shear rates, however, it was found that a length to diameter ratio of greater than 35 was required in order for entrance effects to be negligible i.e. less than 10% of the total pressure drop.

2.11.4 Bruhns (2004)

Bruhns (2004) carried out an investigation into the viscosity of massecuite using a double tube pipeline viscometer, as shown in Figure 2-19. Corrections for end effects and wall slip were carried out and the relative viscosity of massecuite was expressed as a function of only molasses viscosity and volume fraction of crystals, as shown in equation 2-62.

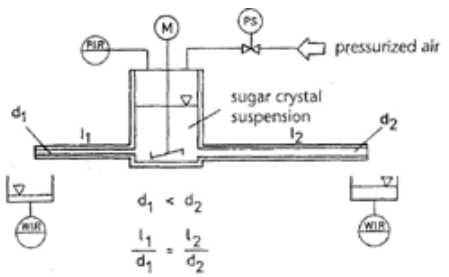

Figure 2-19: Double tube pipeline viscometer used by Bruhns (2004)

$$\frac{\mu_{\text{massecuite}}}{\mu_{\text{molasses}}} = 1 + 2.8\left(\frac{\phi}{\phi_m - \phi}\right)^{\frac{4}{3}} \qquad \textit{2-62}$$

Where ϕ_m represents the maximum volume fraction of crystals as 0.62

2.11.5 Barker (2008)

Barker (2008) carried out a comparative study and investigation on the suitability of the pipeline viscometer for measurement of C-massecuite viscosity, comparing results with a Brookfield rotating viscometer. Samples of C-massecuite were prepared by mixing C-sugar and C-molasses and were tested at 55°C and 65°C. The pipeline viscometer tests were conducted with a single pipe with a length-to-diameter ratio of 40. End effects were ignored as they are reported to be small at low flow rates and for length to diameter ratios of 10-20 (Ness, 1980).

Barker (2008) reported higher consistencies with the pipeline viscometer than with the rotating viscometer, an observation opposite to that reported by Ness (1980). A linear relationship with crystal content was observed for each sample, however, the slope of each linear relationship was found to be different.

Regarding experimental work with final molasses, the flow behaviour indices were comparable between the two methods with relatively good agreement between the two methods.

2.12 Falling Ball viscometry and associated correlations for massecuite viscosity

The introduction of the falling ball viscometer was perceived as an improvement upon the glass capillary viscometer. The fluid viscosity is determined by the time taken for a ball of known geometry and density to fall through the fluid held within a cylinder.

According to Ness (1984), the Hoppler falling ball viscometer was once very popular and used by Micheli & de Gyulay (1938) on C molasses to determine whether C-massecuite should be re-heated or diluted to aid in curing of C-massecuite. Reheating was found to be the method yielding the lower viscosity and was thus favoured. However, Ness (1984) describes the applicability of this type of viscometer to Newtonian fluids only.

2.13 Orifice viscometry and associated correlations for massecuite viscosity

Experimentation with the orifice and pipeline viscometers were pioneered in response to the recommendation from the 16th ICUMSA session to find a suitable measuring device for massecuite viscosity, as referenced by Maudarbocus (1980). The orifice viscometer, like the pipeline viscometer,

allowed for a method of viscosity measurement that was independent of the heterogeneous nature of massecuite.

2.13.1 Maudarbocus (1980)

Maudarbocus (1980) investigated the suitability of the orifice viscometer to measurement of massecuite viscosity and carried out a comparative study with a pipeline viscometer. The orifice viscometer, seen in Figure 2-20, consisted of two reservoirs with a division plate and orifice hole.

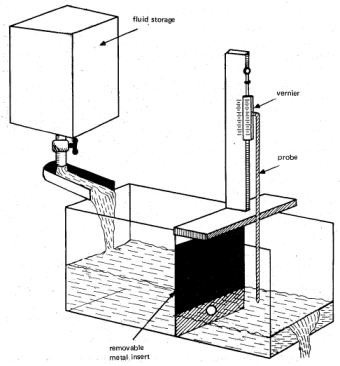

Figure 2-20: Orifice viscometer used by Maudarbocus (1980)

Tests were carried out at temperatures between 17°C – 21°C with molasses and massecuite using both a pipeline and orifice viscometer at a shear rate of $10s^{-1}$. The orifice viscometer was found to a reliable method for massecuite viscosity measurement and provided results consistent with that of the pipeline viscometer, as seen in Figure 2-21.

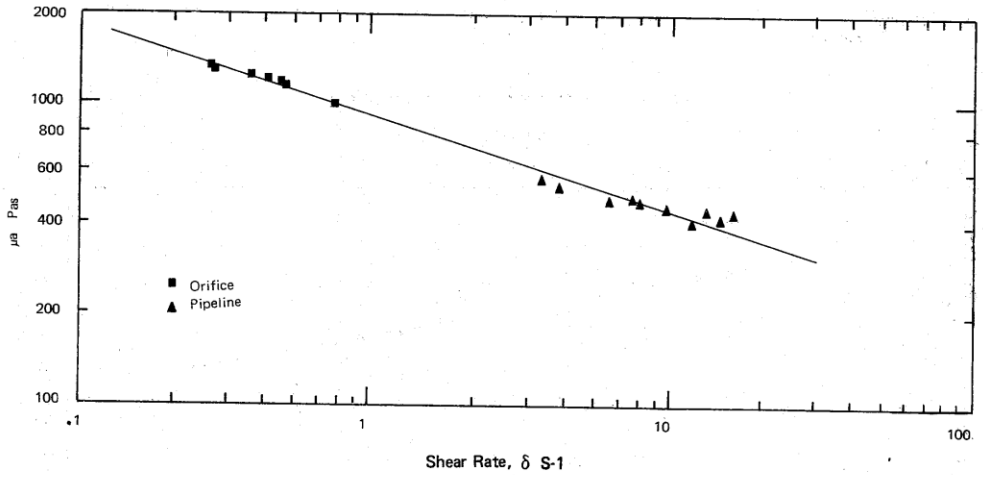

Figure 2-21: Apparent viscosity for C-massecuite using an orifice and a pipeline viscometer (Maudarbocus, 1980)

Statistical analysis of the two sets of results showed no significant difference with a 95% confidence limit.

2.14 Summary of literature review

The rotating viscometer is extremely popular within the sugar industry and is highly accurate for sugar cane juices that exhibit Newtonian behaviour, however, little confidence exists with the results obtained from measurements made with massecuite. The International Commission for Uniform Methods of Sugar Analysis (ICUMSA) does not endorse the use of the rotational viscometer for massecuite viscosity measurement and promoted the investigation of alternative methods for massecuite viscosity measurement from as early as 1974 (Maudarbocus, 1980). The Sugar Milling Research Institute is also hesitant with the use of the rotating viscometer for massecuite applications (Barker, 2008) and measurement with a rotating viscometer is not included as an approved test method for massecuite.

Of the correlations developed using the rotating viscometer, the correlations most widely used are that of Broadfoot et al. (1998) which included a correlation for molasses consistency (equation 2-58) and the modified Awang & White correlation and modified Metzler correlation with re-fitted coefficients (equations 2-59 and 2-60, respectively). However, Tongaat Hulett continues to utilise the viscosity chart developed by Rouillard (1984) as shown in Figure 2-9. Despite a wide range of published data, all correlations developed using the rotating viscometer possess an inherent uncertainty regarding then extent of the interference of crystals on the viscosity measurement.

The design pressure of the glass capillary viscometer is too low for applicability to massecuite measurements and the Falling ball viscometer was considered appropriate for Newtonian fluids only.

The pipeline viscometer and orifice viscometer were shown to be reliable methods of viscometry, however, there remains a need for additional research in this area before a correlation can be accepted as representative. The correlation proposed by Ness (1980) does not take into account the effects of temperature, leaving the correlation by Bruhns (2004) as the only correlation for massecuite viscosity from a suitable method of viscometry (equation 2-62).

CHAPTER 3: EXPERIMENTAL APPARATUS AND PROCEDURE

The design of the pipeline viscometer was based on the principle that when a fluid flows in a pipeline, a pressure drop results due to an inherent resistance to flow.

The pipeline viscometer, as shown in Figure 3-1, consisted of a pipe attached to the base of a tank, which was classified as a pressure vessel. It was designed according to the PD 5500 design code, fabricated according to the pressure vessel regulations as outlined in the South African Occupational Health and Safety Act of 1993 and approved by an Approved Inspection Authority.

Figure 3-1: 3D illustration of pipeline viscometer from Solid Edge

The pipeline viscometer TK-01 was submerged in a temperature controlled water bath TK-02, as shown in Figure 3-2. Only a small section of the pipeline was exposed to facilitate collection of samples.

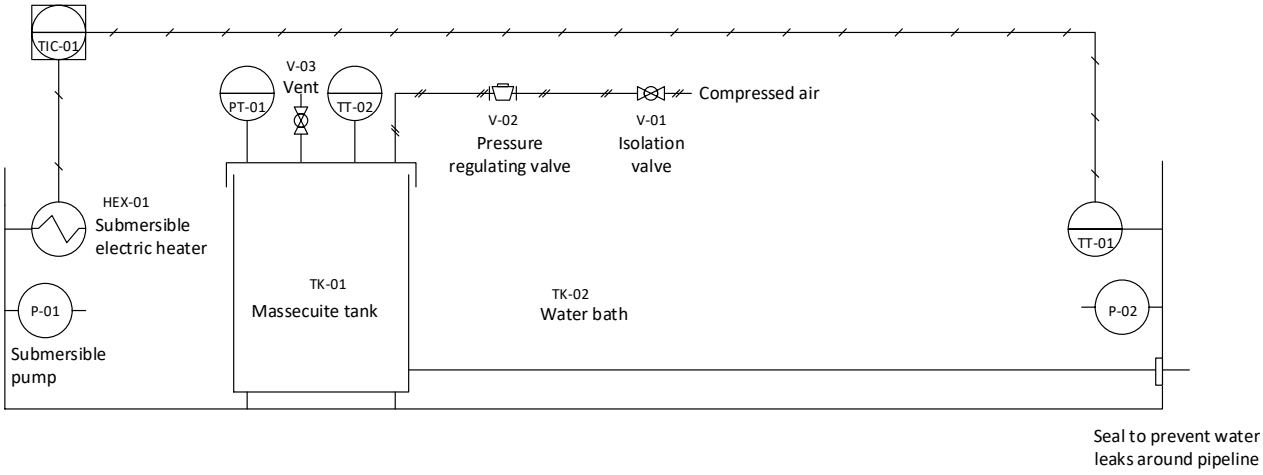

Figure 3-2: Piping and instrumentation diagram of the experimental apparatus

The water temperature was controlled by an electric heater HEX-01. Two submersible pumps P-01 and P-02 assisted with water circulation and prevented localised heating. Compressed air was used to create the pressure driving force and was adjusted using a pressure regulating valve V-02. The differential pressure

was measured using an absolute pressure transmitter PT-01 and massecuite temperature was recorded using a PT-100 thermocouple TT-02. A stirrer was not considered necessary due to the high viscosity associated with C-massecuite, allowing the effects of crystal settling to be ignored (Ananta et al., 1989). The applied pressure on the surface of the massecuite in the tank was not believed to promote crystal settling as the applied pressure did not affect the properties that affect crystal settling. The particle size and the density of the suspended particles and suspending liquor remained unchanged by the applied pressure.

The pipeline viscometer is suitable for both Newtonian and non-Newtonian fluids however it is not suitable for viscosity measurement of fluids with low viscosity or those exhibiting time-dependent behaviour. Many guidelines exist on the design and use of pipeline viscometers, where the length-to-diameter ratio of the pipe was reported to be critical in the design (Broadfoot and Miller, 1990). Allowing for pipes sufficiently large and long allows inaccuracies due to wall slip and end effects to be minimised (Mathlouthi & Kasprzyk, 1984) but increases the scale of the apparatus. This chapter outlines important considerations taken into account during the design of the experimental apparatus and procedure.

3.1 Massecuite selection

The viscometer was designed for C-massecuite duty with the flexibility to be used on A- or B-massecuite as well. As discussed in chapter 2.7.2, the high viscosity and smaller crystal size and crystal content associated with C-massecuite allowed the effects of crystal settling to be ignored (Ananta et al., 1989). C-massecuite possesses a stable suspension of crystals, however, if the viscometer is to be used for A or B massecuite measurements, the installation of a stirrer must be considered to prevent crystal settling.

3.2 Pipeline design

The pipeline viscometer was designed for a maximum pressure of 600kPa.g to ensure that the vessel can withstand the maximum air pressure delivered by the compressor at Maidstone mill. A pressure regulator on the air inlet to the viscometer further restricted the pressure to a maximum of 300kPa.g, ensuring a steady air pressure well below the maximum design limit.

3.2.1 Selection of pipe diameters

In order for the fluid properties to be representative of the average prevailing conditions, the characteristic length of the measuring instrument, in this case the pipe diameter, was recommended to be at least ten times larger than that of the average crystal size (Bruhns, 2004).

The pipe diameters were selected to accommodate A-massecuite with an average crystal size of 0.65mm, allowing the pipeline to be conservative for experimentation with C-massecuite with an average crystal size

of 0.12mm. For C-massecuite, the smallest pipe diameter was selected as 15mm nominal bore (NB) and is approximately 131 times the average crystal size.

Whilst the smallest diameter of the pipeline was selected primarily to accommodate the average crystal size, the impact on the scale of the entire apparatus must be taken into account and cannot be too large to manage. A minimum length-to-diameter ratio is required to minimise the impact of entrance effects with minimum ratios quoted as 35 by Broadfoot and Miller (1990), 25 by Barnes (2000) and 30 by Schramm (2000). Entrance effects can be ignored if the length to diameter ratio is between 100-120 (Chhabra & Richardson, 2008), however, the selection of a larger pipe diameter would require a longer pipeline, larger massecuite holding tank and larger water bath.

Taking this into account, a pipe diameter of 15NB was selected for routine experimentation with a length of 1.4m and a length to diameter ratio of 89. In order to correct for wall slip, pipelines of at least three diameters with the same length were tested. Standard pipe diameters of 15NB, 25NB and 32NB were selected, all 1.4m in length as shown in Table 3-1.

3.2.2 Selection of pipe lengths

In order to determine the entrance effects, three lengths of 15NB pipe were selected. The pipeline used for routine experimentation was specified as 1.4m in length and a minimum pipe length of 0.6m would be required to satisfy the minimum length-to-diameter ratio of 40. A third and intermediate pipe length of 1m was thus selected.

Five pipelines were required for all routine and correction tests, as summarised in Table 3-1.

Table 3-1: Summary of pipeline dimensions

Tube number	Diameter, NB	Internal diameter (m)	Length (m)	LD ratio	Purpose
T1	15	0.01576	0.6	38	Entrance effects
T2	15	0.01576	1	63	Entrance effects
T3	15	0.01576	1.4	89	Routine experiments / Entrance effects / Wall slip
T4	25	0.02664	1.4	53	Wall slip
T5	32	0.03508	1.4	40	Wall slip

3.2.3 Pipeline adaptor fitting

In order for three pipes of different diameters to fit into a single massecuite tank nozzle, three adaptor fittings were required to be designed with the pipelines protruding from the adaptor, pre-cut to specified

lengths. An 80mm round bar was used to manufacture the adaptors in order to ensure the material thickness was sufficient before and after threading and machining.

The outer diameter of each adaptor was designed to screw into the socket on the massecuite tank, with the edge of each adaptor rounded to the same radius to ensure standardisation of entrance losses and to assist in the development of a laminar velocity profile, as recommended by Broadfoot and Miller (1990).

3.3 Massecuite tank design

The massecuite tank was designed to accommodate 3L of massecuite per experimental run, allowing at least three experimental runs to be carried out before the tank is to be refilled. The drop in massecuite level associated with filling the empty pipe was also taken into account, thus ensuring the pipeline remains fully flooded with massecuite under all conditions, with no risk of air ingress. The working volume was determined from the level above the outlet pipe and calculated as 10L.

The massecuite tank diameter was specified as 250NB to fit into an existing rectangular trough that would be modified to act as a water bath. The outlet nozzle on the massecuite tank was sized to accommodate the largest pipe diameter of 32NB.

In order to prevent air ingress into the pipe or additional pressure drop as a result of eddy currents associated with a sharp change in direction of fluid flow, the outlet pipe was positioned one pipe diameter (32NB) above the base of the massecuite tank (Daugherty et al., 1989). Once the orientation and elevation of the outlet nozzle was finalised, the height of the massecuite tank was selected to be 300mm, amounting to a total volume of 14L. The viscometer and pipelines can be seen in Figure 3-3.

Figure 3-3: Pipeline viscometer with pipelines

3.3.1 Fittings and instrumentation

The massecuite tank lid accommodated five fittings, two for instrumentation, one for compressed air and a pressure breaker valve used to relieve pressure at the end of each run, before opening the massecuite tank lid.

Massecuite temperature was measured using a PT100 thermocouple and thermowell, shown in Figure 3-4. The calibration of the PT100 probe was carried out by the supplier and checked against a Digitherm temperature probe with a calibration certificate valid for one year.

Figure 3-4: PT 100 temperature probe and thermowell

Compressed air pressure was measured using a digital absolute pressure transmitter, shown in Figure 3-5. The pressure transmitter was calibrated using the compressed air system connected to an independent calibrated pressure transmitter.

Figure 3-5: Digital pressure transmitter, thermocouple and pressure breaker valve

A nylon gasket was inserted between the massecuite tank and lid to create a seal and prevent air leakage during experimentation. The lid was secured with nuts and bolts with washers on either side of the tank lid.

3.4 Water bath design and modification

3.4.1 Modification of original trough

A rectangular stainless steel trough, as shown in Figure 3-6, was modified to serve as a water bath. The water bath was 2m long, 0.4m wide and 0.4m high. Only the straight section of the trough was utilised, with the length of the water bath designed to accommodate the longest pipe length of 1.4m, the massecuite tank with a diameter of 250NB and allowing ancillary instrumentation and equipment to be installed.

Figure 3-6: Rectangular stainless steel trough

3.4.2 Fittings and instrumentation

A nozzle was installed on the side of the water bath to allow a 3kW submergent heating element to be installed in a horizontal position. A horizontal position was favoured as this allowed the entire heating element to be submerged at a height well below the water level, utilising the maximum heat transfer area even with a slight drop in water level. The heating element was installed to accommodate the viscometer with the longest pipe length of 1.4m installed, taking care to be as far from the massecuite tank as possible to prevent localised heating. The heating element was also installed at the opposite end from the water temperature probe to prevent a premature response from the temperature controller.

A supporting bracket was installed to allow the PT 100 thermocouple to be mounted in a vertical position in the water bath at a suitable distance to accommodate the position of the pipeline viscometer with the shortest pipe length of 0.6m installed. A drain valve was installed at the base of the water bath and a hole was cut into the side of the tank large enough to allow the largest pipeline to protrude for collection of product. The experimental set up is shown in Figure 3-7.

Figure 3-7: Pipeline viscometer in the water bath

3.4.3 Collection of product

In order to collect samples passing through the viscometer, the pipeline was required to protrude through the water bath. A seal between the water bath and the pipe was required for all three pipe diameters. For this purpose, three silicon seals with rubber o-rings were fabricated, each with the same outer diameter but different inner diameters to suit the individual pipelines, as shown in Figure 3-8.

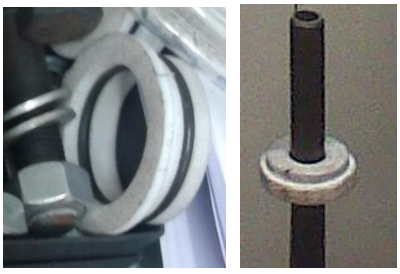

Figure 3-8: Seal between pipeline and water bath

Four legs were added to the trough, raising the water bath and allowing a suitably large collection beaker to be utilised comfortably to collect sample from the protruding pipeline.

3.4.4 Insulation

The water bath was coated with an insulation paint designed to minimise heat losses. In addition, wooden boards were placed above the bath to minimise evaporative losses.

3.5 Power supply unit

The power supply unit converted 220V alternating current to 24V direct current and provided power to all instruments with varying requirements. The unit consisted of an alternating current circuit and direct current circuit, each protected from overcurrent by circuit breakers, as shown in Figure 3-9 and 3-10. The 3kW heating element and Yokogawa recorder were powered by 220V AC, however, the digital pressure transmitter was powered using 24V DC.

A relay was included in the circuit design to switch the heating element on and off and to protect the temperature controller in the event of a malfunction of the heating element. The use of a contactor was considered as the contactor allows for a higher load and thus more rapid heating, however, concerns regarding the capacity of the controller and risk of burnout resulted in the use of a relay rather than a contactor.

Figure 3-9: Power supply unit

The power supply circuit was wired in terms of voltage rather than current, as voltage loops are arranged in parallel and current loops are arranged in series. A fault in a current loop would result in the entire power supply unit failing, however, in a voltage circuit, only the faulty loop will fail.

The circuit was wired in a normally open mode such that, in the event of a failure, the heating element will cool down rather than overheat.

3.5.1 Water temperature controller

A constant massecuite temperature was required during each experimental run. A PT100 thermocouple with re-transmission was thus used to measure the water temperature in the water bath and was connected to a Yokogawa temperature controller. The temperature controller was in turn connected to a relay that regulated a 3kW heating element. Two submersible pumps were mounted on either end of the water bath to promote circulation and prevent localised heating. The water temperature was maintained to the required set point, with a maximum deviation of 0.5°C.

The possibility of localised heating was of concern, however, this was checked at the start of each experimental run as massecuite was allowed to flow through the pipe whilst monitoring the massecuite temperature. The massecuite temperature probe was located within the massecuite tank above the entrance to the pipeline, ensuring the temperature of the massecuite flowing through the pipe was being recorded. The change in temperature set points were small (2-3°C), minimising the risk of high temperature gradients between massecuite at the wall of the tank and at the centre of the tank. Care was taken to allow the massecuite temperature to stabilise for a period of 45 minutes prior to experimentation. Localised heating was not evident during experimentation, however, thermal inertia was a problem as the massecuite temperature was initially slow to respond to changes in water temperature but increased rapidly after a period of time. This was resolved by allowing small step changes in the water temperature set point of 2°C at a time.

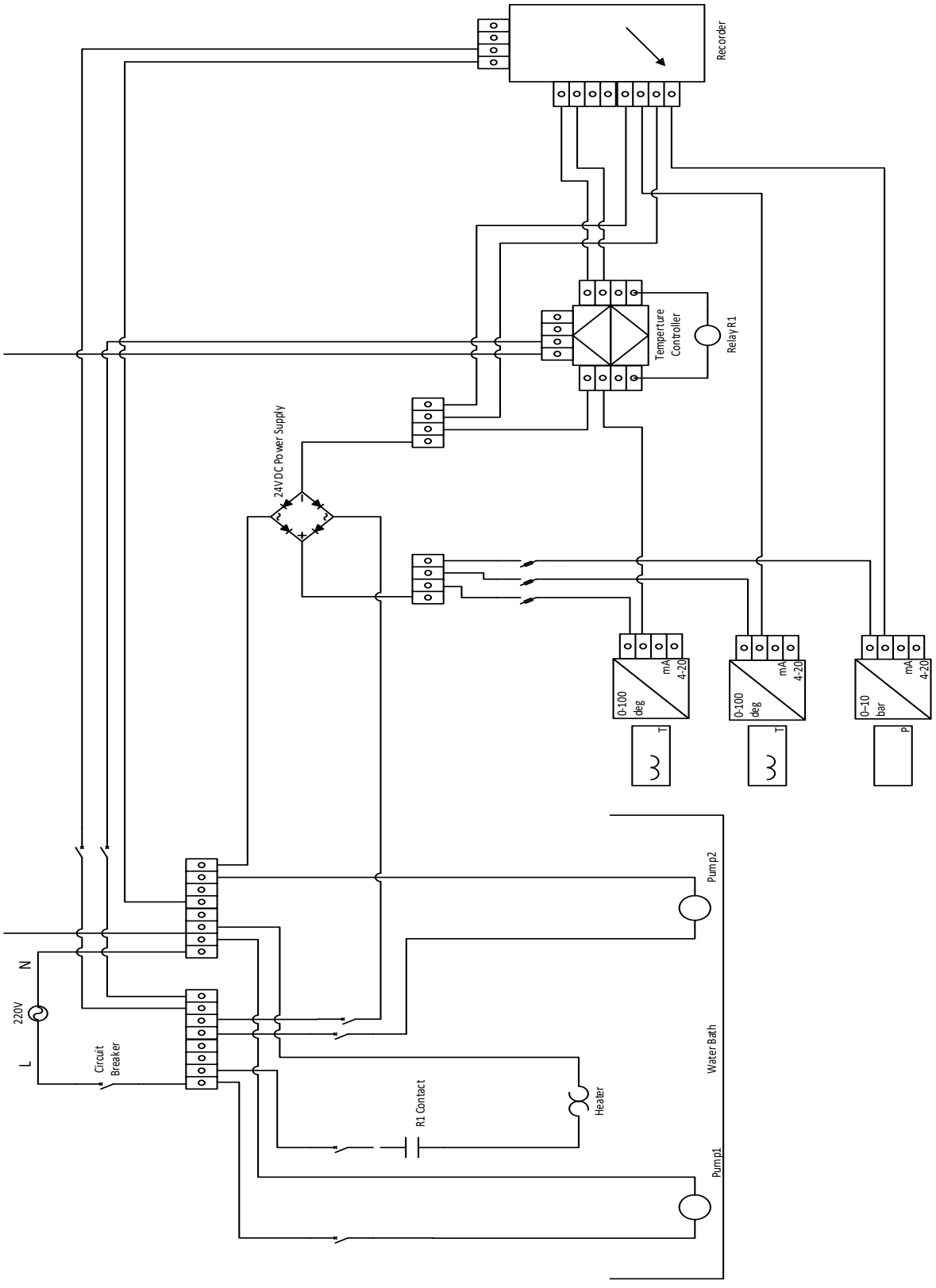

Figure 3-10: Power supply circuit

Experiments were carried out within a temperature range of 45°C to 60°C, however, in order to achieve temperatures at the upper end of the range, additional heat energy was required in the form of a 1kW immersion heating element as shown in Figure 3-11.

Figure 3-11: Additional heat energy from 1 kW immergent heating element

The output of the temperature controller was sent to a relay, which in turn transmitted a signal to the heating element, switching the heating element on and off based on the measured water temperature relative to the set point.

3.5.2 Pressure control

Compressed air was supplied from the mill compressors rated for a maximum pressure of 600kPa.g. The compressed air pressure to the pipeline viscometer was regulated using a pressure regulator with a maximum pressure rating of 300kPa.g, as shown in Figure 3-12.

Figure 3-12: Pressure regulator

3.5.3 Recorder

The recorder was configured to receive only resistance and voltage inputs. PT 100 thermocouples measuring water and massecuite temperatures transmitted resistance signals directly to the recorder. The temperature controller transmitted a 4-20mA signal to a transducer in the recorder, converting it to a voltage of 1-5V corresponding to a temperature range of 0-100°C. The recorded information was stored and used only in the event of an emergency if for some reason the pressure or temperature readings fluctuated or manually recorded data was lost.

3.6 Sampling and lab analysis

Massecuite samples were analysed at the Maidstone mill laboratory for massecuite pol, massecuite brix, nutsch molasses pol and nutsch molasses brix using the apparatus shown in section 2.5. Massecuite samples were also sent to the Sugar Milling Research Institute NPC (SMRI) for analysis for crystal size, shape and dextran.

3.7 Experimental procedure

Experiments were carried out to facilitate the collection of sufficient shear stress and shear rate data, allowing the flow behaviour index and massecuite consistency to be evaluated over a range of physical properties and conditions.

The compressed air pressure was regulated to allow different massecuite velocities, and thus shear rates, to be achieved. The corresponding shear stress was calculated based on the applied compressed air pressure and height of massecuite in the tank.

3.7.1 Range of shear rates for massecuite

Correlations for massecuite viscosity are applicable for a given range of shear rates. Broadfoot & Miller (1990) recommended an applicable range of shear rates of $0.1 – 10s^{-1}$. However, in order to include massecuite flow under gravity which is of great industrial importance, a narrower range of shear rates between $0.01 – 4s^{-1}$ was explored.

3.7.2 Development of flow curve

The flow curve is generated using a ln-ln plot of shear stress vs shear rate for at least five data points (Broadfoot and Miller, 1990), corrected for end effects and wall slip. The slope of the flow curve represents the flow behaviour index, n, and the intercept is a function of ln(K), the natural logarithm of massecuite consistency.

In order to generate a flow curve, six flow measurements were recorded by measuring the mass of massecuite collected for a pre-determined time at six different pressure set points.

3.7.3 Experimental procedure for routine analysis

The calculation of massecuite viscosity required several experimental runs with increasing pressure. To assess the dependence on temperature, each experimental run with increasing pressure was repeated at incrementally higher temperatures.

For repeatability purposes, the temperature set points were increased incrementally from 45°C to 60°C, then decreased incrementally to 45°C, and subsequently increased incrementally to 60°C. A more detailed procedure is summarised below.

3.7.3.1 Preparation of water bath

- Prior to routine experimentation, the installed pipeline was verified as being T3 (15NB,1.4m long).
- The integrity of the o-ring seal was checked to ensure a positive seal around the pipeline as it extrudes from the water bath
- The water bath drain remained closed
- The heating element remained switched off, so as to prevent over-heating of the element in the absence of water
- Water is filled in the water bath via a hose-pipe connected to a tap
- Once the water level covered the heating element, the heating element was switched on and the water set point adjusted to 45°C.
- The water circulation pumps were switched on
- The water temperature was allowed to reach the set point

3.7.3.2 Collection of massecuite and preparation of viscometer

- The pressure regulator was fully closed
- The compressed air isolation valve was opened
- The cork stopper was inserted at the end of the pipeline as shown in Figure 3-13.

Figure 3-13: Stopper for pipeline

- A sample of massecuite was collected in a 20L bucket and was poured into the empty, dry tank, as shown in Figure 3-14.

Figure 3-14: Collection of massecuite and filling of the tank

- The negative height of massecuite was recorded from the top of the tank
- The gasket was repositioned prior to replacing the tank lid as shown in Figure 3-15.

Figure 3-15: Repositioning of gasket

- The tank lid was secured by inserting the bolts and tightening the nuts using an M25 spanner to ensure no air leakage
- Massecuite was allowed to stand over-night in the water bath to achieve a temperature of 45°C
- The air vent valve was opened the following day to release air and de-gas the massecuite

3.7.3.3 Start of experimental run at 45°C

- All collection beakers were weighed and empty masses recorded (transition and experimental beakers were clearly labelled)
- Once the temperature set point was achieved, a single experiment could be carried out and involved the following:
    - The air vent valve was closed
    - The compressed air pressure was adjusted using a pressure regulator
        - Initial flow of sample was collected in transition beaker 1, shown in Figure 3-16.

Figure 3-16: Collection of sample

Once the air pressure was stable, massecuite was cut using a massecuite knife, the stop watch was started and the sample was collected in experimental beaker 1 for a pre-determined time.

- At the end of the pre-determined period, the timer was stopped as the massecuite was cut and the subsequent sample was collected in transition beaker 2 while the next pressure was set. The new pressure set point stabilised within a matter of seconds.

- The compressed air pressure was adjusted to the next set point and the experiment repeated until six pressures were completed.

- After experiments at six pressures were completed
  - The pressure regulating valve was closed
  - The air vent valve was opened
  - Residual samples flowing from the pipe were collected in a residual beaker
  - The masses of all beakers were recorded and re-used for experiments at the next temperature set point.

- For the same sample of massecuite, the experimental procedure was repeated for increasing temperatures of 48°C, 50°C, 53°C, 56°C, 59°C.

  - Attempting to carry out repeatability tests, the experimental procedure was repeated for decreasing temperatures of 59°C, 56°C, 53°C, 50°C, 48°C, 45°C and repeated once more for increasing temperatures of 45°C, 48°C, 50°C, 53°C, 56°C, 59°C.

As a result of the highly viscous nature of massecuite, the product required hours to reach the temperature set point. Three temperature set points, at most, were tested per day with additional heating in the form of

an immersion heater required at higher temperatures. One week per massecuite sample was required for complete experimentation.

3.7.3.4 Collection of samples for lab analyses

- A 3L sample of massecuite was required for nutsch analysis
- Additional samples were collected in sample bottles for the following analyses
    - Bottle 1 - Brix and Pol
    - Bottle 2 - Crystal size, shape
    - Bottle 3 - Dextran

3.7.4 Experimental procedure for end effects and wall slip

The experimental procedure for routine analysis was repeated for a sample of massecuite with the following changes

- Experiments were carried out at only 45°C
- All pipelines were tested (T1, T2, T3, T4, T5)

As per the procedures outlined in chapters 3.7.3.1 to 3.7.3.4, water was filled in the water bath, a sample of massecuite was filled into the massecuite tank and experimental runs were carried out for a single temperature of 45°C. Once the experiment at 45°C was completed, the pipeline was changed.

In order to change the pipeline with massecuite in the tank, the following procedure was employed:

- The heating element and water circulation pumps were switched off
- Water was drained from the water bath via the drain valve
- Once the water level was below the massecuite tank outlet level, the pipeline was pulled out of the water bath protrusion and removed from the massecuite tank using a spanner.
- The tank was pulled back further to allow a longer length pipe, for example T2, to be inserted
- The new pipeline was held in place as the old pipeline was being removed to allow for a quick replacement, minimising spillage of massecuite
- As a result of the highly viscous nature of massecuite, pipelines were neatly interchanged with no spillage
- The position of the tank was adjusted such that the newly inserted pipeline protruded slightly from the water bath, with the o-ring seal in place.
- The water bath drain was closed
- The water bath was once again filled with water

- Once the water covered the heating element, the heating element and circulation pumps were switched on and the water bath was allowed to reach the set point of 45°C.
- Once the temperature set point was achieved, the experimental run was carried out with the newly fitted pipeline as described above.

This procedure was repeated for all five pipelines.

3.8 Expected margin of error

The relative error associated with a variable j can be expressed using the deviation σ_j from the measured value x_j, as seen in equation 3-1.

$$\text{Relative error}\% = \frac{\sigma_j}{x_j} \times 100 \qquad \textit{3-1}$$

Where an error can be attributed to a number of different variables, the error propagation method for uncorrelated variables was used, as shown in equation 3-2 for a number of variables i.e. j = 1, 2, 3…i.

$$\text{Combined relative error}\% = \sqrt{\sum_{j=1}^{i}\left(\frac{\sigma_j}{x_j} \times 100\right)^2} \qquad 3\text{-}2$$

3.8.1 Shear stress

The calculation of shear stress is dependent on the tube length, diameter and pressure driving force as seen in equation 2-8. The tube length and diameter were measured accurately, however, a manual pressure regulating valve was used to maintain the desired pressure set point. In the calculation of shear stress, the error associated only with fluctuating compressed air pressure was taken into account, where a maximum deviation of 1kPa from the desired set point was observed. The maximum error was calculated using the lowest pressure set point of 50kPa.a. Using equation 3-1, the maximum relative error for shear stress was calculated to be 2%.

For plots containing the the natural logarithm of shear stress, the relative deviation can be expressed as $\frac{1}{x_j}.\sigma_j$, the same as the relative error. The error bar included in plots of ln(shear stress) thus represent an error of 2%.

3.8.2 Shear rate

The calculation of shear rate was dependent on the tube diameter and massecuite velocity as seen in equation 2-11. The tube diameter was measured accurately, however, the error associated with massecuite velocity was in turn dependent on the time taken to collect the sample and mass measurement of the sample. Seeing as the mass flow was converted to a volumetric flow using a correlation that is dependent on temperature, massecuite brix, nutsch molasses brix and pol, the errors associated with these analyses were taken in to account. The errors associated with all components of the calculation are summarised in Table 3-2 and were taken into account using the error propagation method for uncorrelated variables, shown in equation 3-2.

Table 3-2: Summary of individual errors used to calculate error associated with shear rate

		Expected deviation	**Expected measured value providing maximum error**	**Maximum relative error, %**
Time	s	1	20	5
Mass	g	0.5	10	5
Nutsch molasses purity	%	0.5	33	1.5
Temperature	^{0}C	0.5	45	1
Nutsch molasses brix	%	0.5	92	0.5
Massecuite brix	%	0.5	95	0.5

The greatest errors were expected to be associated with time and mass measurement. The digital mass meter reading was expected to fluctuate by 0.5g as a result of disturbances from the air conditioner. To establish the maximum relative error, the smallest sample mass of 10g was used together with equation 3-1 and calculated to be 5%.

The time taken to collect each sample at various pressures was pre-determined. Inaccuracies associated with the time measurement arose from the speed at which the massecuite sample could be cut from the pipe, ensuring this coincided accurately with the time set point. A reasonable deviation of 1s was expected. To establish the maximum relative error, the shortest experimental run of 20s was used together with equation 3-1 and calculated to be 5%.

The error associated with the laboratory analyses were estimated with a focus on handling of the product rather than the accuracy of the measuring instruments. The laboratory analyses were expected to deviate by a maximum of 0.5% for each measurement and with respect to massecuite and nutsch molasses brix, this error was small, however, with nutsch molasses purity, a greater error of 1.5% was introduced.

The massecuite temperature was expected to remain constant for the duration of each run. However, during the longer experimental runs of 10 minutes and above, a maximum temperature drift of 0.5°C was expected as a result of the thermal inertia of massecuite.

Using equation 3-2, the maximum combined relative error associated with shear rate was calculated as $\sqrt{(5)^2 + (5)^2 + (1.52)^2 + (1.11)^2 + (0.54)^2 + (0.53)^2} = 7.4\%$. Where the natural logarithm of shear rate is plotted, the error bar contains a maximum combined relative error of 7.4%.

3.8.3 Consistency and flow behaviour index

The consistency and flow behaviour indices were dependent on the shear stress and shear rate and the maximum combined relative error was calculated from equation 3-2 as $\sqrt{(2)^2 + (7.36)^2} = 7.6\%$. Where the natural logarithm of consistency is plotted, the error bar contains a maximum combined relative error of 7.6%.

3.8.4 Apparent viscosity

Apparent viscosity was calculated using the consistency and flow behaviour index. The maximum combined relative error was calculated from equation 3-2 as $\sqrt{(7.62)^2 + (7.62)^2} = 10.8\%$.

A summary of the maximum relative errors associated with the experimental method can be seen in Table 3-3.

Table 3-3: Summary of maximum relative errors

		Maximum relative error
Shear stress	%	2
Shear rate	%	7.4
Consistency, K	%	7.6
Flow behaviour index, n	%	7.6
Apparent viscosity	%	10.8

3.9 Validation

In order to validate the accuracy of the pipeline viscometer, the viscometer was tested with a fluid of known viscosity, preferably a fluid exhibiting pseudoplastic behaviour, similar to massecuite.

3.9.1 Validation test fluid

Carboxymethyl Cellulose (CMC) was originally selected as the test fluid; however, the composition of CMC was found to change from one supplier to the next. The composition of CMC from local suppliers contained quantities of salts that were not explicitly specified and it was difficult to match the composition of CMC samples received with viscosity data from literature.

Viscosity standard gels as seen in Figure 3-17, used by the SMRI , were also considered as test fluids; however, the quantity required for validation of the pipeline viscometer was found to be too large and would have been cost prohibitive.

Figure 3-17: Viscosity standard used to calibrate Brookfield viscometer

Broadfoot & Miller (1990) carried out extensive research on the viscosity of molasses and massecuite using both a Brookfield RVT rotational viscometer and a pipeline viscometer with water-jacketted tubes attached to the base of a reservoir tank.

No statistically significant difference (at the 5% level) in the molasses consistencies and flow behaviour indices were found, however, it was noted that better agreement of flow behaviour indices was achieved at low length to diameter ratios. Higher length to diameter ratios resulted in flow behaviour indices elevated consistently by 0.05units (Broadfoot & Miller,1990).

When comparing rheological behaviour using two different measuring devices, it is recommended that the range of shear rates be similar for the results to be comparable.

Based on the close correlation of the values for consistency and flow behaviour index for molasses from the two rheological methods, together with the inability to source a suitable test fluid in sufficient quantities, it was decided to use the Brookfield viscometer as the test apparatus and final molasses as the test fluid to validate the pipeline viscometer using a similar range of shear rates.

Validation of the pipeline viscometer was carried out using final molasses and compared with independent viscosity analyses carried out by the SMRI. Experiments were conducted at 30°C, allowing the viscosity parameters from the pipeline viscometer to be comparable with that of the Brookfield viscometer.

Final molasses was sourced from Maidstone mill with an expected brix of 88%. However, the brix of final molasses from the storage tank during the week of validation was significantly lower than expected which made management of molasses slightly difficult. The first sample was at 73% brix and the remaining samples were between 80- 82% brix, as shown in Table 3-4.

Table 3-4: Summary of final molasses analyses

Sample number	Sample name	Brix %	Pol %	Purity %
1	20161108am	73.85	30.03	40.66
2	20161108pm	80.65	28.06	34.79
3	20161109am	80.80	28.22	34.93
4	20161109pm	81.00	28.22	34.84
5	20161110	81.95	28.73	35.06

3.9.2 Validation test using the pipeline viscometer

Final molasses is a homogenous product and corrections for wall slip were not required. However, corrections for end effects were carried out using pipelines T1, T2 and T3, with routine experimentation carried out using pipeline T3 only.

The standard procedures as outlined in sections 3.7.3 and 3.7.4 were followed, however, the pipeline stopper was required to be used more frequently in order to prevent molasses from pouring out of the pipeline, especially between changes in pressure set point. Large fluctuations in pressure were noted at the start of the run, however, the mass of sample collected only during the stable pressure was used in the calculation. As a result of the low viscosity of molasses, and in order to collect a reasonable amount of molasses and allow for repeatability of the experiment, the duration of each run was minimised with all runs less than 40s. A summary of results for molasses validation using the pipeline viscometer can be seen in Table 3-5 and 3-6.

Table 3-5: Summary of results for molasses viscosity measurements using the pipeline viscometer

Sample number	Sample name	n	K, Pa.s^n
1	20161108am	0.75	4.75
2	20161108pm	0.83	9.64
		0.83	10.00
		0.83	9.83
3	20161109am	0.77	18.29
		0.77	17.81
		0.77	17.59
4	20161109pm	0.79	13.02
		0.80	12.89
		0.80	13.00
5	20161110	0.78	28.98
		0.79	30.15

Table 3-6: Summary of average results for molasses viscosity measurements using the pipeline viscometer

Sample number	Sample name	Average n	Average K, Pa.s^n
1	20161108am	0.75	4.75
2	20161108pm	0.83	9.82
3	20161109am	0.77	17.90
4	20161109pm	0.80	12.97
5	20161110	0.78	29.56

3.9.3 Validation test using the Brookfield viscometer

Five molasses samples were analysed by the SMRI using a Brookfield rotating viscometer, as shown in Figure 3-18, with T-type spindles, shown in Figure 3-19.

Figure 3-18: Brookfield viscometer and water bath

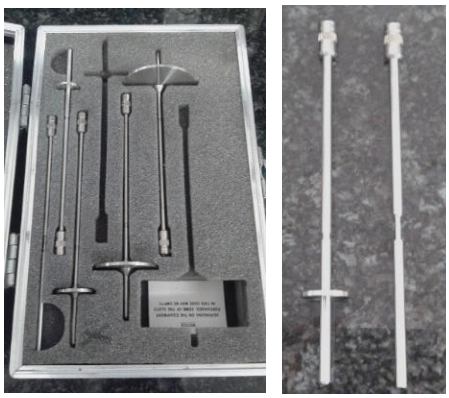

Figure 3-19: T-type spindles, with T6 and T7 used for molasses at high speed

The maximum torque for the Brookfield viscometer was 0.00072N.m and details of the T-spindles are summarised in Table 3-7.

Table 3-7: Summary of radius and effective length for T-spindles

Spindle number	Radius (m)	Effective length (m)
2	0.02355	0.025
3	0.0174	0.018
4	0.0137	0.015
5	0.01062	0.012
6	0.007325	0.01
7	0.0016	0.051

Spindles T6 and T7, as shown in Figure 3-19, were used for molasses measurements based on the range of shear rates required.

3.9.3.1 Range of shear rate for validation

In order to validate the pipeline viscometer, the molasses viscosity measurements were required to be carried out within a similar range of shear rates to that of the pipeline viscometer. A comparison of the ranges of shear rates used by each equipment is summarised in Table 3-8.

Table 3-8: Summary of range of shear rates used for Brookfield and pipeline viscometers

Sample number	Sample name	Shear rate, s^{-1}	
		Brookfield viscometer	**Pipeline viscometer**
1	20161108am	17 – 70	58-160
2	20161108pm	7 – 30	10-66
3	20161109am	17 – 68	9-40
4	20161109pm	17 – 68	13-50
5	20161110	17 – 67	5-22

Samples of molasses were placed in a water bath with a temperature set point of 30°C. The appropriate spindle was attached to the viscometer and lowered into the molasses sample. The torque, as a percentage of the maximum torque, was recorded for four different shear rates within a range corresponding to the range of shear rates used for the pipeline viscometer.

The results for the molasses measurements using the Brookfield viscometer are summarised in Table 3-9.

Table 3-9 : Summary of results for molasses viscosity measurements using the Brookfield viscometer

Sample number	Sample name	Spindle	Speed, rpm	Torque, %
1	20161108am	6	250	29.4
			187.5	23.8
			125	17.7
			62.5	10.6
2	20161108pm	6	120	85.6
			90	66.2
			60	47
			30	27
3	20161109am	7	250	55.6
			187.5	44.7
			125	32.9
			62.5	19.1
4	20161109pm	7	250	37.4
			187.5	30.2
			125	22.1
			62.5	12.7
5	20161110	7	250	98.8
			187.5	78.7
			125	57.7
			62.5	33.2

3.9.3.2 Flow behaviour index, n

The speed of the T-spindle was recorded in revolutions per minute (rpm) and converted to revolutions per second, *N*, by dividing by 60.

The torque was calculated from the percentage using the maximum torque of 0.00072N.m. The flow behaviour index, *n*, was calculated as the slope of the ln-ln plot of torque as a function of speed in revolutions per second.

3.9.3.3 Shear rate

The shear rate γ was calculated according to equation 3-3 using the spindle speed *N*.

$$\gamma = \frac{4\pi N}{n} \qquad 3\text{-}3$$

3.9.3.4 Shear stress

The shear stress τ was calculated according to equation 3-4 using the torque *t*, spindle radius R_s and spindle effective length L_{eff}.

$$\tau = \frac{t}{2\pi R_S{}^2 L_{eff}} \qquad 3\text{-}4$$

3.9.3.5 Consistency

The consistency was calculated from the intercept of the ln-ln plot of shear stress as a function of shear rate as shown by equation 2-32.

The results for the flow behaviour index and consistency are summarised in Table 3-10.

Table 3-10: Summary of results for Brookfield viscometer

Sample number	Sample name	n	K, Pa.s^n
			Pa.s^n
1	20161108am	0.74	2.72
2	20161108pm	0.83	10.65
3	20161109am	0.77	18.92
4	20161109pm	0.78	12.37
5	20161110	0.79	31.98

3.9.4 Comparison of results

The pipeline viscometer was found to correlate well with the Brookfield viscometer for molasses measurements, with good agreement among the flow behaviour index. The consistency for the pipeline viscometer was found to lie between 95 – 105% of the Brookfield viscometer figures as seen in Table 3-11, with the exception of sample number 1. This sample possessed a low brix and was difficult to handle, which can contribute to the large discrepancy. The brix of the subsequent samples were higher and meticulous care was taken to ensure accurate timing and mass measurements were taken.

Table 3-11: Comparison of results

		n			K		
Sample number	**Sample name**	**Brookfield viscometer**	**Pipeline viscometer**	**n Pipeline as % of n Brookfield**	**Brookfield viscometer**	**Pipeline viscometer**	**as % of Brookfield**
1	20161108am	0.736	0.749	102%	2.720	4.751	175%
2	20161108pm	0.830	0.829	100%	10.648	9.824	92%
3	20161109am	0.771	0.770	100%	18.917	17.896	95%
4	20161109pm	0.781	0.796	102%	12.374	12.970	105%
5	20161110	0.786	0.785	100%	31.981	29.562	92%

CHAPTER 4: RESULTS AND DISCUSSION

For each massecuite sample, the consistency was calculated from a flow curve generated under conditions of constant temperature, for a temperature range of 45°C – 60°C.

Development of the correlations used to correct for end effects and wall slip were outlined allowing for accurate determination of the flow behaviour index *n* and consistency *K*. The flow behaviour index is represented as the gradient on each flow curve in Appendix 2 (chapter 7.2, Figure 7-1 to Figure 7-102) and massecuite consistencies for all temperatures are summarised in Tables 7-1 to 7-8 of Appendix 3 (chapter 7.3). Laboratory analyses summarised in Table 4-1 were then used together with the rheological data to develop an empirical correlation for the prediction of massecuite consistency shown by equation 4-18.

4.1 Laboratory analyses

Laboratory analyses for massecuite brix, purity and crystal content were carried out as well as nutsch molasses brix and purity. The dextran content, crystal size and shape were also determined for each massecuite sample. The dry substance content was calculated according to equation 2-40. The results from internal and external laboratory analyses are summarised in Table 4-1.

Table 4-1: Summary of laboratory analyses

Sample name	Massecuite brix, %	Dry Substance, %	Massecuite purity, %	Nutsch molasses brix, %	Nutsch molasses purity, %	Crystal content, %	Dextran, ppm
20160901	95.75	92.88	52.53	92.25	38.37	41.88	272.72
20160905	96.05	93.24	53.81	92.45	42.23	35.77	276.6
20160919	95.85	93.08	54.37	93.25	38.83	44.78	278
20160926	96.40	93.58	53.95	93.75	37.93	46.12	263
20161003	96.75	94.05	56.27	95.35	38.98	48.71	267
20161017	98.30	95.26	52.36	97.65	37.43	44.80	275
20161024	95.75	92.99	54.39	92.83	39.05	44.31	265
20161031	96.20	92.84	45.02	92.75	32.66	39.23	312

The crystal shapes in all massecuite samples were found to be D-type crystals, as seen in Figure 4-18, and crystal sizes ranged from 0.96mm to 0.127mm. The dextran content on massecuite brix was found to be between 263 – 312ppm.

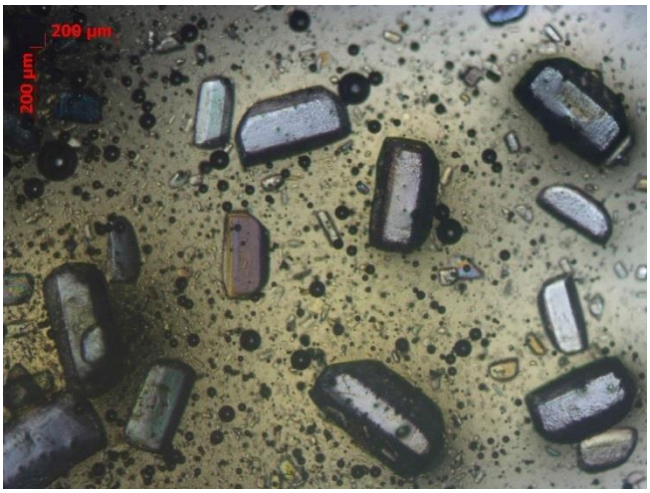

Figure 4-1: Sugar crystals in C-massecuite

4.2 Correction and repeatability tests

4.2.1 Correction for end effects

In order to evaluate the pressure loss due to end effects, flow curves were generated using pipelines of the same diameter but three different lengths, as shown in Figures 4-2 to 4-4 (shear stress was calculated in Pa and shear rate in s^{-1}). Pipelines T1, T2 and T3 were used.

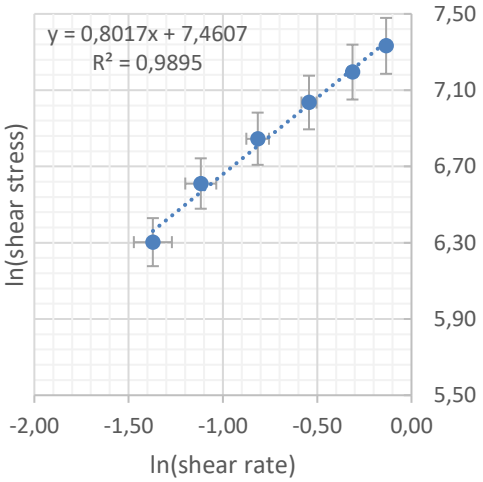

Figure 4-2: Flow curve using pipeline T1

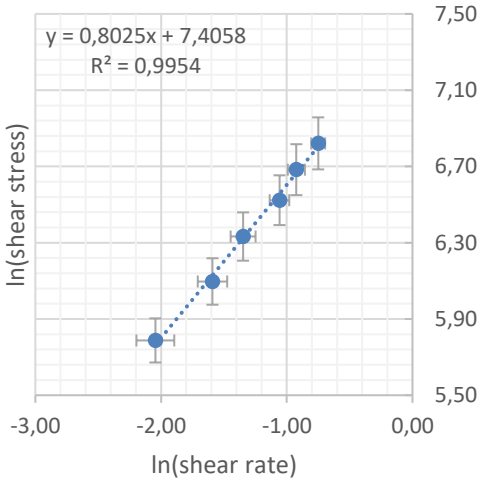

Figure 4-3: Flow curve using pipeline T2

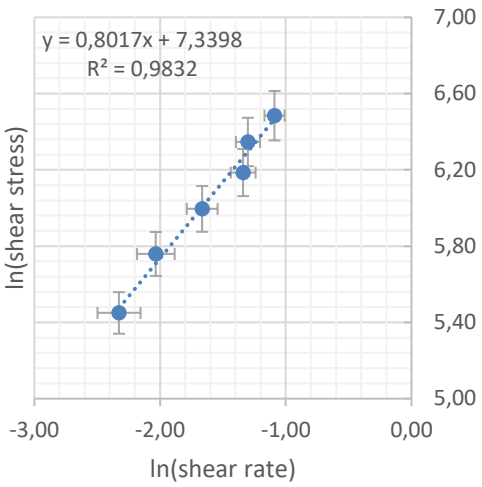

Figure 4-4: Flow curve using pipeline T3

The linear relationship between the natural logarithms of shear stress and shear rate allowed the equation for the linearised plot to be used to determine the shear stress at fixed values of shear rates. The shear stress was calculated for each pipeline at shear rates from 0.1 - 0.35s^{-1}, a range of shear rates within the expected range during operation.

Pressure drop was calculated from shear stress using equation 2-8. A plot of pressure drop vs pipe length at constant shear rate was then developed as shown in Figure 4-5.

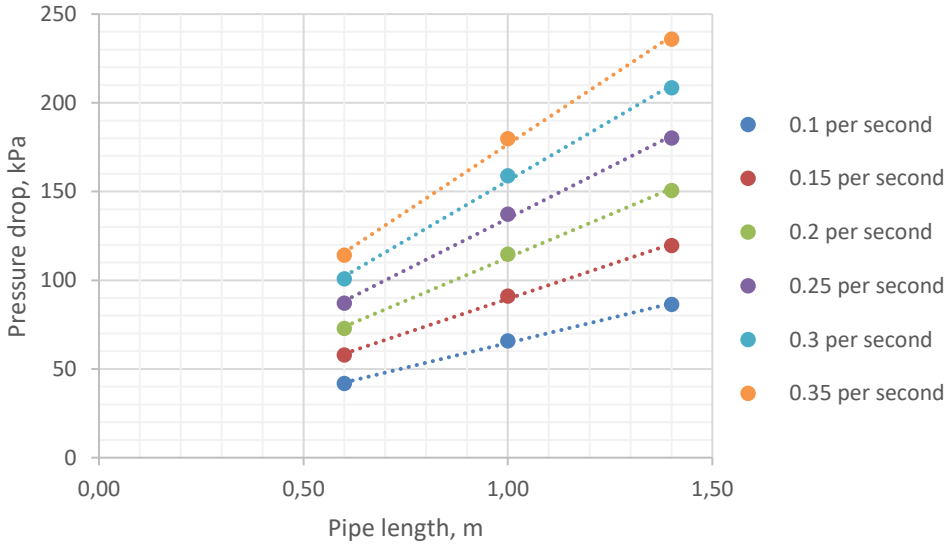

Figure 4-5: Pressure drop as a function of pipe length

Equations 4-1 to 4-6 were found from the plot of pressure drop as a function of pipe length

$$\Delta P = 152.25L + 24.37 \quad \textit{at a shear rate of 0.35 } s^{-1} \quad \textit{4-1}$$

$$\Delta P = 134.55L + 21.53 \quad \textit{at a shear rate of 0.3 } s^{-1} \quad \textit{4-2}$$

$$\Delta P = 116.25L + 18.60 \quad \textit{at a shear rate of 0.25 } s^{-1} \quad \textit{4-3}$$

$$\Delta P = 97.21L + 15.54 \quad \textit{at a shear rate of 0.2 } s^{-1} \quad \textit{4-4}$$

$$\Delta P = 77.19L + 12.34 \quad \textit{at a shear rate of 0.15 } s^{-1} \quad \textit{4-5}$$

$$\Delta P = 55.77L + 8.91 \quad \textit{at a shear rate of 0.1 } s^{-1} \quad \textit{4-6}$$

The intercept of each plot allowed the pressure drop at the entrance of the pipeline to be calculated for a specific shear rate. A plot of the pressure drop at the entrance of the pipeline was then plotted against shear rate to develop the equation to correct for end effects, as seen in Figure 4-6.

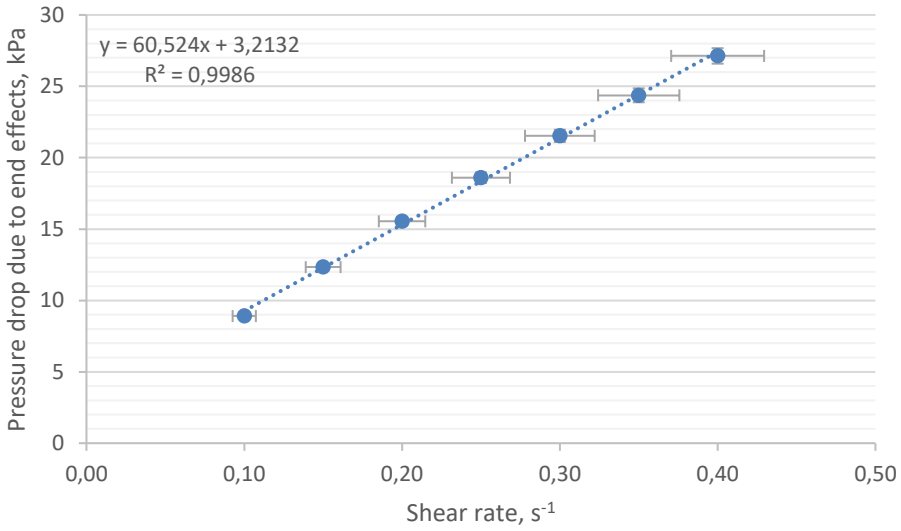

Figure 4-6: Plot of pressure drop due to end effects as a function of shear rate

The correction for pressure loss due to end effects as a function of shear rate was given by equation 4-7.

$$P_{\text{end effects}} = 60.524\gamma + 3.213 \quad \text{4-7}$$

4.2.2 Correction for wall slip

In order to evaluate the pressure loss due to wall slip, flow curves were generated using pipelines of the same length but three different diameters, as shown in Figure 4-7 to 4-9 (shear stress was calculated in Pa and shear rate in s^{-1}). Pipelines T3, T4 and T5 were used.

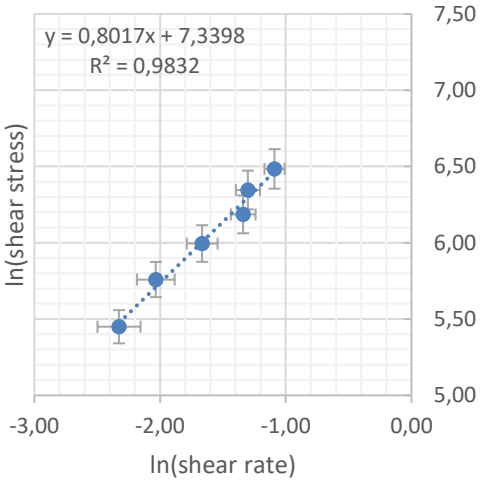

Figure 4-7: Flow curve using pipeline T3

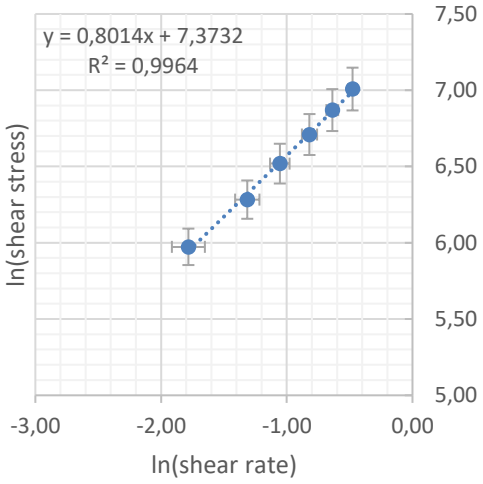

Figure 4-8: Flow curve using pipeline T4

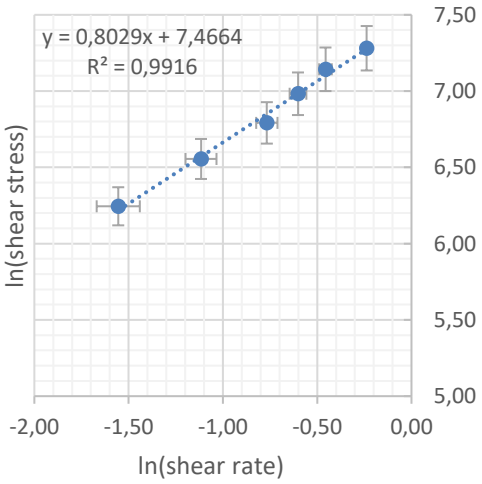

Figure 4-9: Flow curve using pipeline T5

The linear relationship between the natural logarithms of shear stress and shear rate once again allowed the equation for the linearised plot to be used to determine the shear rate at fixed values of shear stress. The

shear rate was calculated for each pipeline at shear stresses from 200 - 700Pa and plotted as a function of $\frac{1}{D}$, as shown in Figure 4-10.

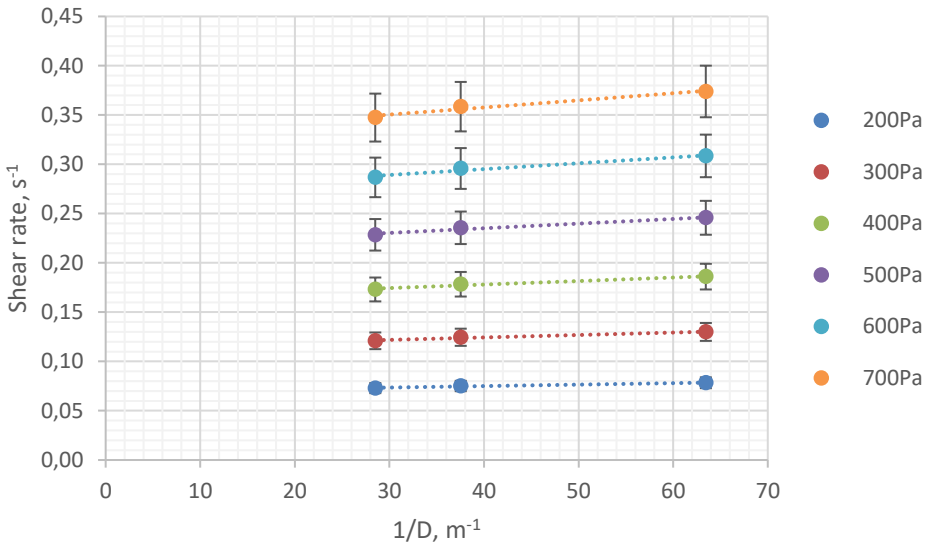

Figure 4-10: Plot of shear rate vs 1/D

Equations 4-8 to 4-13 were found from the plot of shear stress vs. 1/D.

$$\dot{\gamma} = 0.000722\frac{1}{D} + 0.329 \quad \textit{at a shear stress of 700Pa} \quad \textit{4-8}$$

$$\dot{\gamma} = 0.000594\frac{1}{D} + 0.271 \quad \textit{at a shear stress of 600Pa} \quad \textit{4-9}$$

$$\dot{\gamma} = 0.000472\frac{1}{D} + 0.216 \quad \textit{at a shear stress of 500Pa} \quad \textit{4-10}$$

$$\dot{\gamma} = 0.000356\frac{1}{D} + 0.164 \quad \textit{at a shear stress of 400Pa} \quad \textit{4-11}$$

$$\dot{\gamma} = 0.000247\frac{1}{D} + 0.114 \quad \textit{at a shear stress of 300Pa} \quad \textit{4-12}$$

$$\dot{\gamma} = 0.000148\frac{1}{D} + 0.0691 \quad \textit{at a shear stress of 200Pa} \quad \textit{4-13}$$

The wall slip velocity was calculated using equation 2-28 from the gradients in Figure 4-9 and plotted as a function of shear stress, as shown in Figure 4-11 (slip velocity was calculated in ms^{-1} and shear stress was calculated in Pa).

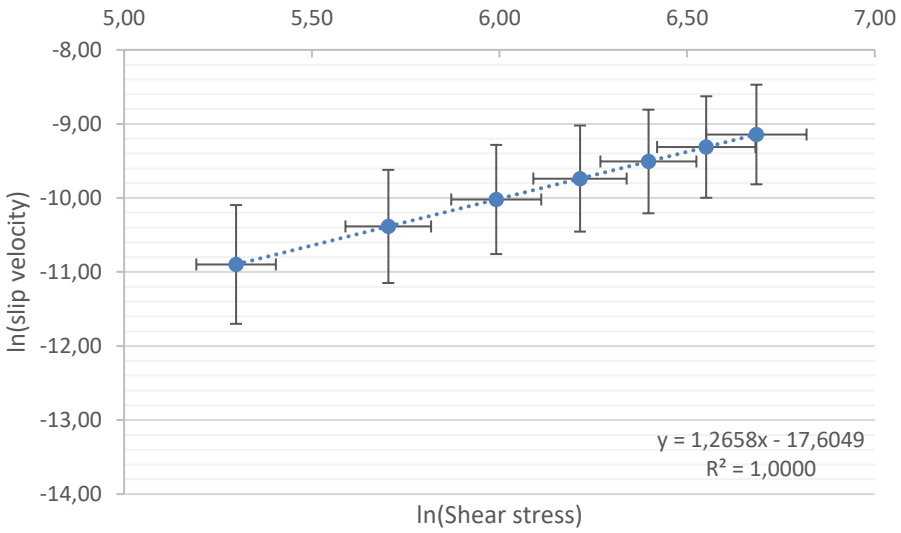

Figure 4-11: Plot of slip velocity as a function of shear stress

The correction for wall slip velocity as a function of shear stress was given by equation 4-14.

$$\ln(u_s) = 1.266 \ln \tau - 17.605 \qquad 4\text{-}14$$

The correction for end effects allowed a corrected shear stress to be calculated based on the pressure loss at a given shear rate, whilst the correction for wall slip allowed the shear rate to be corrected for a given shear stress. The corrected shear stress and shear rate were thus dependent on each other necessitating the use of the solver function to complete the iterative calculation. The massecuite data was thus corrected before plotting of the flow curves and calculation of the flow behaviour index and consistency.

4.2.3 Repeatability tests

Eight massecuite samples were tested using the pipeline viscometer, each at six temperature intervals. No repeatability tests were carried out for the first two massecuite samples, however, the subsequent six samples were tested with repeatability with respect to temperature as shown in Figures 4-12 to 4-17 and Table 7-1 to 7-8 of Appendix 3 (chapter 7.3).

Experiments were first carried out at increasing temperatures (blue markers), then decreasing temperatures (green markers) and once again at increasing temperatures (red markers), with the aim to achieve the same temperature set points along each trajectory.

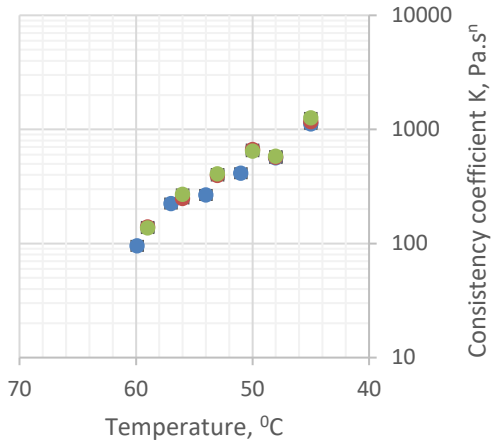

Figure 4-12: Repeatability - sample 20160919

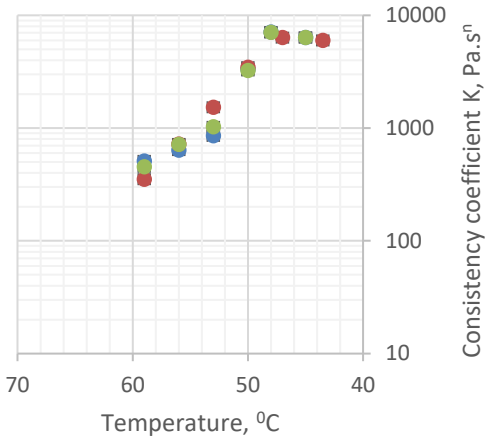

Figure 4-13: Repeatability - sample 20160926

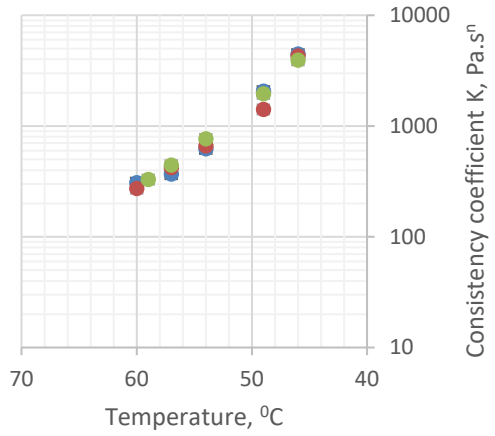

Figure 4-14: Repeatability - sample 20161003

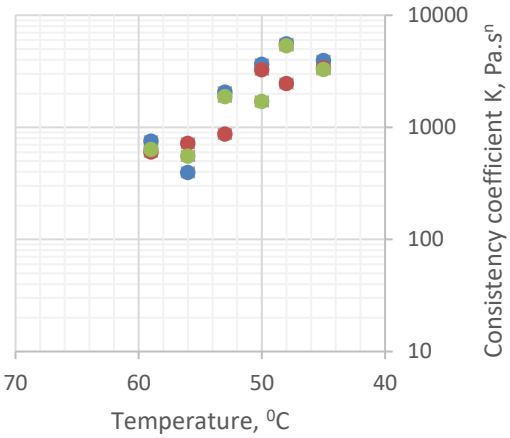

Figure 4-15: Repeatability - sample 20161017

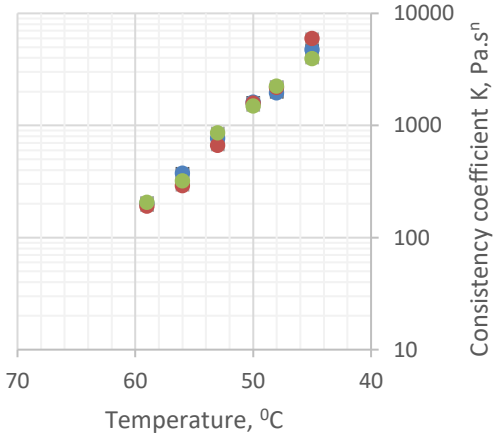

Figure 4-16: Repeatability - sample 20161024

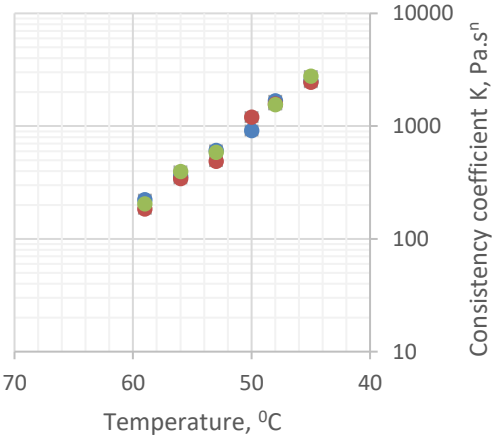

Figure 4-17: Repeatability - sample 20161031

Slight fluctuations in air pressure of up to 2kPa were noted whilst testing sample 20161017, contributing toward poor repeatability as seen in Figure 4-15. The source of fluctuations was attributed to fluctuations in the main header pressure resulting in constant manual pressure regulation in order to achieve a constant pressure.

The deviation of each consistency measurement from the average consistency for each temperature is summarised in Figures 7-103 to Figure 7-108 in Appendix 2 (chapter 7.2). Whilst the individual consistency measurements fluctuated around the average value with a maximum deviation of 35%, the average deviation for each temperature was found to be less than 25% of the average consistency. The variability in results can be attributed to the errors discussed in chapter 3.8 as well as the difficulty in achieving the same temperature set point whilst ramping temperatures up and down where a temperature difference of up to 1^0C may be present in the consistency comparison. One such example was evident in Table 7-3 where massecuite sample 20160919 achieved a temperature of 51°C for run 1 but only 50°C for the subsequent two runs, resulting in a larger deviation in consistency for run 1.

The experiments for each massecuite sample with repeatability were carried out over a period of one week with no concern of breakdown in structure as massecuite is a stable product with a low water content, minimising the possibility of degradation. The retention time of C-massecuite in industrial crystallisers is typically 48hours, with longer retention times common due to breakdowns. A comparison of the consistency results at each temperature as the week progressed did not yield any trends of increasing consistency with time, confirming that no breakdown in structure with time was observed.

Care was taken to ensure massecuite temperatures remained constant for the duration of the flow measurement however massecuite temperature fluctuations of up to 0.5°C were noted as a result of thermal inertia. The massecuite temperature increased slightly at first, followed by a sharp rise in temperature. A similar trend was evident during cooling of massecuite. The temperature set point of the water bath was adjusted manually and required careful attention once the desired massecuite temperature was achieved to prevent temperature drift.

4.3 Experimental results for C-massecuite

4.3.1 Flow behaviour index

The flow behaviour indices for all massecuite samples ranged between 0.8 - 0.9, consistent with the range reported by Awang & White (1976) and Barker (2008). Histograms were recommended as the most effective form of representation of results for data sets greater than 100 (Montgomery & Runger, 1999). A histogram for the flow behaviour index can be seen in Figure 4-18 where the average flow behaviour index

was found to be 0.85. The flow behaviour indices are summarised in Tables 4-1 to 4-9 of Appendix 3 (chapter 7.3)

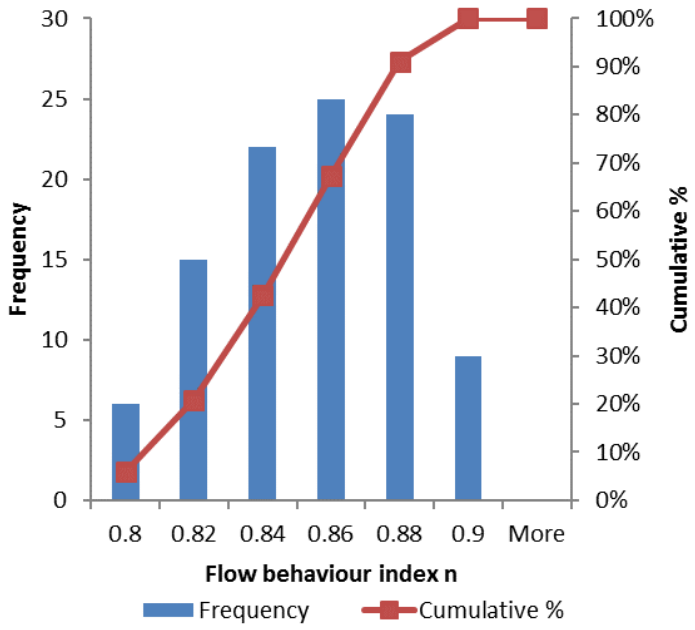

Figure 4-18: Histogram of flow behaviour index

The flow behaviour indices were not seen to fluctuate with temperature, as seen in Figure 4-19, and no observable trend of flow behaviour index with varying physical properties such as dry substance, dextran or crystal content was noted.

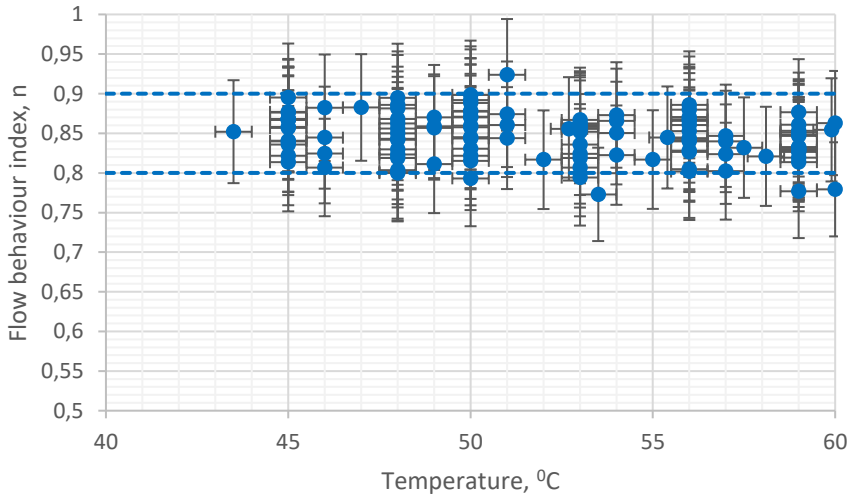

Figure 4-19: Flow behaviour index

4.3.2 Consistency

A histogram of experimental consistencies can be seen in Figure 4-20 where 65% of the consistencies were found to be less than 1000Pa.s^n. The consistencies are summarised in Tables 7-1 to 7-9 of Appendix 3 (chapter 7.3).

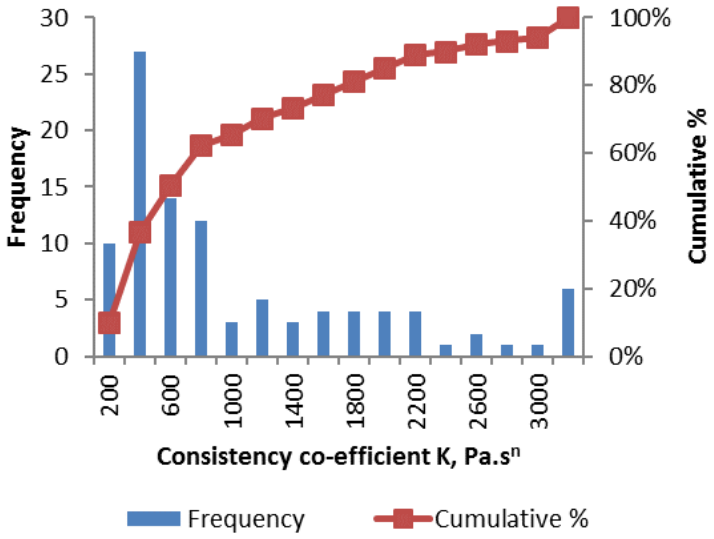

Figure 4-20: Histogram of consistency

4.4 Development of the empirical correlation for apparent viscosity of massecuite

The apparent viscosity of massecuite is written according to equation 4-15.

$$\mu_{apparent} = \frac{\tau}{\gamma} = K\gamma^{n-1} \qquad 4\text{-}15$$

In order to predict the apparent viscosity of massecuite, an average flow behaviour index of 0.85 is recommended to be used. The calculation of the consistency, however, is somewhat more complex.

The massecuite consistency was seen to increase with an increase in dry solids and crystal content and decrease with an increase in temperature. A linear relationship between lnK and lnT can be expected (Perry, 1950) and was evident. All lnK – lnT trends exhibited an average slope of approximately -10.5 units. Evidence of a definite shift in the linear trend of each graph due to inherent massecuite properties can be seen in Figure 4-21 (consistency was measured in Pa.s^n and temperature was measured in °C), resulting in the proposal of an empirical correlation of a linear form (i.e. y= mx + c), as seen in equation 4-16.

$$lnK = (alnT + b)(c) \qquad 4\text{-}16$$

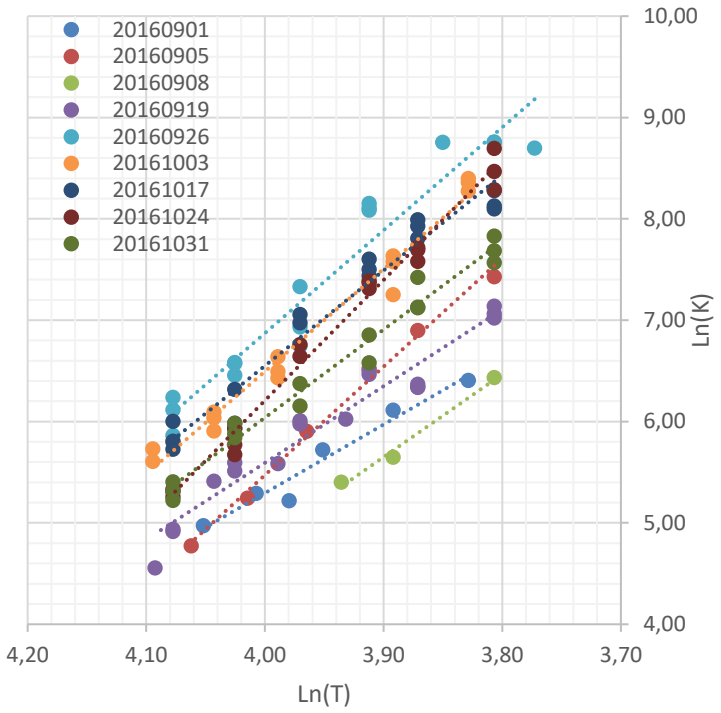

Figure 4-21: Relationship between consistency and temperature

Whilst the gradient of each line was strongly dependent on the natural logarithm of temperature, the vertical shift in the linear relationship for each sample was attributed to changes in either massecuite dry solids or crystal content, or a combination of the above. A term "c" was added to equation 4-16 to account for the vertical shift in each linear trend with varying properties of each sample.

Taking into account the average gradient of -10.5 units from the linear trend seen in Figure 4-21 and the vertical shift in the linear trend of each sample, equation 4-17 was transformed as follows.

$$lnK = (-10.5lnT + b)(c) \qquad 4\text{-}17$$

The "b" and "c" terms describing the intercept and vertical shift in the linear trend were determined using a sensitivity analysis based on the massecuite dry substance, crystal content, massecuite purity and dextran. A coefficient for each variable was assumed and the square of the difference between the experimental and correlated consistencies was calculated and summed. The solver function was used to minimise the sum of the squared errors by optimising the coefficients associated with each variable. The coefficients for massecuite purity and dextran were found to be zero whilst dry substance and crystal content were found

to impact massecuite consistency, with temperature showing the greatest effect. The intercept "b" was found to be a function of massecuite dry solids and the shift in the linear trend "c" was found to be a strong function of crystal content. The proposed empirical correlation for massecuite consistency can be expressed according to equation 4-18 with a regression coefficient of 0.7672.

$$lnK = \left(-10.5lnT + \frac{DS}{1.892}\right)\left(\frac{CC+36}{100}\right) \qquad 4\text{-}18$$

A comparison of the experimental and correlated consistencies can be seen in Figure 4- 22.

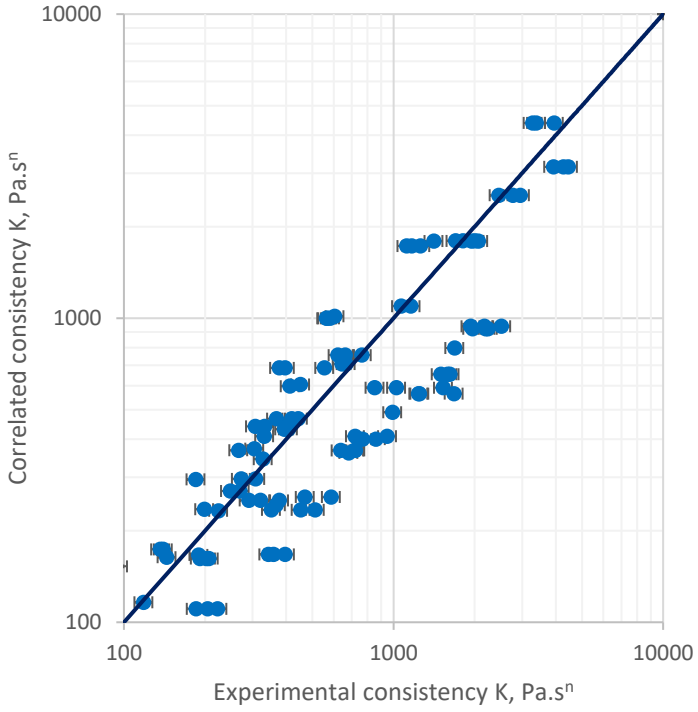

Figure 4-22: Comparison of experimental and calculated consistency

Although no direct relationship was evident between consistency and massecuite purity or dextran, there is a large amount of scatter in the comparison of correlated and experimental consistencies, suggesting that massecuite viscosity remains a function of impurities not taken into account during analyses and is discussed further in section 4.5.2.

Assuming a flow behaviour index of 0.85, the apparent viscosity based on experimental data and the proposed empirical correlation were compared for shear rates of $0.1s^{-1}$ and $1s^{-1}$, and can be seen in Figures 4-23 and 4-24 respectively.

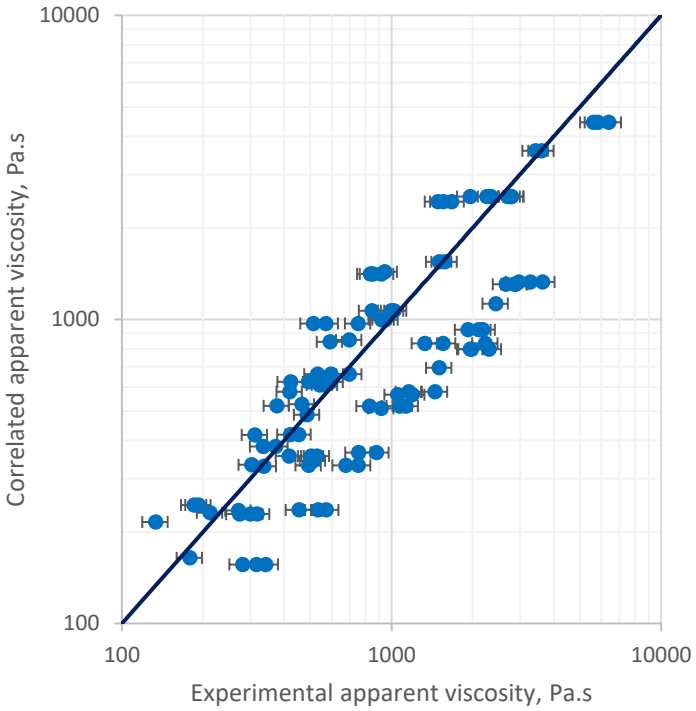

Figure 4-23: Comparison of experimental and calculated apparent viscosities (shear rate of $0.1s^{-1}$)

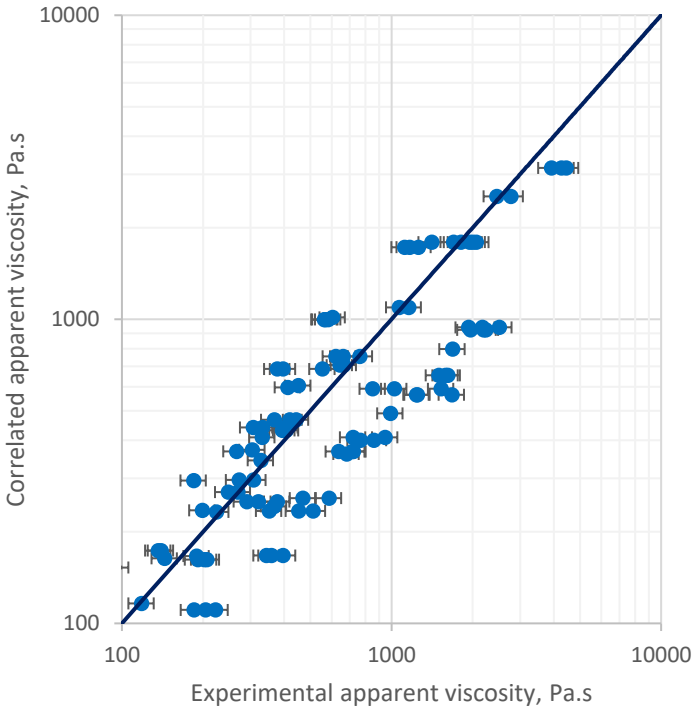

Figure 4-24: Comparison of experimental and calculated apparent viscosities (shear rate of $1s^{-1}$)

A strong linear correlation was found to exist between the consistency and temperature. A weaker correlation was found to exist with massecuite dry solids and crystal content both with co-efficients less than 1. The crystal content was found to account for a shift in the linear trend of the massecuite consistency. The correlated consistencies were compared to experimental data and a statistical analysis was performed.

4.5 Statistical analysis of data

Dependent and independent variables can be classified as either categorical or continuous variables (http://www-users.cs.umn.edu/~ludford/stat_overview.htm). Categorical variables have a finite value whereas continuous variables can take on a range of values, or a continuum, dependent on sampling and measurement procedures or factors outside of the control of the experimental method (Montgomery and Runger, 1999). The independent variables of temperature, concentration and crystal content and the dependent variable, namely the consistency *K*, are all classified as continuous variables. In selecting an appropriate statistical test to analyse the proposed empirical correlation with continuous independent and dependent variables, the Regression test was found to be most appropriate, as shown in Table 4-2 (http://www-users.cs.umn.edu/~ludford/stat_overview.htm).

Table 4-2: Guide for selection of appropriate statistical test

Statistical test selection		Dependent variables	
		Categorical	Continuous
Independent variables	Categorical	Chi square	T test, ANOVA
	Continuous	LDA, QDA	Regression

4.5.1 Regression analysis

A regression analysis allows the adequacy of a model to be assessed using a number of statistical tools. The co-efficient of determination R^2, commonly referred to as the regression coefficient, represents the adequacy of a model and expressed as a function of the total, error and residual sum of squares. A value of 1 represents a perfect linear fit (Montgomery and Runger, 1999) and is calculated using equation 4-19.

$$R^2 = \frac{SS_R}{SS_T} = 1 - \frac{SS_E}{SS_T} \qquad 4\text{-}19$$

A regression analysis of the 102 data points was carried out. The multiple correlation co-efficient, a measure of linearity between the experimental and correlated values, was found to be 0.8759. The R^2 value, or co-efficient of determination, was found to be fairly good at 0.7672 and the standard error was found to be 452 units, as seen in Table 4-3.

Table 4-3: Summary of results for regression analysis of correlation against experimental values

Regression Statistics	
Multiple R	0.8759
R Square	0.7672
Adjusted R Square	0.7649
Standard Error	451.8
Observations	102

4.5.2 Residual plot

The residual is calculated as the difference between the correlated and observed values, plotted against the correlated value. A residual plot with normally distributed errors is expressed by errors mirrored around the x-axis. However, the residual plot for this study seen in Figure 4-25 showed a funnel-shaped scatter of residuals and is indicative of an increasing non-constant error (heteroskedasticity).

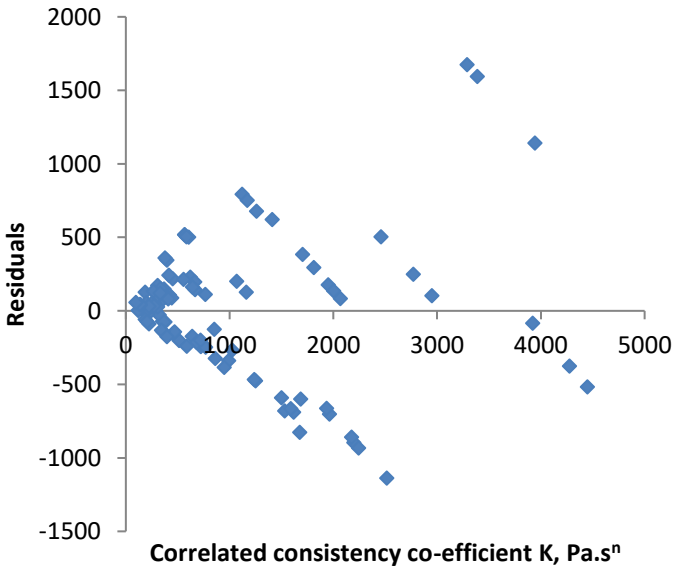

Figure 4-25: Residual plot

Heteroskedasticity is believed to be caused by the impact of an unmeasured parameter on massecuite consistency that was not analysed for during experimentation and is thus unaccounted for in the proposed empirical correlation.

The observed deviation can be attributed to the presence of gums, reducing sugars and ash (Rouillard, 1983). Whilst the dextran content did not correlate well with massecuite consistency, is still reported as an

important factor in molasses and thus massecuite viscosity (Rein, 2007). The inclusion of a combination of these parameters could allow for the development of a more accurate massecuite consistency correlation.

4.6 Sensitivity analysis with respect to temperature, dry solids and crystal content

Table 4-4 illustrates the effect of each parameter on C-massecuite consistency resulting from the proposed empirical correlation. A strong dependence on temperature and dry solids can be seen and a weaker dependence on crystal content.

Table 4-4: Sensitivity of massecuite consistency correlation

Temperature, °C	Massecuite Dry Solids, %	Crystal content, %	Consistency K, $Pa.s^n$
Sensitivity with respect to massecuite temperature			
45	93	30	429
46	93	30	368
47	93	30	317
48	93	30	274
49	93	30	238
Sensitivity with respect to massecuite dry solids			
50	**91**	30	103
50	**92**	30	146
50	**93**	30	207
50	**94**	30	293
50	**95**	30	415
Sensitivity with respect to crystal content			
50	93	**28**	176
50	93	**29**	191
50	93	**30**	207
50	93	**31**	224
50	93	**32**	243

4.7 Comparison of experimental results with Rouillard (1984)

The viscosity data published by Rouillard (1984) assumed a dependence on only temperature and not shear rate and is thus comparable to experimental results for a shear rate of $1s^{-1}$ i.e. when massecuite consistency is equal to massecuite viscosity. Assuming a shear rate of $1s^{-1}$, the experimental massecuite viscosities (represented by data points) were superimposed on the range of C- massecuite viscosity published by Rouillard (1984) (represented by two solid lines), as shown in Figure 4-26. A strong correlation between experimental massecuite viscosity and temperature was found, with an R^2 value of 0.64.

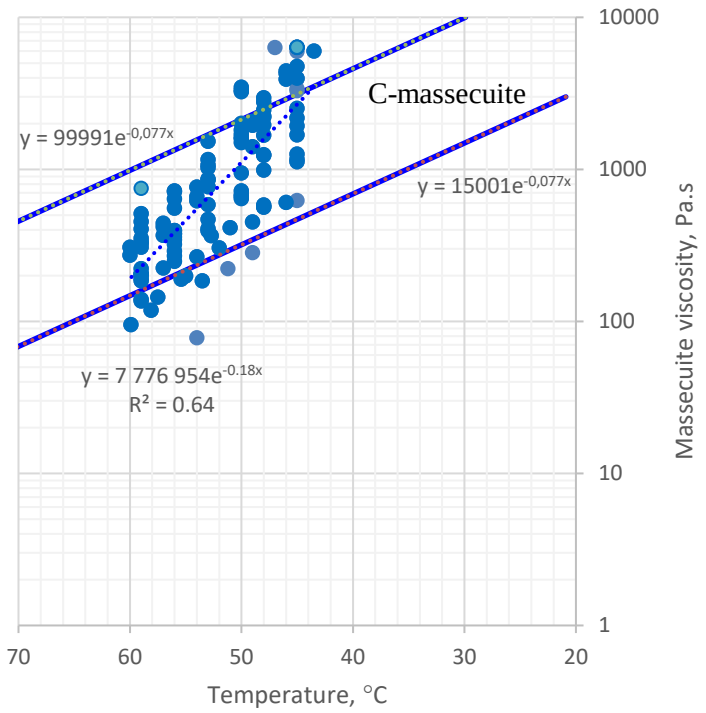

Figure 4-26: Experimental results compared to published range from Rouillard (1984) (shear rate of $1s^{-1}$)

The upper and lower limits for C-massecuite viscosity are shown in Figure 4-26 as two solid lines (adapted from Figure 2-9 for C-massecuite) and was based on the viscosity chart developed by Rouillard (1984). The current practice involves the graphical determination of the upper and lower-limits for C-massecuite viscosity at the desired temperature using Figure 2-9 developed by Rouillard (1984), allowing a sensible estimate to be made thereafter. The upper and lower limits for C-massecuite viscosity, as recommended by Rouillard (1984), can be represented by equation 4-20 and 4-21 respectively, as a function of temperature.

$$\mu_{\text{upper limit}} = 99991e^{-0.077T} \qquad 4\text{-}20$$

$$\mu_{\text{lower limit}} = 15001e^{-0.077T} \qquad 4\text{-}21$$

The experimental data was found to fit within the band of values as represented by Rouillard (1984) confirming that the band currently used and represented by two solid lines is appropriate, however, the rate of increase in viscosity with decreasing temperature was found to be greater than the prediction from Rouillard (1984) as represented by the dotted lines in Figures 4-26 and 4-27.

Based on the experimental results, a new upper limit and a new lower limit for C-massecuite viscosities can be used, as shown by the dotted lines in Figure 4-27 and represented by equation 4-22 and 4-23 respectively, as a function of temperature.

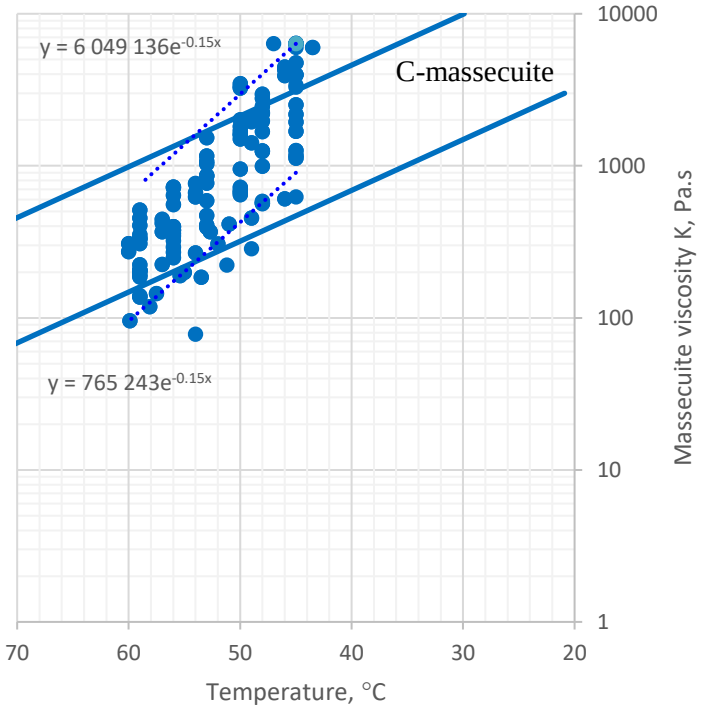

Figure 4-27: Experimental results compared to published range from Rouillard (1984) with proposed upper and lower limits (shear rate of $1s^{-1}$)

In order to apply the upper and lower limit equations to various shear rates, the proposed equations (4-22 and 4-33) are thus presented in terms of consistency rather than viscosity.

$$K_{\text{upper limit}} = 6\ 049136e^{-0.15T} \qquad 4\text{-}22$$

$$K_{\text{lower limit}} = 765\ 243e^{-0.15T} \qquad 4\text{-}23$$

4.7.1 Improvement in estimating C-massecuite viscosity

C-massecuite viscosity is currently obtained using Figure 2-9, a viscosity chart developed by Rouillard (1984) assuming non-Newtonian behaviour of massecuite, assuming a dependence on temperature only and is thus applicable only for shear rates of $1s^{-1}$. The proposed method of obtaining C-massecuite viscosity is to acknowledge the pseudoplastic nature of massecuite and utilise the power law model to calculate the

apparent viscosity, as shown in equation 2-33 using an estimate for the flow behaviour index and consistency.

The flow behaviour index was assumed to be 0.85 and the consistency can be predicted using the empirical correlation as per equation 4-18. Due to the variation in results, a sense check can be carried out by using equations 4-22 and 4-23 to ensure the viscosity estimate is within the correct range.

CHAPTER 5: CONCLUSION

The rotating viscometer is extremely popular within the sugar industry and is highly accurate for sugar cane juice exhibiting Newtonian behaviour, however, little confidence exists with the results obtained from measurements made with massecuite. Massecuite is classified as a pseudoplastic fluid, but was reported to approach Newtonian behaviour at higher shear rates. Massecuite fluid behaviour was best described using the power law model as seen in equation 2-2 (Adkins, 1951; Behne, 1964; Awang and White, 1976 and Broadfoot and Miller, 1990) where the apparent viscosity is expressed as a function of shear rate, flow behaviour index and consistency.

Despite a wide range of correlations and viscosity charts available for the determination of C-massecuite viscosity, most massecuite viscosity measurements were carried out using rotating viscometry and thus possessed an inherent uncertainty due to the interaction and displacement of crystals around the rotating spindle (Behne, 1964). Whilst the rotational viscometer was accepted as the ICUMSA standard technique for measurement of molasses viscosity, no standard technique was available for massecuite viscosity measurement (Ananta et al., 1989). Nonetheless, of the correlations developed using the rotating viscometer, the correlations most widely used are those of Broadfoot et al. (1998) which included a correlation for molasses consistency (equation 2-58) and the modified Awang and White correlation and modified Metzler correlation with re-fitted coefficients (equations 2-59 and 2-60, respectively).

The pipeline viscometer was shown to be a reliable method of viscometry but with few correlations developed using this method of viscometry. The correlation proposed by Ness (1980) did not take into account the effects of temperature and the correlation proposed by Bruhns (2004) was dependent on the accuracy of the molasses viscosity correlation utilised.

In order to improve upon the estimation of C-massecuite viscosity, a pipeline viscometer was designed, constructed and validated using final molasses measurements from a rotating Brookfield viscometer. Results from the pipeline viscometer were found to correlate well with the Brookfield viscometer for molasses measurements, with good agreement between the flow behaviour indices. The consistencies for the pipeline viscometer were found to be acceptable ranging between 95% to 105% of the Brookfield viscometer figures.

Eight massecuite samples were tested using the pipeline viscometer, each at six temperature intervals and taking into account a correction for end effects and wall slip. No repeatability tests were carried out for the first two massecuite samples, however, the subsequent six samples were tested with repeatability with respect to temperature. The flow behaviour index for C-massecuite was found to lie between 0.8 and 0.9,

consistent with the findings of Awang and White (1976) and Barker (2008), with an average value of 0.85 recommended for use. An empirical correlation (equation 4-18) was proposed for massecuite consistency as a function of temperature, dry substance and crystal content with a regression co-efficient of 0.7672, and with dry substance calculated according to equation 2-40.

The proposed empirical correlation for massecuite consistency was found to be weakly dependent on massecuite dry substance and crystal content, with temperature showing the greatest effect. Although no direct relationship was evident between consistency and massecuite purity or dextran, there is a large amount of scatter in the comparison of correlated and experimental consistencies, suggesting that massecuite viscosity remains a function of impurities not taken into account during analyses.

The experimental results were compared to the range of C-massecuite viscosities recommended by Rouillard (1984) as seen in Figure 2-9. Assuming a shear rate of $1s^{-1}$, the experimental viscosities were found to fit within the range of C-massecuite viscosities recommended by Rouillard (1984) as shown in Figure 4-26, confirming that the band currently used in Figure 2-9 was appropriate and the experimental results were within the expected viscosity range. However, the rate of increase in viscosity with decreasing temperature was found to be greater than the prediction from Rouillard (1984). Based on the experimental results and in conjunction with the viscosity chart proposed by Rouillard (1984), a new upper limit and a new lower limit for C-massecuite consistency were proposed as shown by the dotted lines in Figure 4-27 and equations 4-22 and 4-23 respectively, and can be used to assist with estimation of C-massecuite viscosity.

Whilst the residual plot does indicate the presence of an unmeasured parameter impacting on the experimental massecuite consistency, the proposed empirical correlation as shown in equation 4-18 remains an improvement upon the manual estimation of massecuite viscosity currently employed, facilitating capital savings in the back end of a sugar mill.

CHAPTER 6: REFERENCES

Ackermann, N. L. & Shen, H. T., 1979. Rheological characteristics of solid-liquid mixtures. *AIChE Journal,* Volume 25, pp. 327 - 332.

Adkins, B. G., 1951. Notes on the viscosity of molasses and massecuite. *Proc. Qd. Soc. Sugar Cane Technol.,* Volume 18, pp. 43-52.

Ananta, T., Delavier, H. J., Kamarijani & Mugiono, 1989. The applicability of rotational viscometers to measure rheological properties of massecuites. *Proc. Int. Soc. Sugar Cane Technol.,* Volume 20, pp. 78-88.

Anon., 2005. *Laboratory manual for South African Sugar Factories.* 4th ed. Mount Edgecombe: South African Sugar Technologists' Association.

Anon., n.d. *An overview: Choosing the correct statistical test.* [Online]
Available at: http://www-users.cs.umn.edu/~ludford/stat_overview.htm
[Accessed April 2017].

Artyukhov, Y. G. & Garyazha, V. T., 1970. Rheology of massecuites. *Izvest. VUZ. Pisch Tekhnol.,* Volume 4, pp. 157-162.

Awang, M. & White, E. T., 1976. Effect of crystal on the viscosity of massecuites. *Proc. Qd. Soc. Sugar Cane Technol.,* Volume 43, pp. 263-270.

Bagley, E. B., 1957. End corrections in the capillary flow of polyethylene. *Journal of applied physics,* Volume 28, pp. 624-627.

Barker, B., 1998. Theoretical and practical considerations on the rheology of sugar products. *Proc. S. Afr. Sugar Technol. Ass.,* Volume 72, pp. 300-305.

Barker, B., 2008. Massecuite consistency measurement using a pipeline viscometer. *Proc. S. Afr. Sugar Technol. Ass.,* Volume 81, pp. 227-233.

Barnes, H. A., 2000. *A handbook of elementary rheology.* Wales: Penglais.

Bauer, W. H., Weber, N. & Wiberley, S. E., 1958. Entrance effects in capillary flow of Aluminium Dilaurate-Toluene gas. *J. Phys. Chem,* 62(10), pp. 1245-1247.

Bird, R. B., Stewart, W. E., Lightfoot, E. N. 2002. *Transport Phenomena*. 2nd ed. USA: John Wiley & Sons, Inc

Behne, M. F., 1964. Viscometry in massecuites. *Proc. Qd. Soc. Sugar Cane Technol.,* Volume 31, pp. 289-296.

Bernouilli, D., 1738. *Hydrodynamica.* Strasbourg: Dulseker.

Broadfoot, R., 1984. Viscosity limitations on massecuite exhaustion. *Proc. Aust. Soc. Sugar Cane Technol.,* Volume 6, pp. 279-286.

Broadfoot, R. & Miller, K. F., 1990. Rheological studies of massecuites and molasses. *International Sugar Journal,* 92(1098), pp. 107-146.

Broadfoot, R., Miller, K. F. & McLaughlin, R. L., 1998. Rheology of high grade massecuites. *Proc. Aust. Soc. Sugar Cane Technol.,* Volume 20, pp. 388-397.

Broadfoot, R. & Steindl, R. J., 1980. Solubility - crystallisation characteristics of Queensland molasses. *Proc. Int. Soc. Sugar Cane Technol.,* Volume 17, pp. 2557-2581.

Bruhns, M., 2004. The viscosity of massecuite and its suitability for centrifuging. *Zuckerindustrie Journal,* 29(12), pp. 853-863.

Chhabra, R. P. & Richardson, J. F., 2008. *Non-Newtonian flow and applied rheology.* 2nd ed. Oxford: Butterworth-Heinemann.

Daugherty, R. L., Franzini, J. B. & Finnemore, E. J., 1989. *Fluid Mechanics with Engineering Applications.* 8th ed. Singapore: McGraw-Hill.

Doraiswamy, D., 2002. The origins of rheology: A short historical excursion. *Rheology Bulletin,* 71(1), p. 7.

Durgueil, E. J., 1987. Determination of the consistency of non-Newtonian fluids using a Brookfield HBT viscometer. *Proc. S. Afr. Sugar Technol. Ass.,* Volume 61, pp. 32-39.

Echeverri, L. F., Rein, P. W. & Acharya, S., 2005. Numerical and experimental study of the flow in vacuum pans. *Int. Soc. Sugar Cane Technol.,* Volume 25, pp. 212-228.

Einstein, A., 1906. A new determination of molecular dimensions. *Annalen der Physik,* Volume 19, pp. 289-305.

Eisenschitz, R., Rabinowitsch, B. & Weissenberg, K., 1929. *Mittil.-dtsch. Mat. Pruf. Anst.,* 9(91).

Frankel, N. A. & Acrivos, A., 1967. On the viscosity of a concentrated suspension of solid spheres. *Chemical Engineering Science,* 22(6), pp. 847-853.

Gan, Y. X., 2012. *Continuum mechanics: Progress in fundamentals and engineering applications.* Croatia: Rijeka.

Genotelle, J., 1978. *Ind. Aliment. Agric.,* Volume 95, pp. 747-755.

Hagen, G., 1839. Ueber die Bewegung des Wassers in engen cylindrischen Röhren. *Annalen der Physik und Chemie,* 122(3), pp. 423-442.

Holland, F. A. & Bragg, R., 1995. *Fluid flow for Chemical Engineers.* Oxford: Butterworth Heinemann.

Jastrzebski, Z. D., 1967. Entrance effects and wall effects in an extrusion rheometer during the flow of concentrated suspensions. *Ind. Engng. Chem. Fund.,* 6(3), pp. 445-454.

Kadlec, P., Bretschneider, R. & Bubnik, Z., 1983. Measurement and computation of physio-chemical properties of sugar solutions. *Chem. Eng. Commun.,* Volume 21, pp. 263-270.

Keast, W. J. & Sichter, N. J., 1984. Vertical continuous crystallizer - Victoria mill. *Proc. Aust. Soc. Sugar Cane Technol.,* Volume 6, pp. 293-299.

Kelly , F. H. C. & McAntee, H., 1942. The viscosity of molasses and massecuite. *Proc. Qld. Soc. Sugar Cane Technol.,* Volume 13, p. 51.

Kelly, F. H. C., 1958. Viscosity of crystal suspensions. *Sharkara,* Volume 1, pp. 37-45.

Kot, Y. D., Yasinshaya, T. V. & Sushenko, A. K., 1968. Viscous properties of massecuites. *Sakh. Prom.,* pp. 106-125.

Lionnet, G. R. E. & Pillay, M., 2006. Applications of capillary viscometry in cane sugar factories. *Proc. S. Afr. Sugar Technol. Ass.,* Volume 80, pp. 371-377.

Love, D. J., 2002. Estimating dry solids and true purity from brix and apparent purity. *Proc. S. Afr. Sugar Technol. Ass.,* Volume 76, pp. 526-532.

Maron, S. & Pierce, P., 1956. Application of ree-eyring generalized flow theory to suspensions of spherical particles. *J. Colloid. Sci.,* Volume 11, pp. 80 - 95.

Mathlouthi, M. & Kasprzyk, P., 1984. Viscosity of sugar solutions. *Sugar Technology Reviews,* Volume 11, pp. 209-257.

Maudarbocus, S. M. R., 1980. The orifice viscometer: A new technique for measuring rheological properties of massecuites and molasses. *Proc. Int. Soc. Sugar Cane Technol.,* Volume 17, pp. 2257-2263.

Messaâdi, A., Dhouibi, N., Hamda, H., Belgacem, F.B.M., Adbelkader, Y.H., Ouerfelli, N. & Hamzaoui, A.H., 2015. A new equation relating the Viscosity Arrhenius Temperature and the Activation Energy for some Newtonian classical solvents. *Journal of Chemistry,* Volume 2015.

Metzler, E., 1996. *Rheology of suspensions at high solids concentrations.* Brisbane: Thesis for bachelor of engineering, The University of Queensland.

Micheli, L. I. A. & De Gyulay, O. S., 1938. Viscosity-supersaturation relationship of industrial sugar solutions. *Proc. Int. Soc. Sugar Cane Technol.,* Volume 6, pp. 1094-1107.

Montgomery, D. C. & Runger, G. C., 1999. *Applied statistics and probability for engineers.* 2nd ed. New York: John Wiley & Sons.

Mooney, M., 1931. *J. Rheol.,* Volume 2, p. 210.

Mueller, S., Llewellin, E. W. & Mader, H. M., 2011. The effect of particle shape on suspension viscosity and implications for magmatic flows. *Geophysical Research Letters,* 38(13).

Ness, J. N., 1980. Massecuite viscosity - some observations with a pipeline viscometer. *Proc. Aust. Soc. Sugar Cane Technol.,* Volume 2, pp. 195-200.

Ness, J. N., 1983. On the measurement of massecuite flow properties. *Proc. Aust. Soc. Sugar Cane Technol.,* Volume 18, pp. 1295-1303.

Ness, J. N., 1984. Viscometry in cane sugar processing. *Proc. Aust. Soc. Sugar Cane Technol.,* Volume 6, pp. 271-277.

Newell, G. M., 1979. A preliminary investigation into factors affecting gas formation in massecuite and molasses. *Proc. S. Afr. Sugar Technol. Ass.,* Volume 53, pp. 62-65.

Pascal, B., 1663. *Traites de l'equilibre des liqueres et de la pesanteur de la masse de l'air.* Paris: s.n.

Peacock, S. D., 1995. *Selected physical properties of sugar factory process streams,* Durban: Sugar Milling Research Institute Technical report no. 1714.

Perry, J. H., 1950. *Chemical Engineers' Handbook.* 3rd ed. New York: McGraw-Hill.

Poiseuille, J. L., 1841. *Comptes Rendus,* Volume 12, p. 112.

Rein, P., 2007. *Cane Sugar Engineering.* Berlin: Verlag Dr Albert Bartens KG.

Rouillard, E. E. A., 1981. *The measurement of the rheological properties of molasses and massecuite using the Brookfield viscometer,* Durban: Sugar Milling Research Institute Technical report no. 1279.

Rouillard, E. E. A., 1983. *A study of boiling parameters under conditions of laminar non-Newtonian flow with particular reference to massecuite boiling,* Durban: Sugar Milling Research Institute Report No. 1341.

Rouillard, E. E. A., 1984. *Viscosity of factory products,* Durban: Sugar Milling Research Institute Technical report no. 1375.

Rouillard, E. E. A., 1985. *The study of boiling parameters under conditions of laminar non-Newtonian flow with particular reference to massecuite boiling.* Durban: PhD thesis, University of Natal.

Rouillard, E. E. A. & Koenig, M. F. S., 1980. The viscosity of molasses and massecuite. *Proc. S. Afr. Sugar Technol. Ass.,* Volume 54, pp. 89-92.

Schramm, G., 2000. *A practical approach to rheology and rheometry.* 2nd ed. Federal Republic of Germany: Gebrueder HAAKE GmbH.

Schwedoff, T., 1890. *J. Physique,* 2(9), p. 34.

Seeton, C. J., 2006. Viscosity - temperature correlation for liquids. *Tribology Letters,* 22(1), pp. 67-78.

Silina, N., 1953. Viscosity of massecuite. *Sakhar. Prom.,* Volume 8, pp. 4-10.

Walford, S. N., 1996. Composition of cane juice. *Proc. S. Afr. Sugar Technol. Ass.,* Volume 70, pp. 265-266.

Wertz, J., Bedue, O. & Mercier, J. P., 2010. *Cellulose Science and Technology.* Italy: EPFL Press.

CHAPTER 7: APPENDICES

7.1 Appendix 1: Proof of parabolic velocity profile (Holland & Bragg, 1995)

Fully developed flow is characterised by a parabolic flow profile and can be illustrated using a momentum balance across an infinitesimally small cylindrical element δr, as shown in Figure 2-1.

As outlined by Holland & Bragg (1995), the shear stress on the outer surface of the fluid element acts in the negative x direction as a result of the force due to the upstream pressure P_1. The shear stress on the inner surface of the fluid element acts in the positive x direction as a result of the force due to the downstream pressure P_2.

The fluid momentum is conserved and the net force acting on the fluid is thus zero (Holland & Bragg, 1995).

$$2\pi r\delta r.P_1 + 2\pi(r+\delta r)L.\tau \Big|_{r+\delta r} = 2\pi r\delta r.P_2 + 2\pi rL.\tau \Big|_r \quad \textit{7-1}$$

$$\frac{r\tau \Big|_r - (r+\delta r)\tau \Big|_{r+\delta r}}{r\delta r} = \frac{P_1 - P_2}{L} \quad \textit{7-2}$$

$$\lim_{\delta r \to 0}\left(\frac{r\tau \Big|_r - (r+\delta r)\tau \Big|_{r+\delta r}}{r\delta r}\right) = \frac{P_1 - P_2}{L} \quad \textit{7-3}$$

$$-\frac{1}{r}\frac{d}{dr}(r\tau) = \frac{P_1 - P_2}{L} \quad \textit{7-4}$$

$$-\tau = \left(\frac{P_1 - P_2}{L}\right)\frac{r}{2} + \frac{A_1}{r} \quad \textit{7-5}$$

The constant of integration A_1 is zero as the shear stress is required to be finite at r = 0 (Holland & Bragg, 1995), resulting in equation 7-6.

$$-\tau = \left(\frac{P_1 - P_2}{L}\right)\frac{r}{2} \quad \textit{7-6}$$

Substituting equation 2-1 into equation 7-6 yields equation 7-7.

$$-\mu.\gamma = \left(\frac{P_1 - P_2}{L}\right)\frac{r}{2} \qquad 7\text{-}7$$

$$-\mu.\frac{du}{dr} = \left(\frac{P_1 - P_2}{L}\right)\frac{r}{2} \qquad 7\text{-}8$$

$$-\mu.du = \left(\frac{P_1 - P_2}{L}\right)\frac{r}{2}.dr \qquad 7\text{-}9$$

$$-\mu.u = \left(\frac{P_1 - P_2}{L}\right)\frac{r^2}{4} + B \qquad 7\text{-}10$$

Applying the boundary condition $u = 0$ at $r = r_i$

$$u = \frac{1}{4\mu}\left(\frac{P_1 - P_2}{L}\right)\left(r_i^{\,2} - r^2\right) \qquad 7\text{-}11$$

Equation 7-11 thus represents a parabolic velocity profile.

7.2 Appendix 2: Massecuite flow curves

For figure 7-1 to 7-102, shear stress was calculated in Pa and shear rate was calculated in s^{-1}.

7.2.1 Sample 20160901

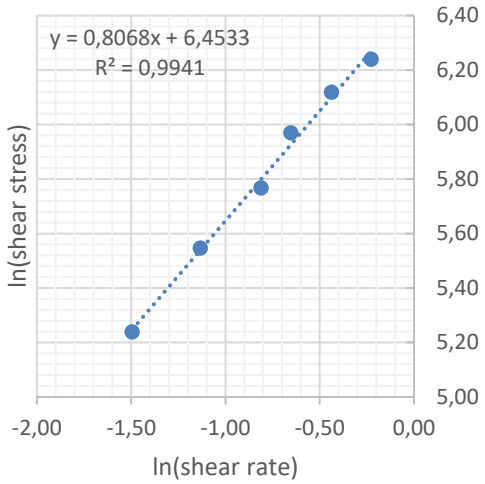

Figure 7-1: Sample 20160901 at 46°C

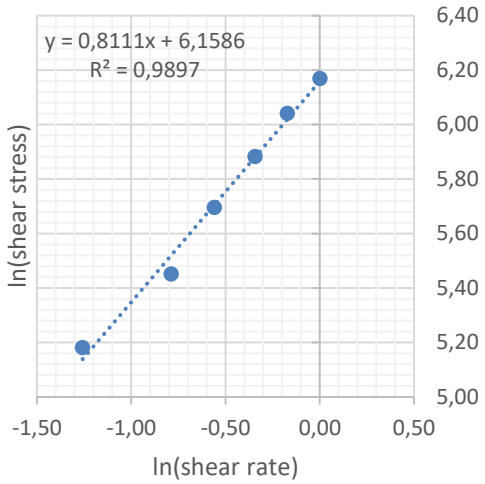

Figure 7-2: Sample 20160901 at 49°C

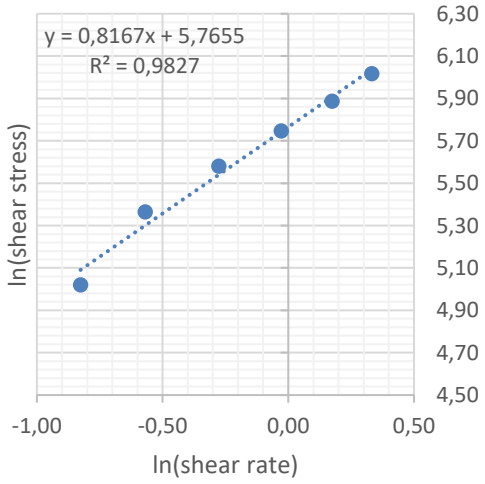

Figure 7-3: Sample 20160901 at 52°C

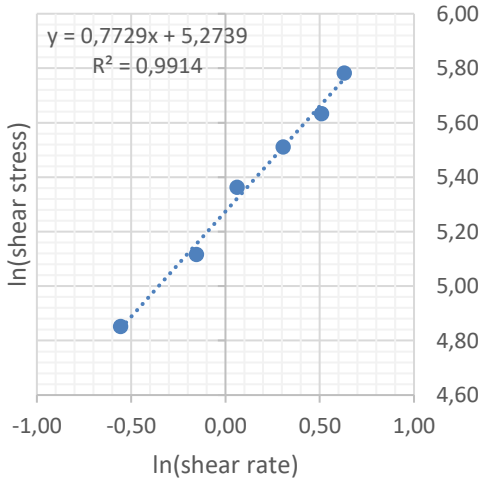

Figure 7-4: Sample 20160901 at 53.5°C

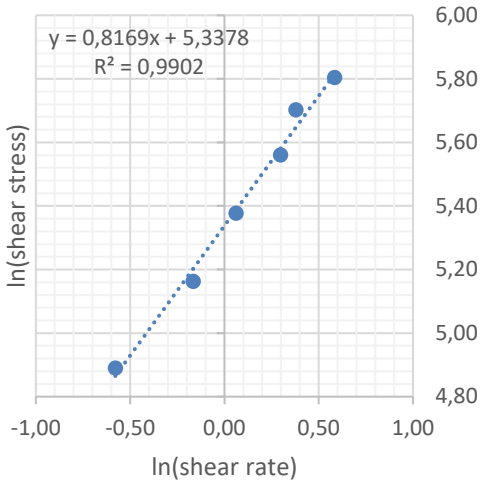

Figure 7-5: Sample 20160901 at 55°C

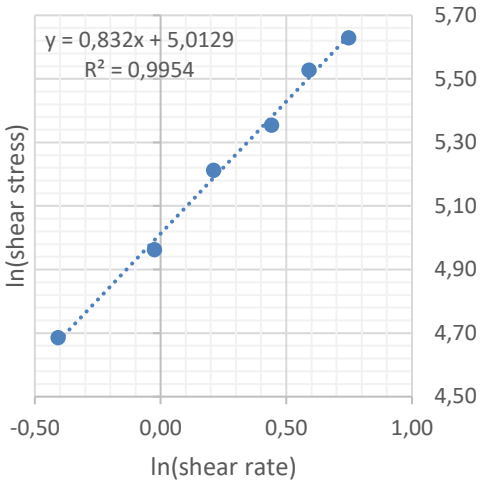

Figure 7-6: Sample 20160901 at 57.5°C

7.2.2 Sample 20160905

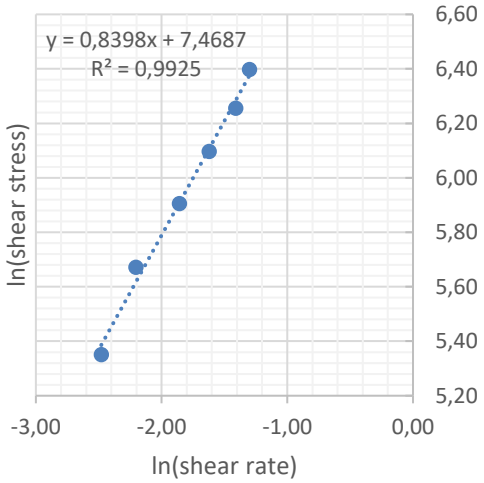

Figure 7-7: Sample 20160905 at 45°C

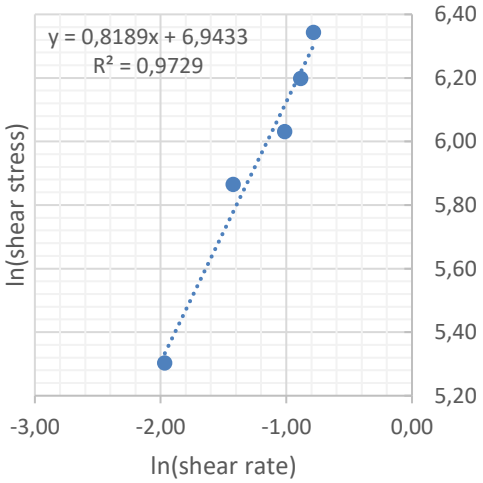

Figure 7-8: Sample 20160905 at 48°C

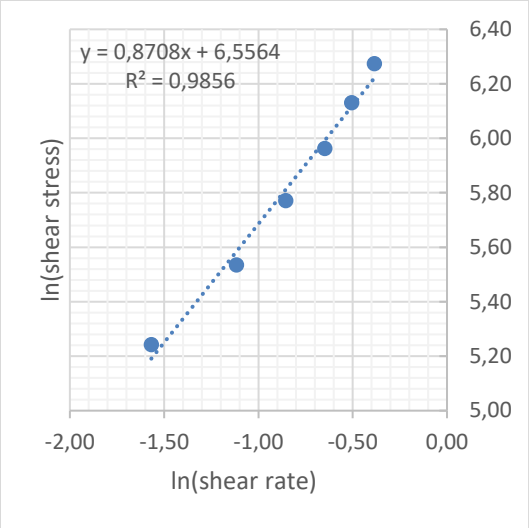

Figure 7-9: Sample 20160905 at 50°C

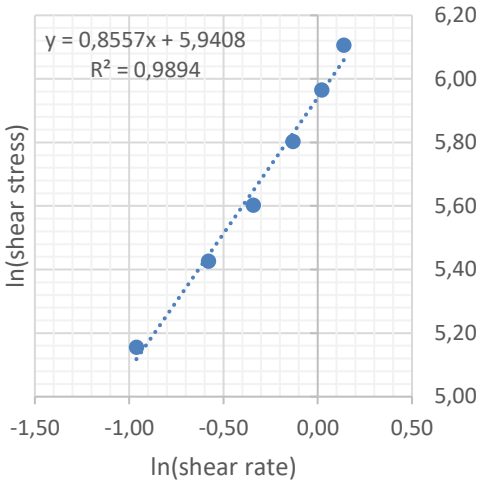

Figure 7-10: Sample 20160905 at 52.7°C

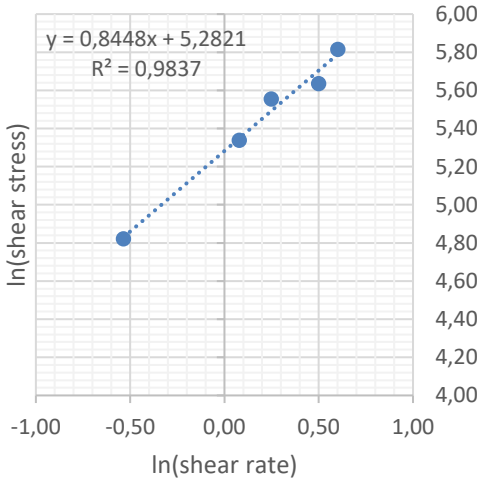

Figure 7-11: Sample 20160905 at 55.4°C

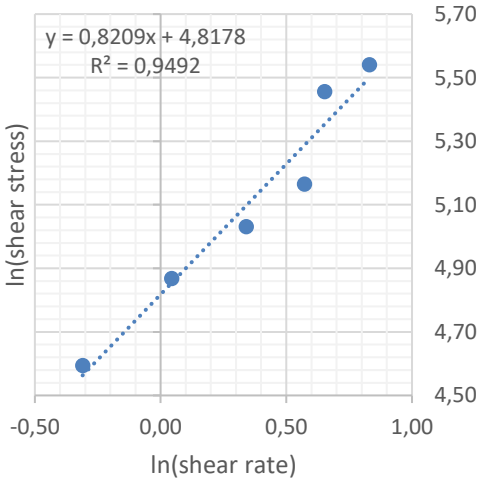

Figure 7-12: Sample 20160905 at 58.1°C

7.2.3 Sample 20160919

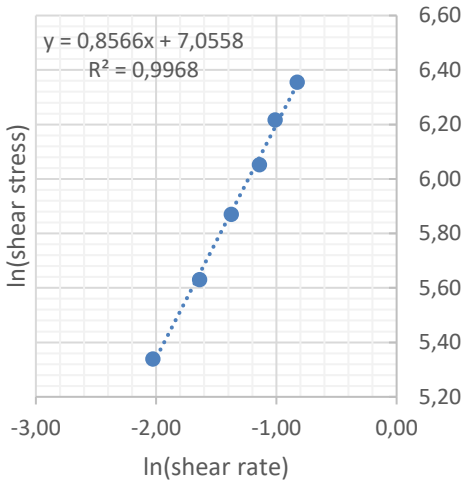

Figure 7-13: Sample 20160919 at 45°C

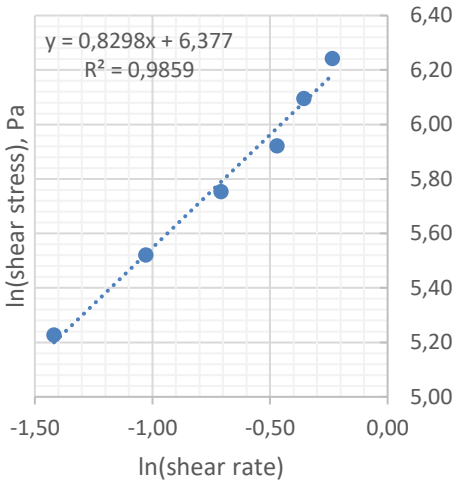

Figure 7-14: Sample 20160919 at 48°C

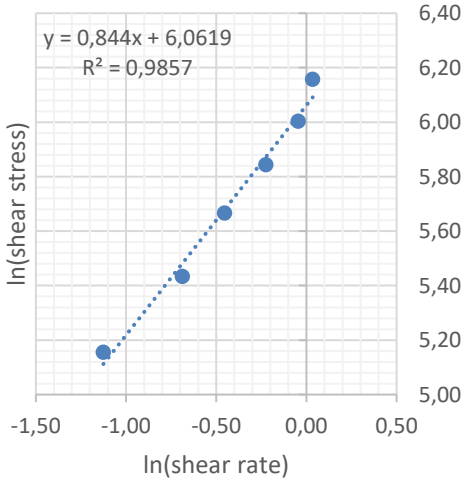

Figure 7-15: Sample 20160919 at 51°C

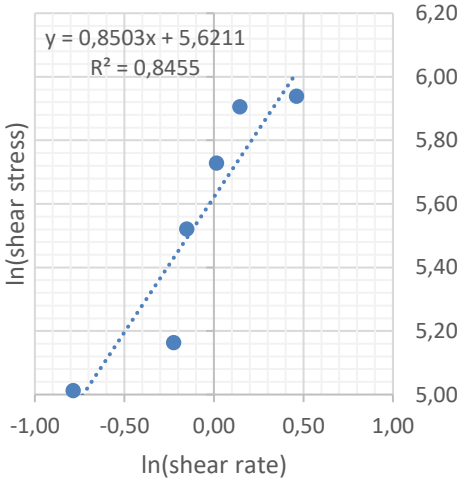

Figure 7-16: Sample 20160919 at 54°C

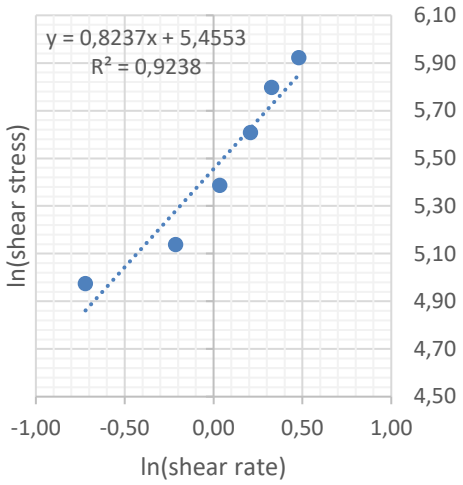

Figure 7-17: Sample 20160919 at 57°C

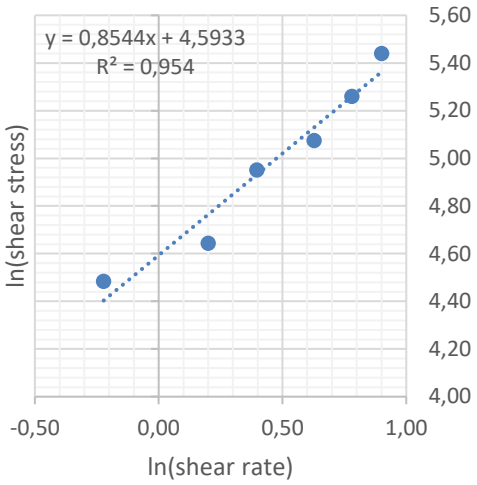

Figure 7-18: Sample 20160919 at 60°C

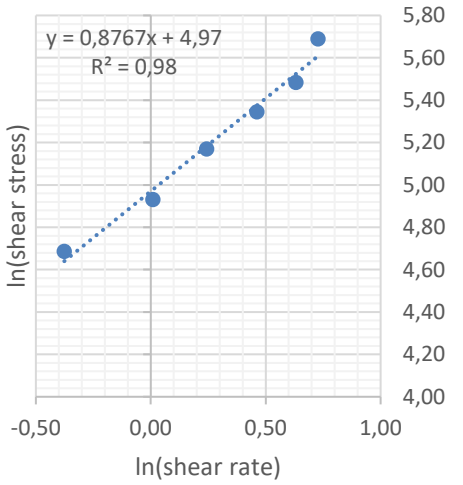

Figure 7-19: Sample 20160919 at 59°C

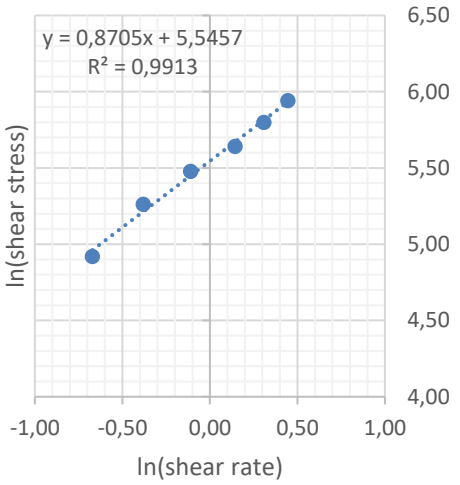

Figure 7-20: Sample 20160919 at 56°C

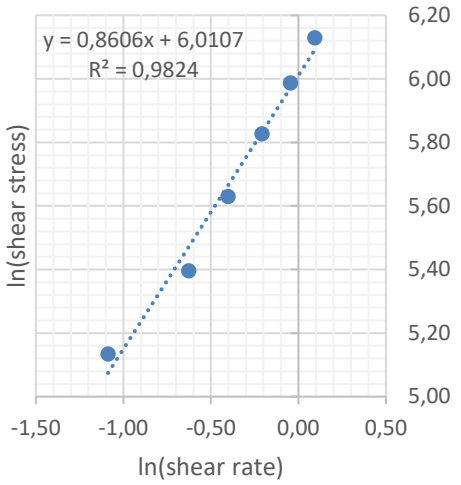

Figure 7-21: Sample 20160919 at 53°C

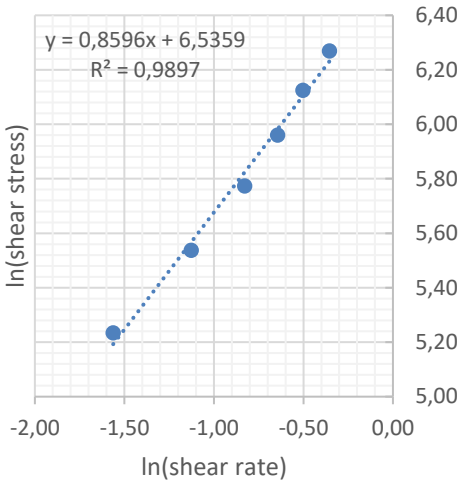

Figure 7-22: Sample 20160919 at 50°C

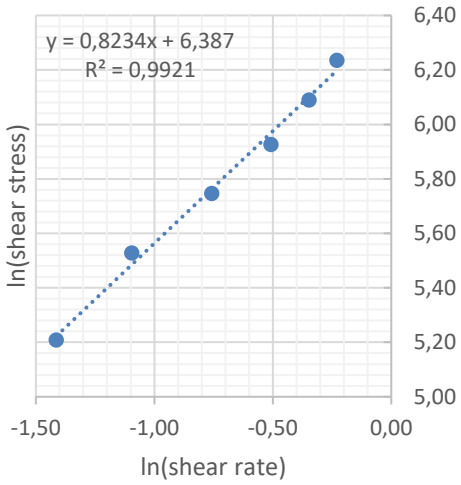

Figure 7-23: Sample 20160919 at 48°C

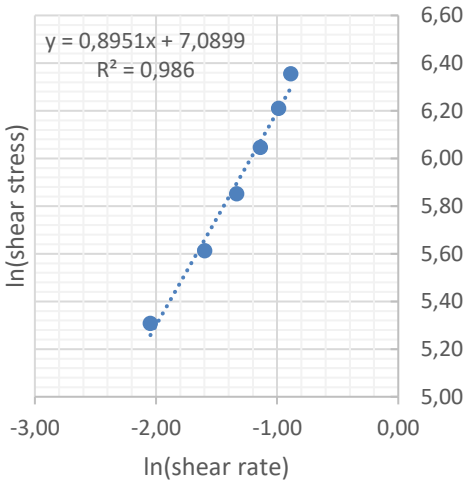

Figure 7-24: Sample 20160919 at 45°C

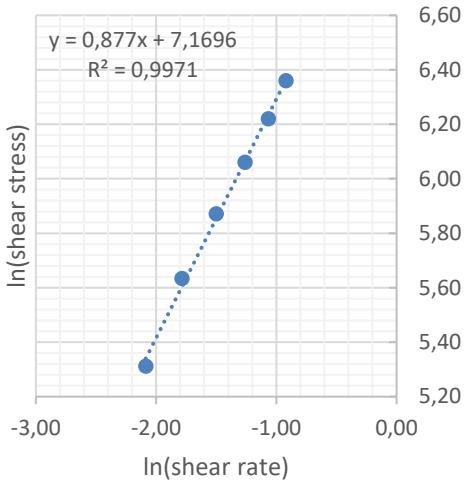

Figure 7-25: Sample 20160919 at 45°C

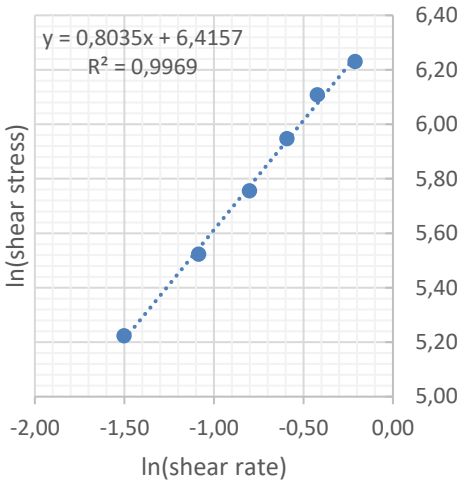

Figure 7-26: Sample 20160919 at 48°C

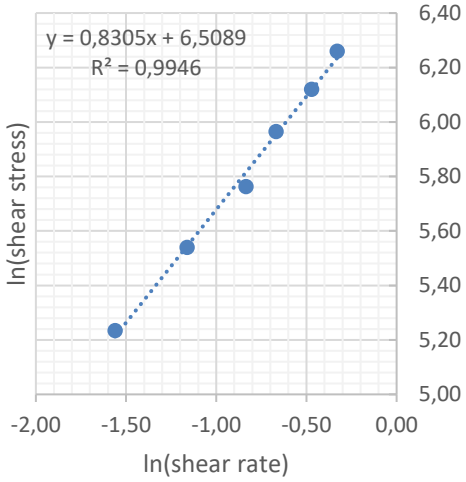

Figure 7-27: Sample 20160919 at 50°C

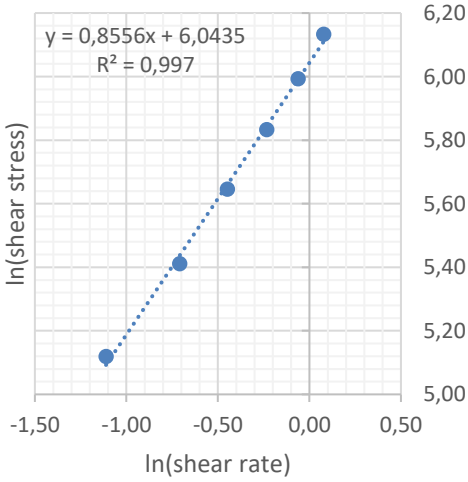

Figure 7-28: Sample 20160919 at 53°C

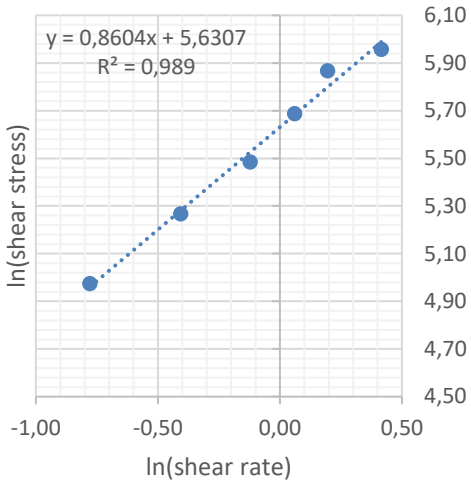

Figure 7-29: Sample 20160919 at 56°C

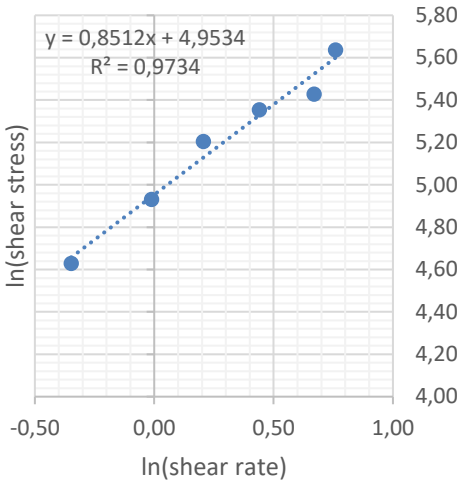

Figure 7-30: Sample 20160919 at 59°C

7.2.4 Sample 20160926

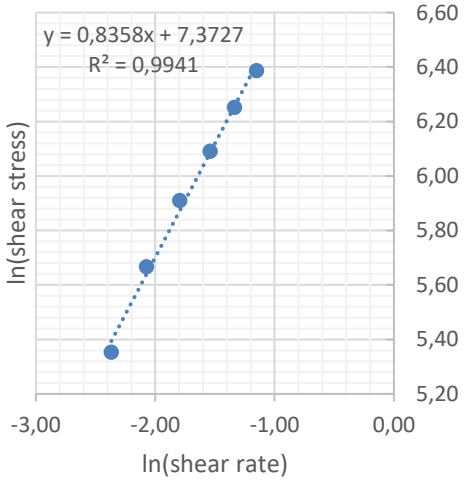

Figure 7-31: Sample 20160926 at 53°C

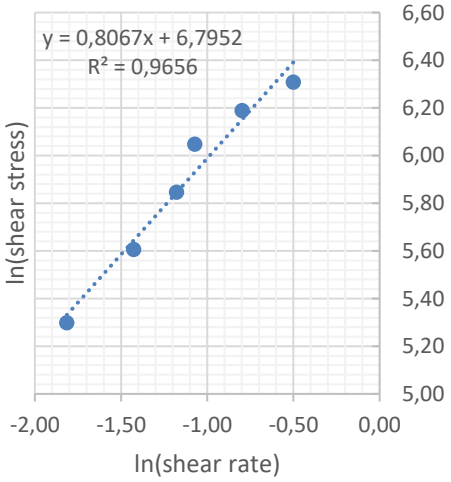

Figure 7-32: Sample 20160926 at 53°C

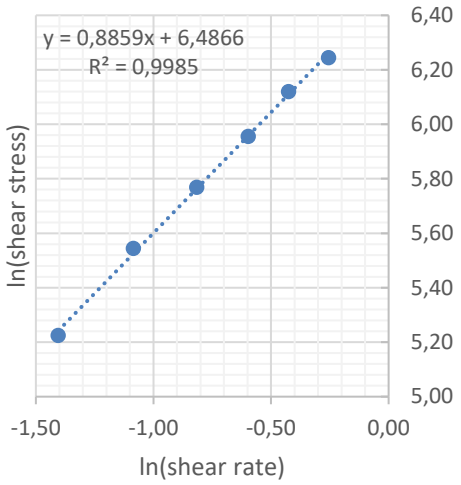

Figure 7-33: Sample 20160926 at 56°C

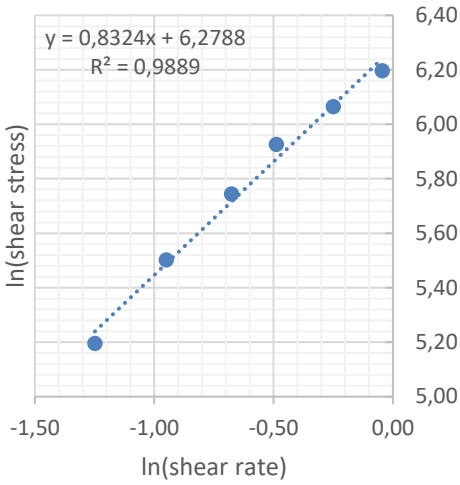

Figure 7-34: Sample 20160926 at 59°C

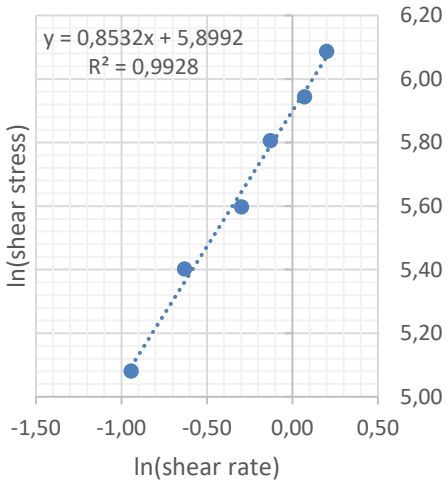

Figure 7-35: Sample 20160926 at 59°C

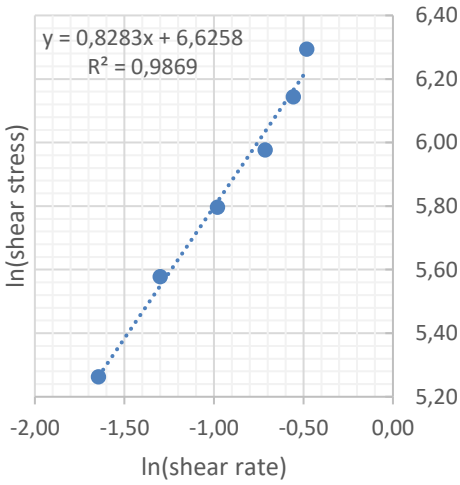

Figure 7-36: Sample 20160926 at 56°C

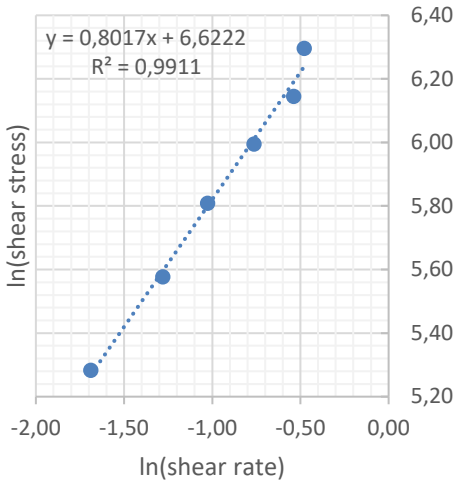

Figure 7-37: Sample 20160926 at 56°C

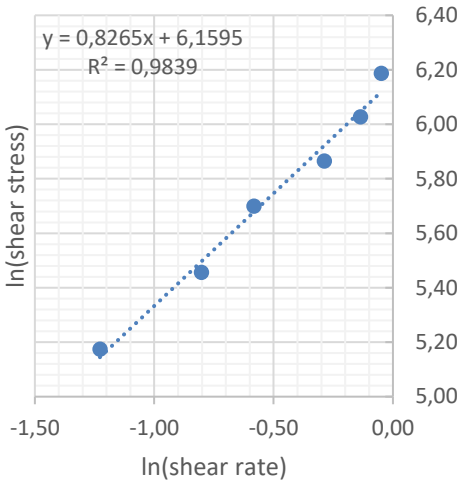

Figure 7-38: Sample 20160926 at 59°C

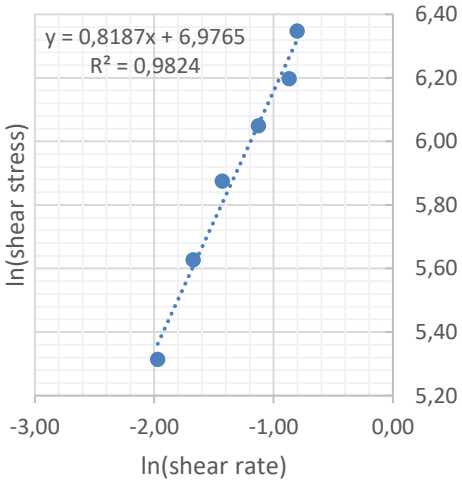

Figure 7-39: Sample 20160926 at 53°C

7.2.5 Sample 20161003

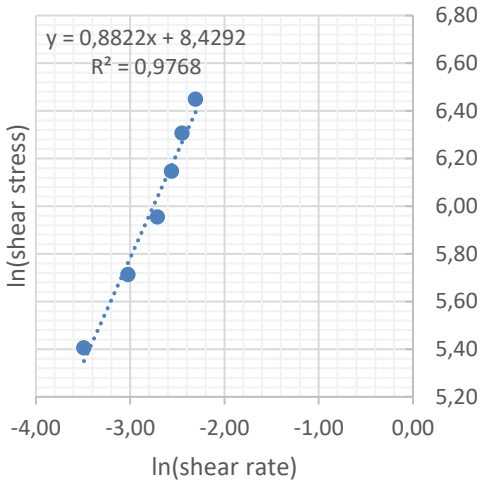

Figure 7-40: Sample 20161003 at 46°C

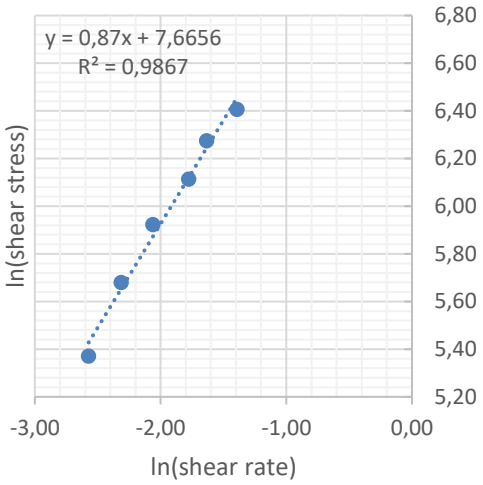

Figure 7-41: Sample 20161003 at 49°C

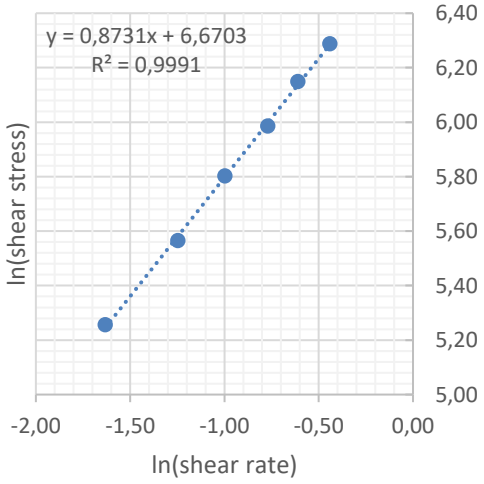

Figure 7-42: Sample 20161003 at 54°C

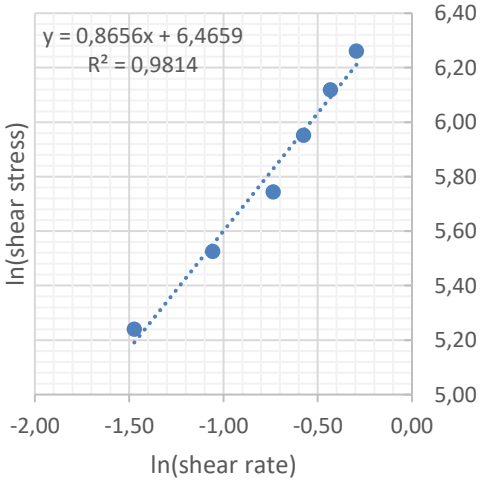

Figure 7-43: Sample 20161003 at 54°C

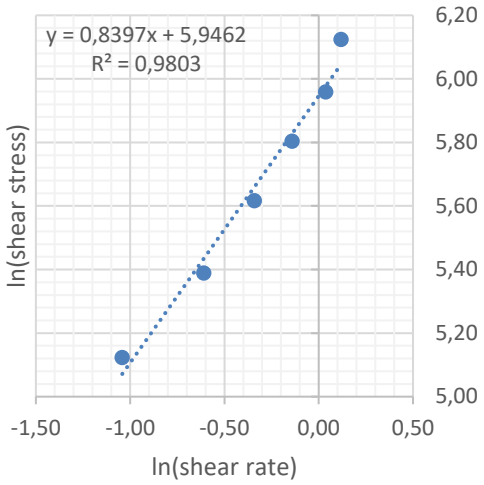

Figure 7-44: Sample 20161003 at 57°C

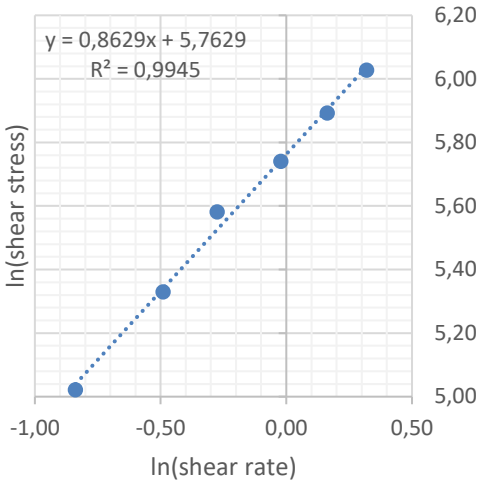

Figure 7-45: Sample 20161003 at 60°C

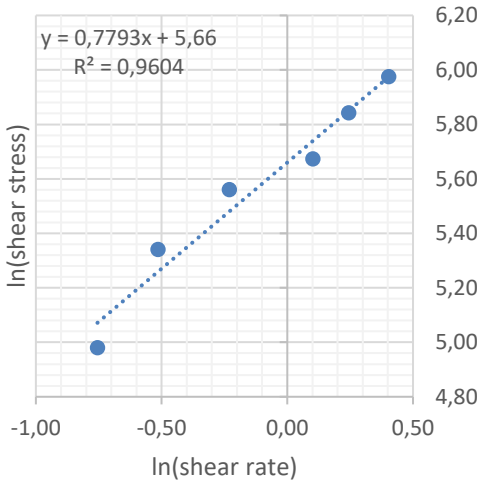

Figure 7-46: Sample 20161003 at 60°C

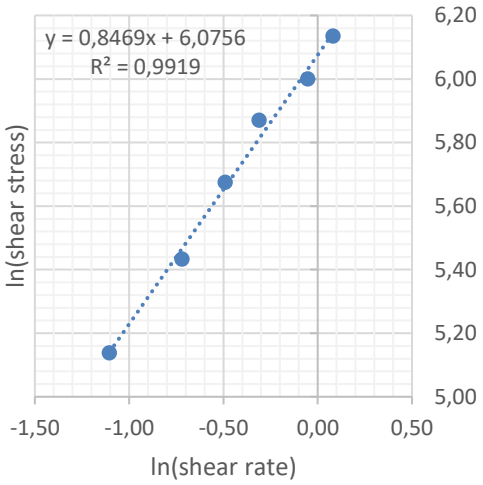

Figure 7-47: Sample 20161003 at 57°C

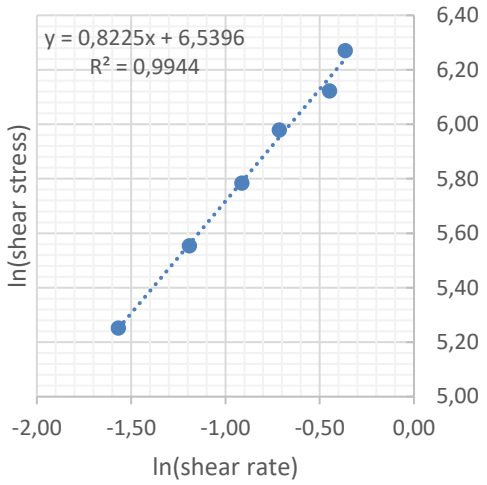

Figure 7-48: Sample 20161003 at 54°C

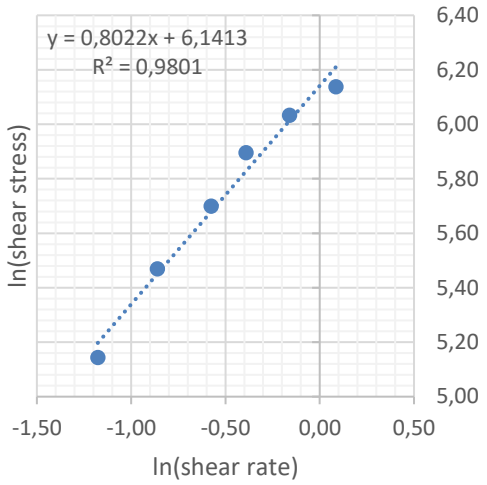

Figure 7-49: Sample 20161003 at 57°C

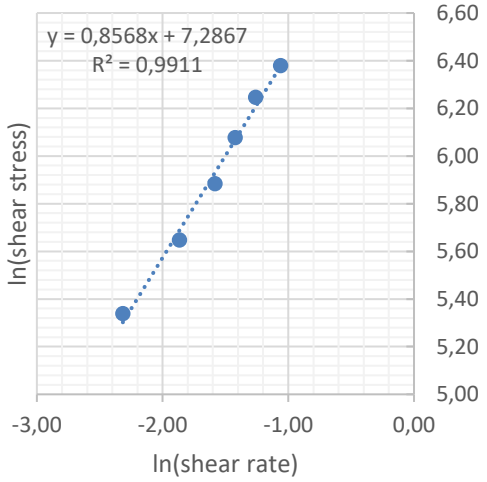

Figure 7-50: Sample 20161003 at 49°C

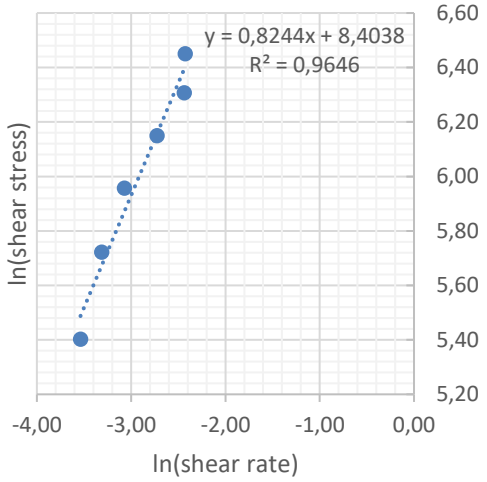

Figure 7-51: Sample 20161003 at 46°C

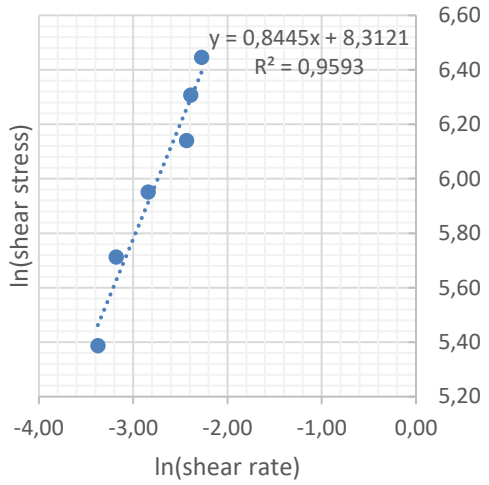

Figure 7-52: Sample 20161003 at 46°C

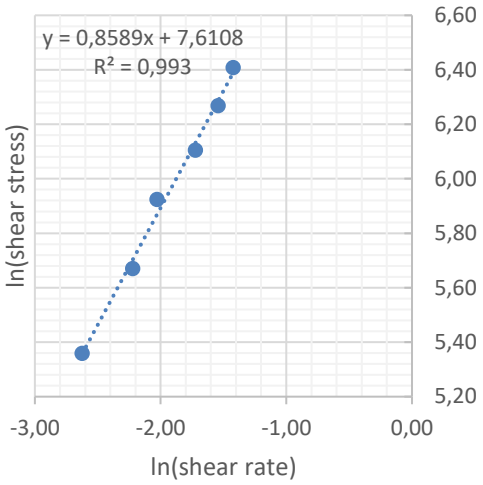

Figure 7-53: Sample 20161003 at 49°C

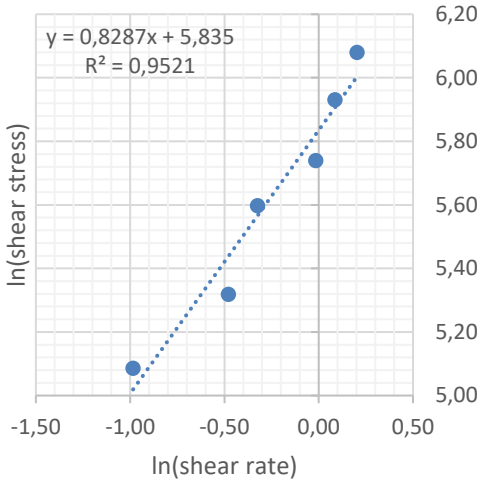

Figure 7-54: Sample 20161003 at 59°C

7.2.6 Sample 20161017

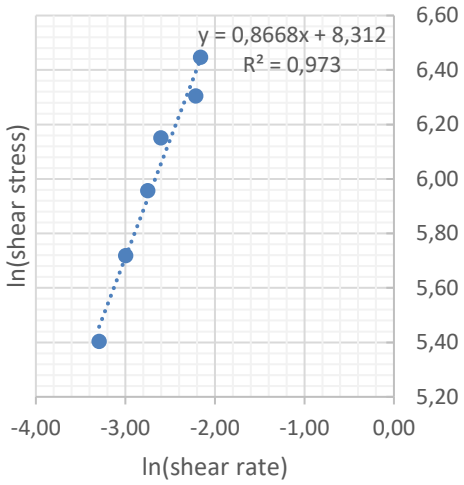

Figure 7-55: Sample 20161017 at 45°C

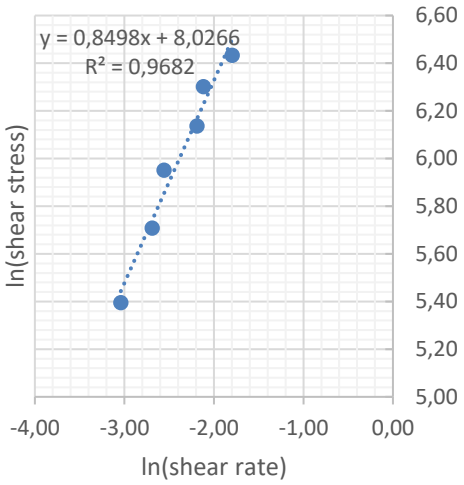

Figure 7-56: Sample 20161017 at 48°C

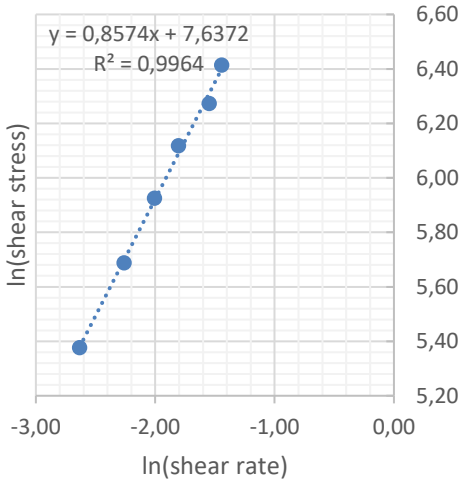

Figure 7-57: Sample 20161017 at 50°C

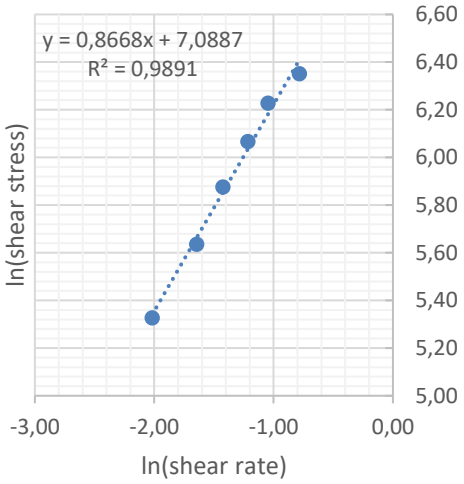

Figure 7-58: Sample 20161017 at 53°C

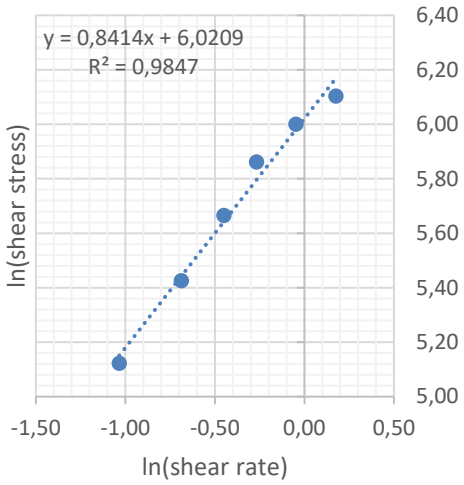

Figure 7-59: Sample 20161017 at 56°C

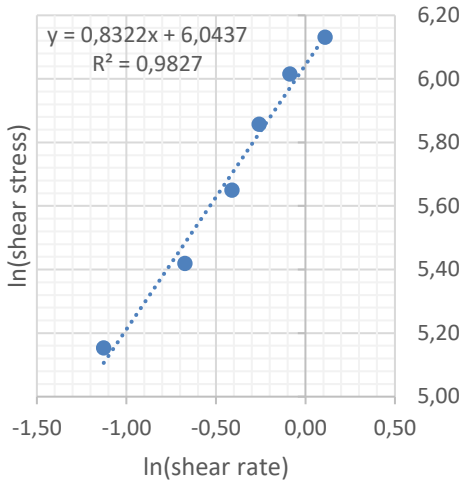

Figure 7-60: Sample 20161017 at 59°C

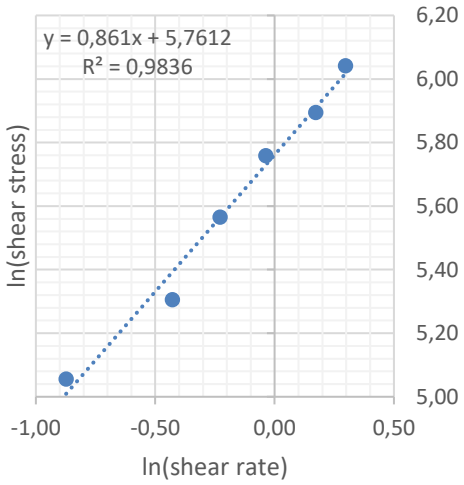

Figure 7-61: Sample 20161017 at 59°C

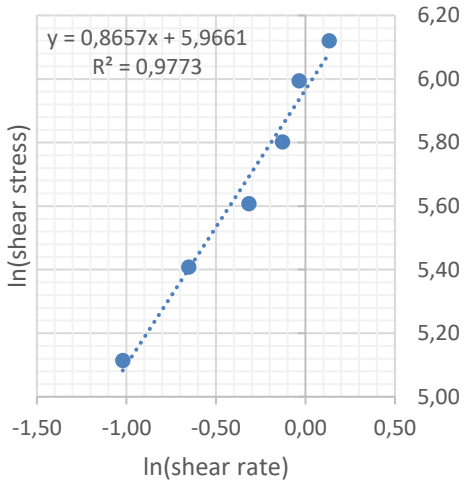

Figure 7-62: Sample 20161017 at 56°C

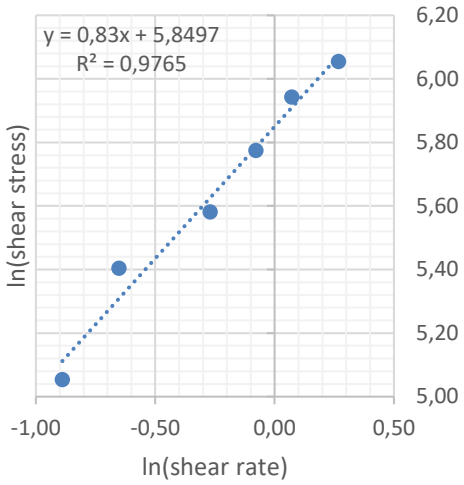

Figure 7-63: Sample 20161017 at 59°C

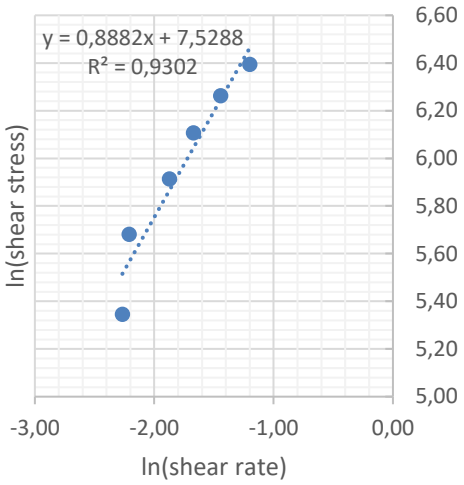

Figure 7-64: Sample 20161017 at 50°C

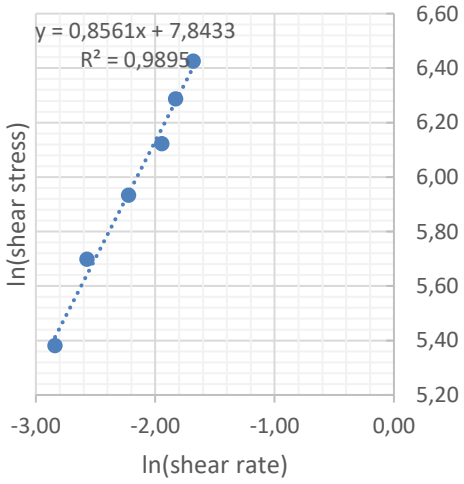

Figure 7-65: Sample 20161017 at 48°C

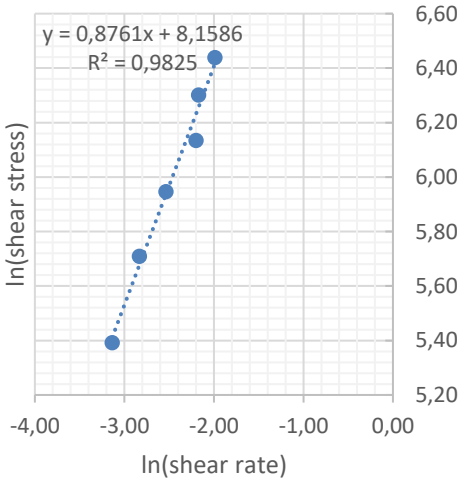

Figure 7-66: Sample 20161017 at 45°C

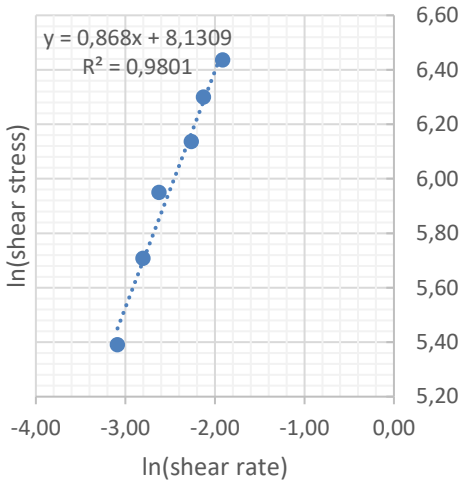

Figure 7-67: Sample 20161017 at 45°C

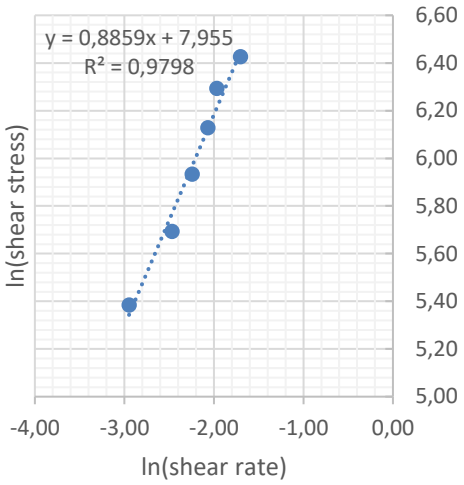

Figure 7-68: Sample 20161017 at 48°C

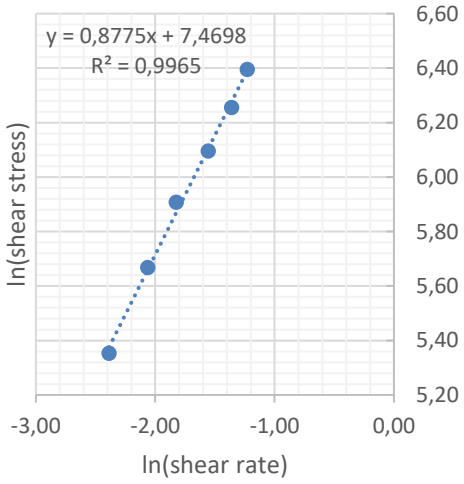

Figure 7-69: Sample 20161017 at 50°C

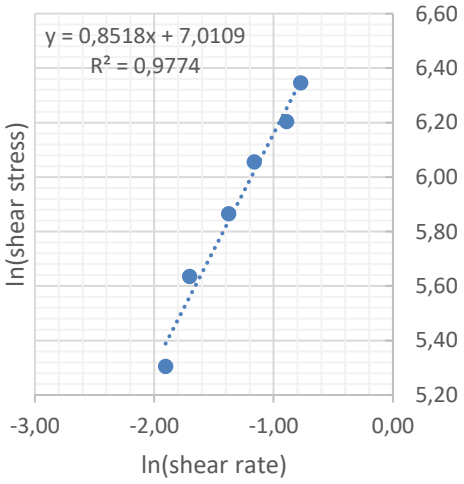

Figure 7-70: Sample 20161017 at 53°C

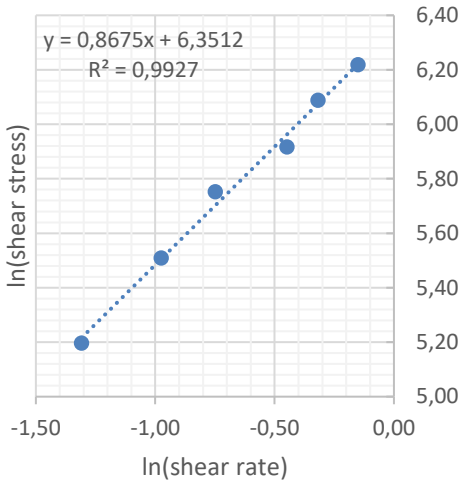

Figure 7-71: Sample 20161017 at 56°C

7.2.7 Sample 20161024

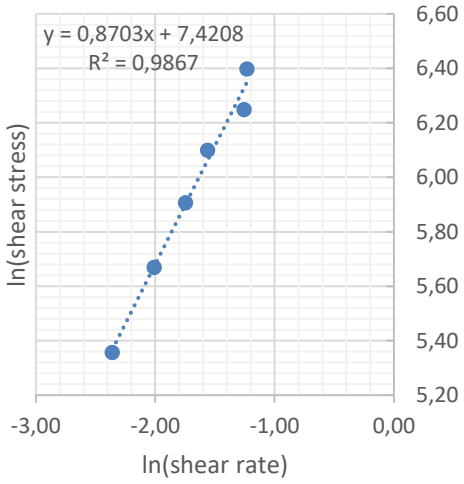

Figure 7-72: Sample 20161024 at 50°C

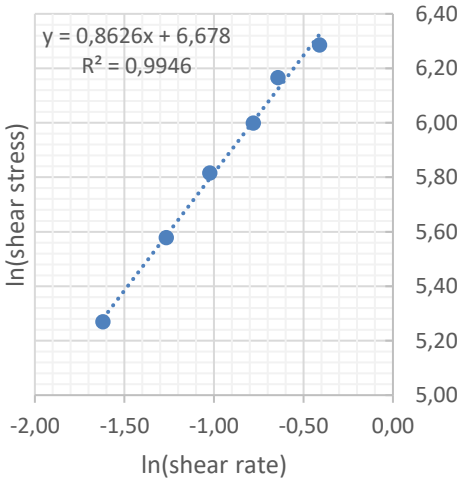

Figure 7-73: Sample 20161024 at 53°C

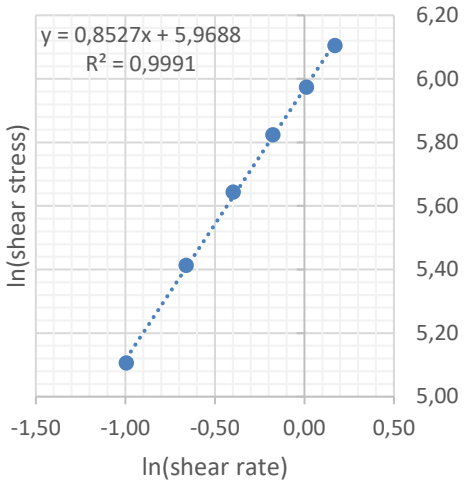

Figure 7-74: Sample 20161024 at 56°C

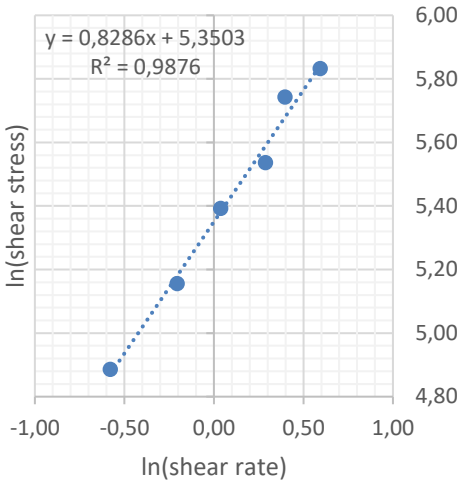

Figure 7-75: Sample 20161024 at 59°C

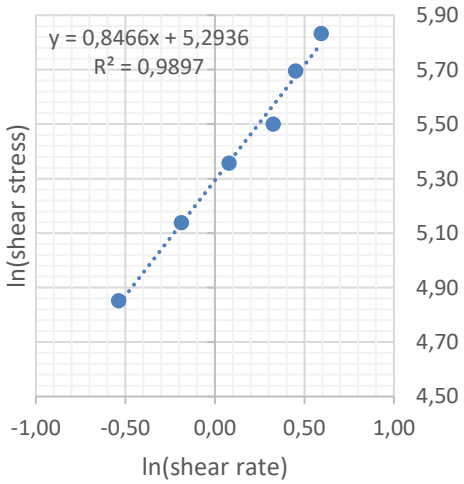

Figure 7-76: Sample 20161024 at 59°C

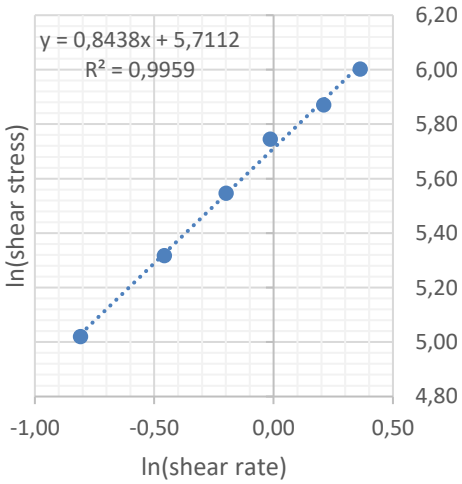

Figure 7-77: Sample 20161024 at 56°C

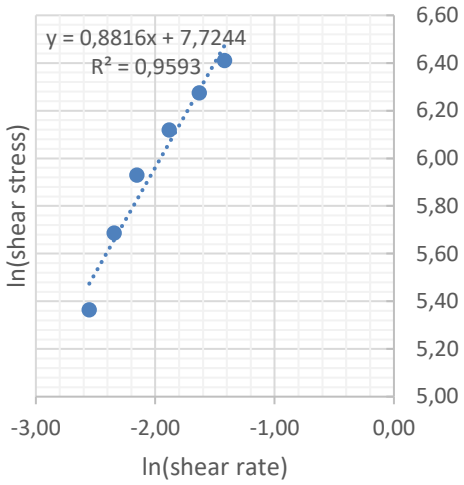

Figure 7-78: Sample 20161024 at 48°C

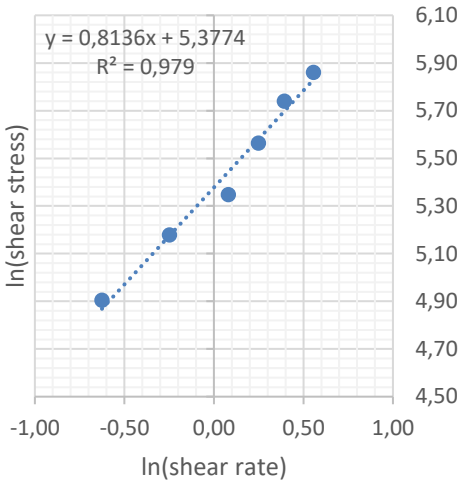

Figure 7-79: Sample 20161024 at 59°C

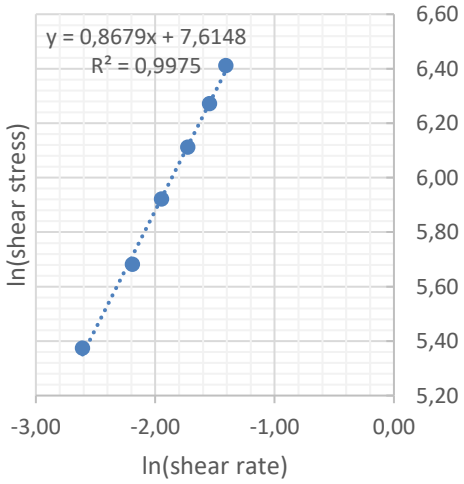

Figure 7-80: Sample 20161024 at 48°C

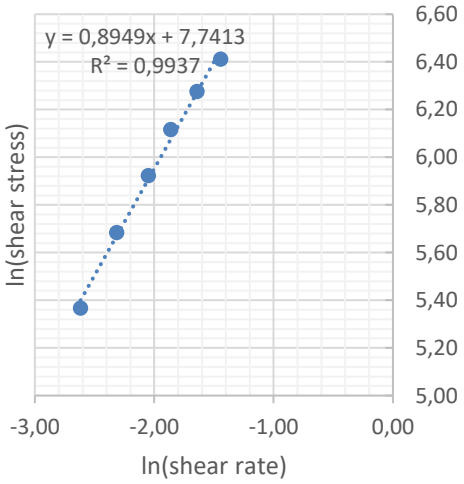

Figure 7-81: Sample 20161024 at 48°C

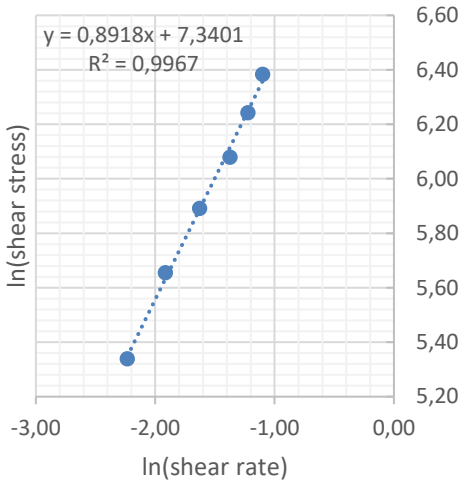

Figure 7-82: Sample 20161024 at 50°C

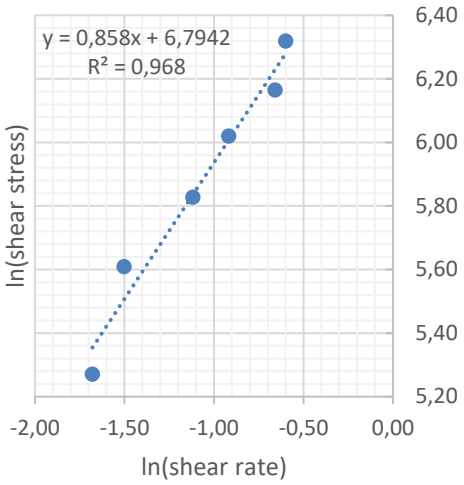

Figure 7-83: Sample 20161024 at 53°C

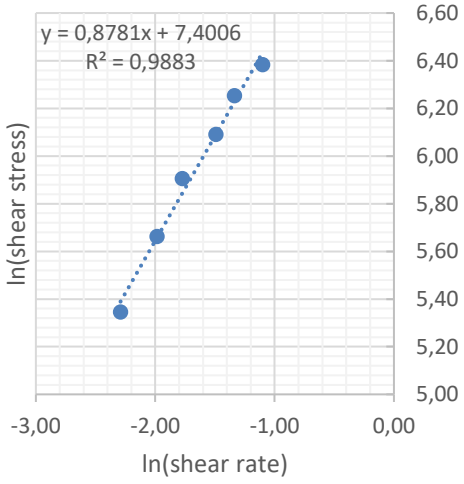

Figure 7-84: Sample 20161024 at 50°C

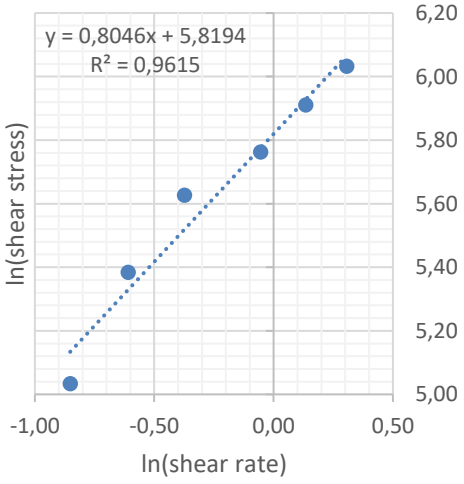

Figure 7-85: Sample 20161024 at 56°C

7.2.8 Sample 20161031

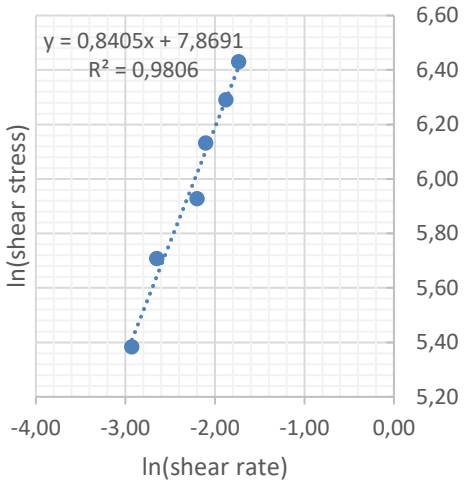

Figure 7-86: Sample 20161031 at 45°C

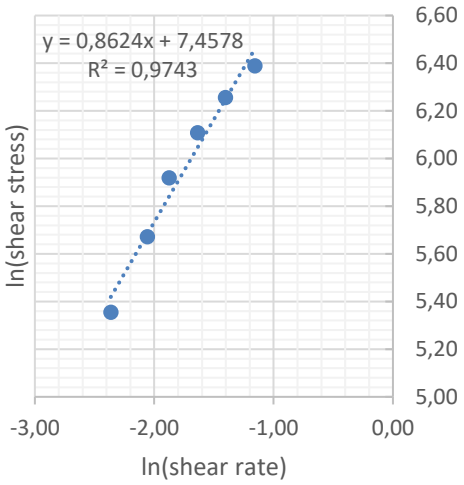

Figure 7-87: Sample 20161031 at 48°C

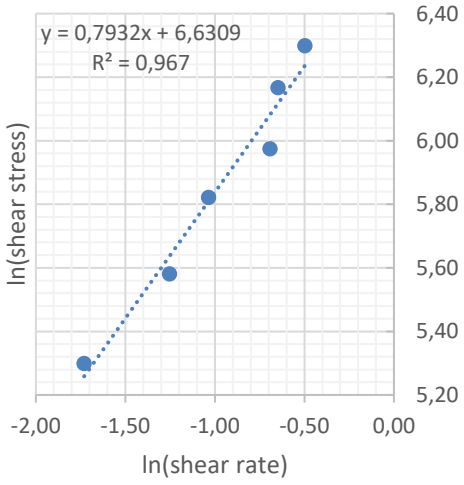

Figure 7-88: Sample 20161031 at 50°C

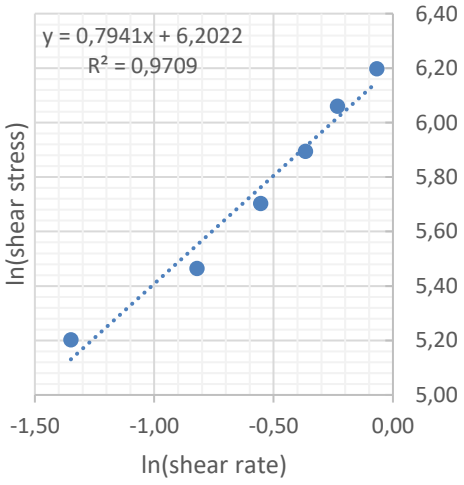

Figure 7-89: Sample 20161031 at 53°C

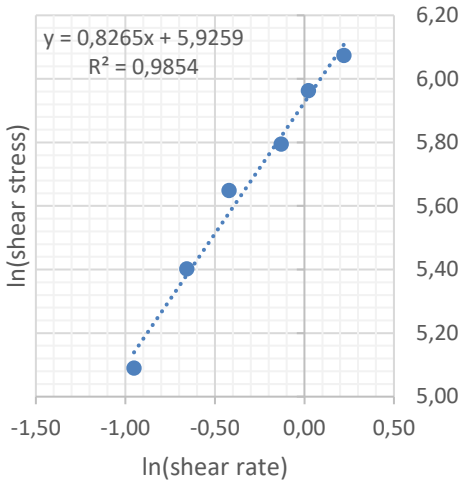

Figure 7-90: Sample 20161031 at 56°C

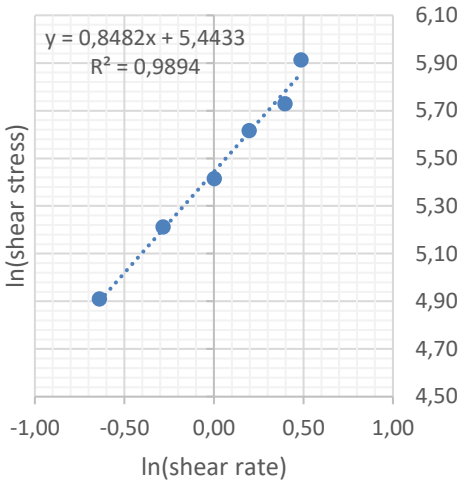

Figure 7-91: Sample 20161031 at 59°C

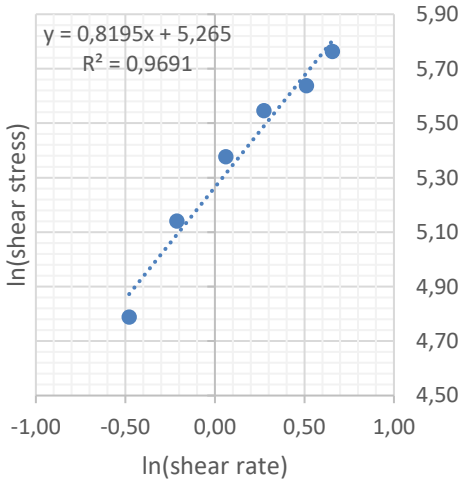

Figure 7-92: Sample 20161031 at 59°C

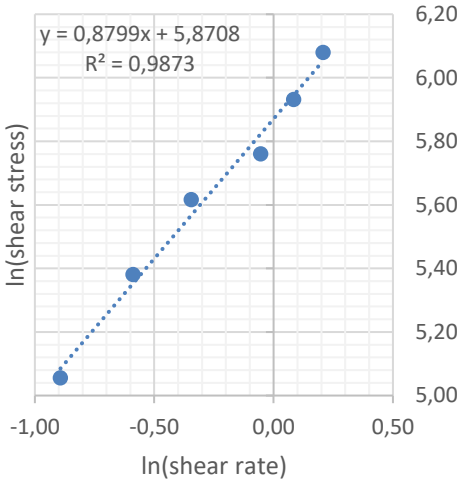

Figure 7-93: Sample 20161031 at 56°C

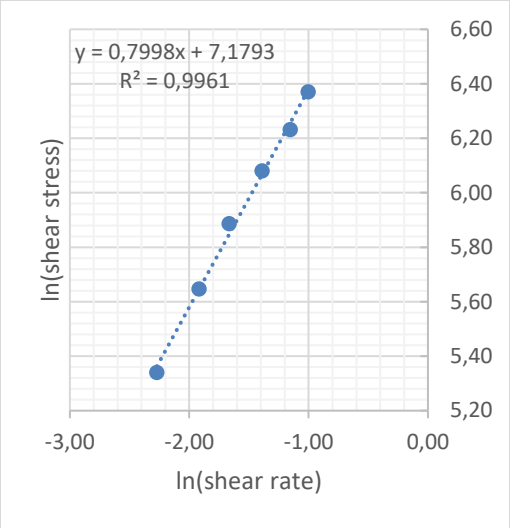

Figure 7-94: Sample 20161031 at 48°C

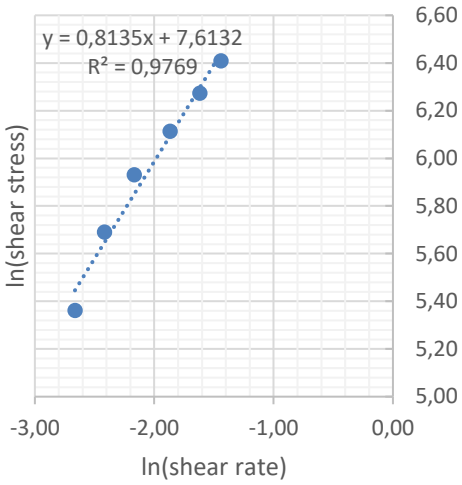

Figure 7-95: Sample 20161031 at 45°C

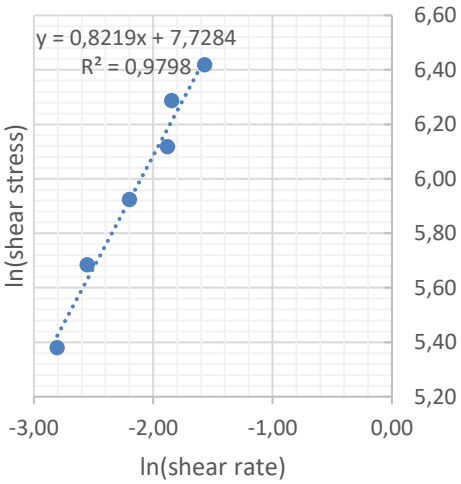

Figure 7-96: Sample 20161031 at 45°C

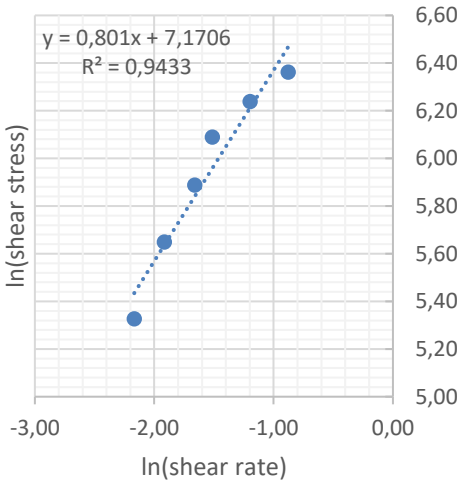

Figure 7-97: Sample 20161031 at 48°C

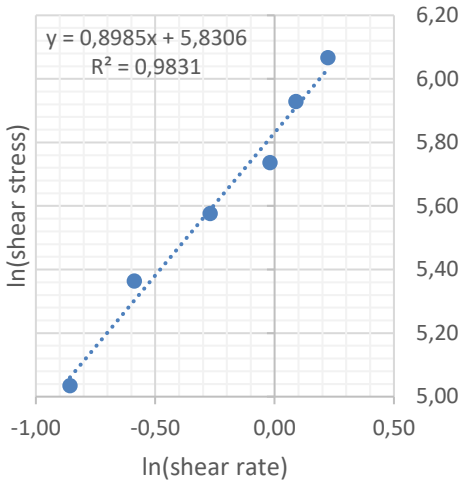

Figure 7-98: Sample 20161031 at 50°C

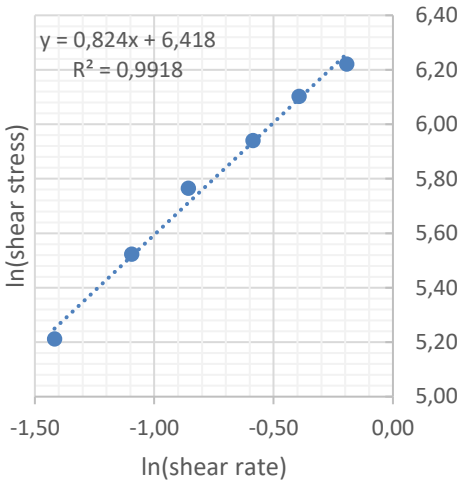

Figure 7-99: Sample 20161031 at 53°C

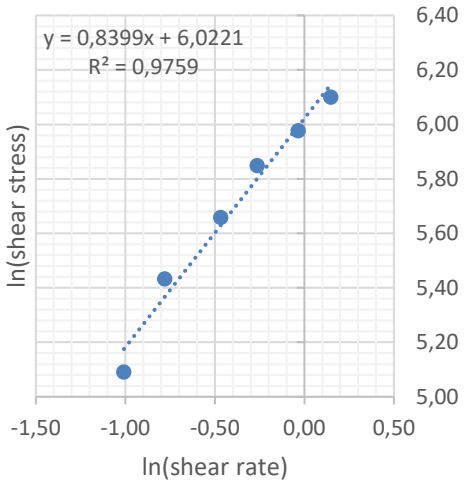

Figure 7-100: Sample 20161031 at 56°C

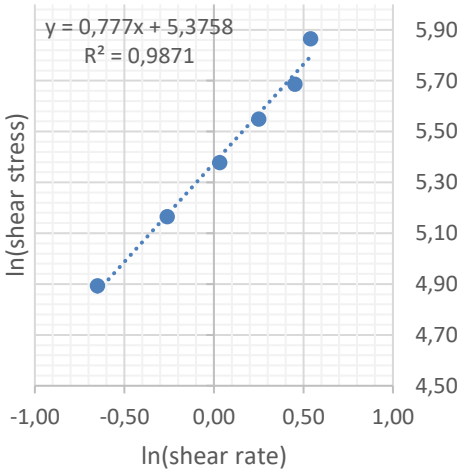

Figure 7-101: Sample 20161031 at 59°C

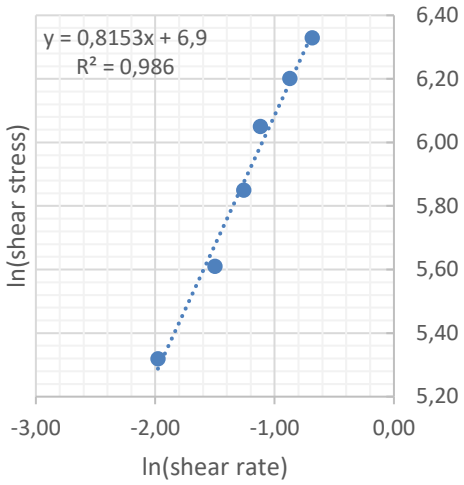

Figure 7-102: Sample 20161031 at 50°C

7.3 Appendix 3: Summary of flow behaviour index and consistency for all massecuite samples at individual temperatures

Table 7-1: Summary of results for tests performed on sample 20160901

Run 1	
Temperature, °C	Consistency K, Pa.s^n
46	606
49	452
52	305
54	185
55	199
58	144

Table 7-2: Summary of results for tests performed on sample 20160905

Run 1	
Temperature, °C	Consistency K, Pa.s^n
45	1685
48	992
50	682
53	367
55	189
58	118

Table 7-3: Summary of results for repeatability tests performed on sample 20160919

Run 1		Run 2		Run 3	
Temperature, °C	Consistency K, Pa.s^n	Temperature, °C	Consistency K, Pa.s^n	Temperature, °C	Consistency K, Pa.s^n
45	1120	45	1169	45	1261
48	564	48	569	48	583
51	413	50	666	50	644
54	266	53	394	53	407
57	224	56	248	56	269
59.9	95	59	140	59	137

Table 7-4: Summary of results for repeatability tests performed on sample 20160926

Run 1		Run 2		Run 3	
Temperature, °C	Consistency K, $Pa.s^n$	Temperature, °C	Consistency K, $Pa.s^n$	Temperature, °C	Consistency K, $Pa.s^n$
53	853	53	1529	53	1025
56	638	56	723	56	716
59	512	59	352	59	454

Table 7-5: Summary of results for repeatability tests performed on sample 20161003

Run 1		Run 2		Run 3	
Temperature, °C	Consistency K, $Pa.s^n$	Temperature, °C	Consistency K, $Pa.s^n$	Temperature, °C	Consistency K, $Pa.s^n$
46	4448	46	4277	46	3921
49	2067	49	1410	49	1951
54	622	54	663	54	764
57	368	57	419	57	443
60	308	60	272	59	328

Table 7-6: Summary of results for repeatability tests performed on sample 20161017

Run 1		Run 2		Run 3	
Temperature, °C	Consistency K, $Pa.s^n$	Temperature, °C	Consistency K, $Pa.s^n$	Temperature, °C	Consistency K, $Pa.s^n$
45	3941	45	3388	45	3290
48	2951	48	2460	48	2771
50	2003	50	1810	50	1702
53	1160	53	873	53	1069
56	396	56	377	56	555
59	405	59	307	59	333

Table 7-7: Summary of results for repeatability tests performed on sample 20161024

Run 1		Run 2		Run 3	
Temperature, °C	Consistency K, $Pa.s^n$	Temperature, °C	Consistency K, $Pa.s^n$	Temperature, °C	Consistency K, $Pa.s^n$
48	1963	48	2198	48	2243
50	1618	50	1589	50	1500
53	768	53	666	53	862
56	377	56	291	56	321
59	202	59	192	59	207

Table 7-8: Summary of results for repeatability tests performed on sample 20161031

Run 1		Run 2		Run 3	
Temperature, °C	Consistency K, Pa.s^n	Temperature, °C	Consistency K, Pa.s^n	Temperature, °C	Consistency K, Pa.s^n
45	2515	45	1935	45	2175
48	1676	48	1250	48	1239
50	721	50	949	0	0
53	470	53	490	53	587
56	359	56	344	56	397
59	223	59	185	59	205

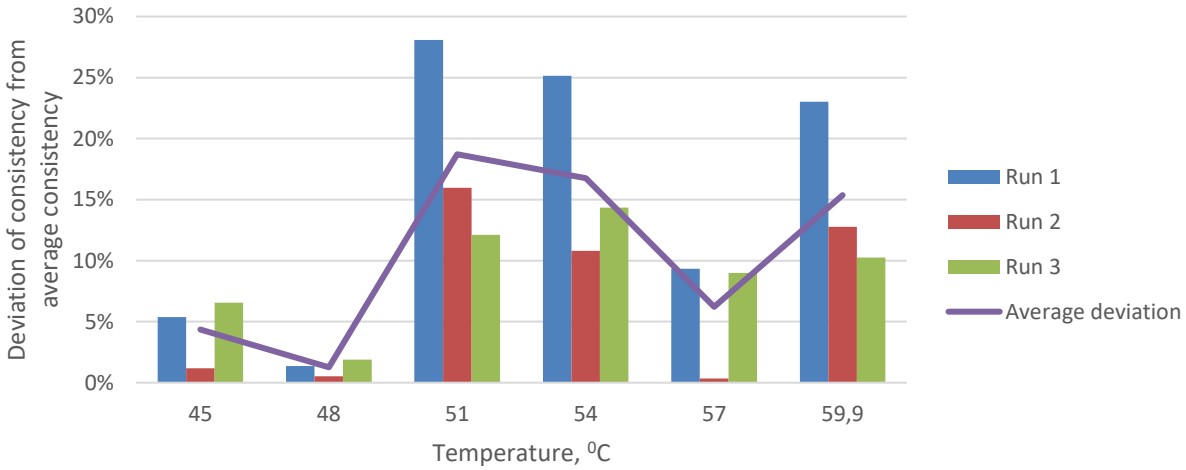

Figure 7-103: Deviation of consistencies for repeatability tests on sample 20160919

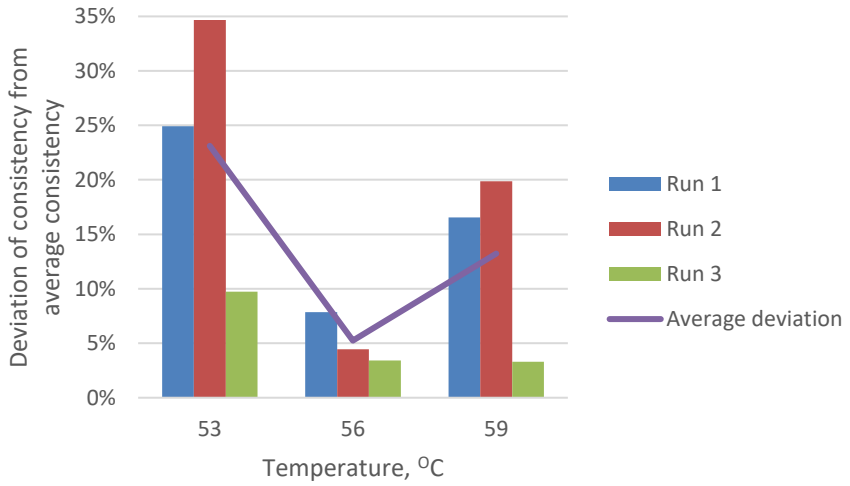

Figure 7-104: Deviation of consistencies for repeatability tests on sample 20160926

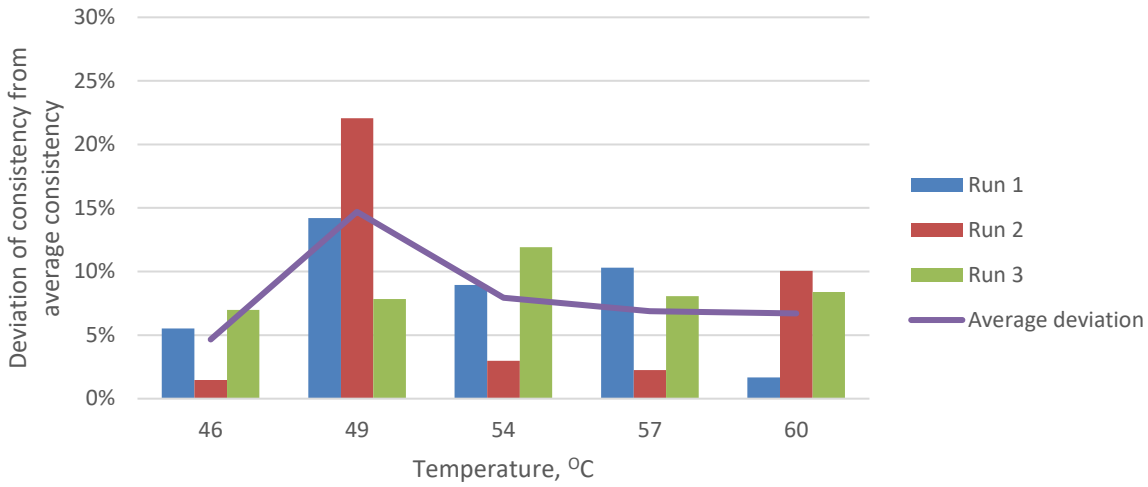

Figure 7-105: Deviation of consistencies for repeatability tests on sample 20161003

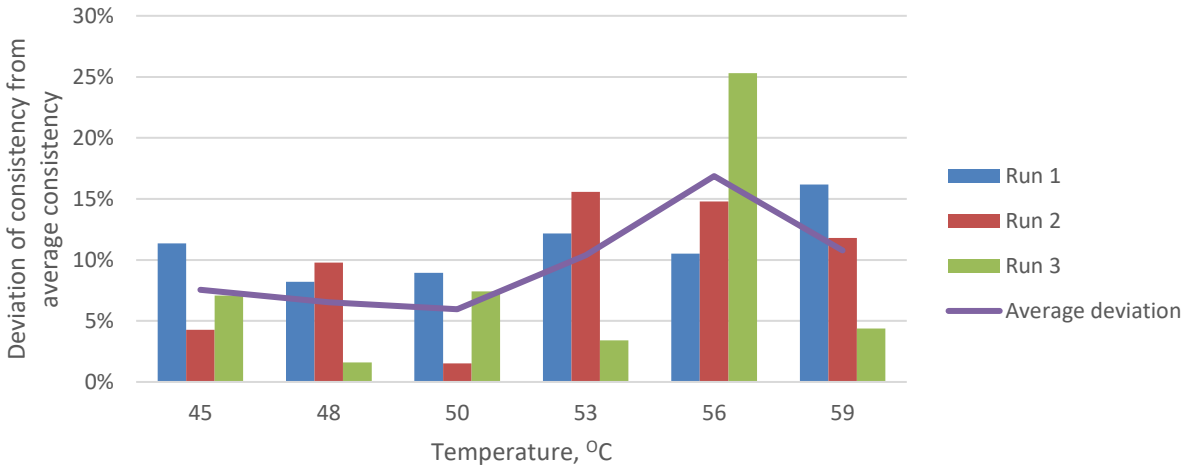

Figure 7-106: Deviation of consistencies for repeatability tests on sample 20161017

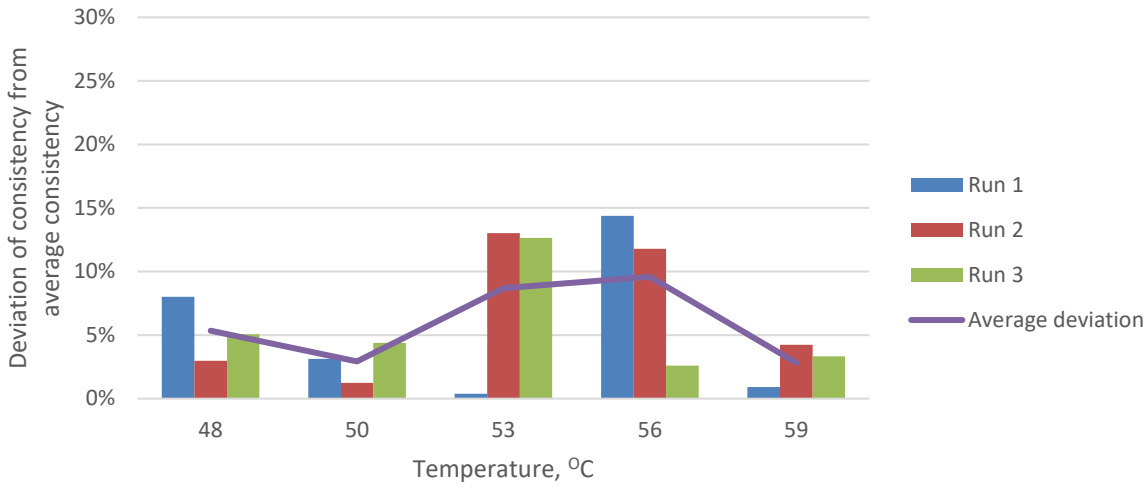

Figure 7-107: Deviation of consistencies for repeatability tests on sample 20161024

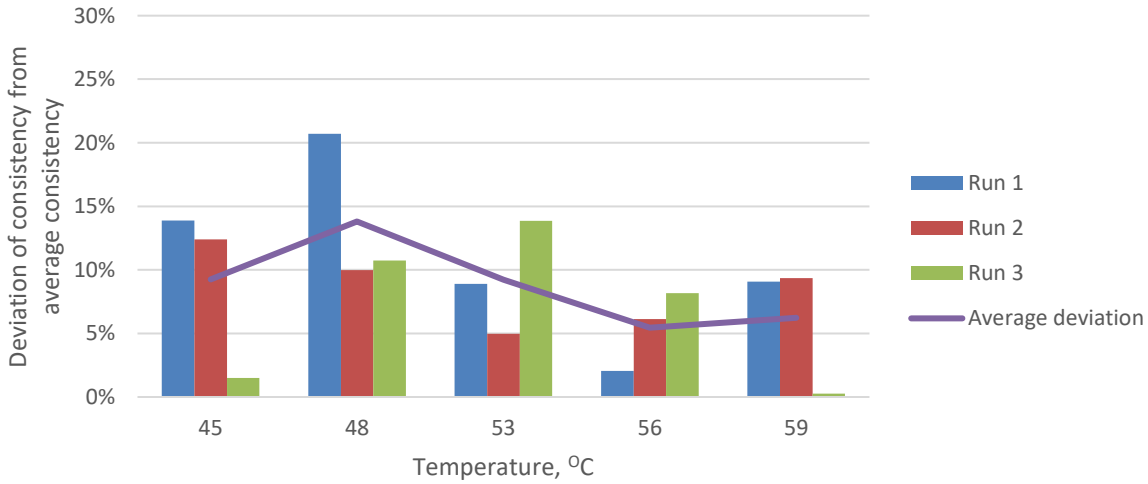

Figure 7-108: Deviation of consistencies for repeatability tests on sample 20161031